

NASA TECHNICAL NOTE



NASA TN D-2327

NASA TN D-2327

LOAN COPY: RETU
AFWL (WLIL-2)
KIRTLAND AFB, N



**COMPARISONS OF EXPERIMENTAL
FREE-JET BOUNDARIES WITH
THEORETICAL RESULTS OBTAINED WITH
THE METHOD OF CHARACTERISTICS**

*by Allen R. Vick, Earl H. Andrews, Jr.,
John S. Dennard, and Charlotte B. Craidon*

*Langley Research Center
Langley Station, Hampton, Va.*





COMPARISONS OF EXPERIMENTAL FREE-JET BOUNDARIES WITH
THEORETICAL RESULTS OBTAINED WITH THE
METHOD OF CHARACTERISTICS

By Allen R. Vick, Earl H. Andrews, Jr., John S. Dennard,
and Charlotte B. Craidon

Langley Research Center
Langley Station, Hampton, Va.

NATIONAL AERONAUTICS AND SPACE ADMINISTRATION

For sale by the Office of Technical Services, Department of Commerce,
Washington, D. C. 20230 -- Price \$2.50

COMPARISONS OF EXPERIMENTAL FREE-JET BOUNDARIES WITH
THEORETICAL RESULTS OBTAINED WITH THE
METHOD OF CHARACTERISTICS

By Allen R. Vick, Earl H. Andrews, Jr., John S. Dennard,
and Charlotte B. Craidon
Langley Research Center

SUMMARY

The characteristics method is presented for computing highly underexpanded free-jet boundary contours. This procedure, permitting extension of the calculations to very high pressure ratios and large distances downstream of the nozzle exit, has been incorporated into a computer program which facilitates rapid calculations of jet exhaust characteristics. Computer programs written in FORTRAN language are presented for the leading characteristic line, corner expansion fan, and the characteristic network. An experimental investigation, undertaken to verify the theoretical procedure, consisted of obtaining schlieren photographs of unheated jet exhaust boundaries from nozzles having design exit Mach numbers of 1.0, 2.22, and 5.0.

Theoretical jet boundaries have been calculated and contour plots developed which permit construction of jet boundaries at any ratio of nozzle-exit pressure to ambient pressure up to 10^7 , 10^6 , and 0.5×10^4 for nozzle-exit Mach numbers of 1.0, 5.0 (flow angle at nozzle lip, 15°), and 4.79 (flow angle at nozzle lip, 26.5°), respectively. It was found that on logarithmic coordinates, the maximum boundary size varied almost linearly with pressure ratio. Reasonable agreement of theoretical and experimental jet plumes was obtained over the complete range of pressure ratios experimentally investigated.

INTRODUCTION

The flow of rocket exhaust gases from highly underexpanded nozzles operating in near-vacuum conditions results in large billowing jet plumes. As a result, various problems arise depending on the vehicle altitude and the proximity of the rocket nozzle to adjacent surfaces, which may be either parts of the main vehicle or surfaces perpendicular to the jet blast, such as would be encountered during lunar landings and take-off. For flights of missiles within the atmosphere jet pluming can produce flow separation over the missile afterbody which in turn affects the stability characteristics. (See refs. 1 to 4.) The radial flow direction of the exhaust gases downstream of the nozzle exit can exceed 90° relative to the nozzle thrust axis, depending upon such factors as nozzle-exit Mach number, ratio of nozzle-exit pressure to ambient pressure,

and the ratio of specific heats of the exhaust products. Under such circumstances, stage separation effects must be evaluated with respect to forces and pressures on booster cases during the separation sequence. (See ref. 5.) Structural and heating problems may be introduced during orbital rendezvous missions in which the use of attitude control rockets for docking or trajectory corrections results in direct impingement of exhaust gases on parts of the vehicle. (See refs. 6 to 8.)

Additional problems, created by the interference of rocket exhaust plumes with communications between missiles and ground stations, have resulted in extensive research into the cause and effects of radio signal attenuation. A general discussion of several of the parameters influencing the propagation of telemetry signals through exhaust plumes is found in reference 9, and a more limited study of a specific missile configuration is contained in reference 10. An extensive summary of the more recent information on signal attenuation in solid-propellant rocket exhaust for many of the current missiles is contained in reference 11, and reference 12 shows that signal attenuation also occurs with liquid-propellant motors.

Jet pluming in connection with soft lunar landings and/or take-off, and the possibility of crater formation due to erosion of the landing area by jet exhaust plumes, has been the object of both experimental and theoretical studies. Jet impingement on hard flat surfaces has been investigated with cold jets (ref. 13) and with hot jets (ref. 14). Experimental investigations of jet impingement on a dust-covered surface (ref. 15) indicate the possibility of visibility impairment and vehicle surface damage. Further theoretical studies of this impingement problem are contained in references 16 and 17.

As a result of the many problems associated with highly underexpanded nozzles, many studies have been made to obtain a clearer understanding of the exhaust plume behavior. A few of these studies are contained in references 18 to 27 for both free jets and jets exhausting into a supersonic stream. Experimental confirmation of jet plume calculations by the method of characteristics or by empirical methods has been limited by lack of experimental data at high pressure ratios.

This report presents experimental studies and theoretical studies by the method of characteristics of free jets exhausting into still air from sonic and supersonic nozzles at relatively high pressure ratios. Experimental tests, conducted with cold air at a total temperature of about 90° F and at stagnation pressures up to approximately 2,400 psia, consisted of obtaining high-speed schlieren photographs of the jet exhaust plume. The initial phase of this investigation concerning experimental tests of free jets impinging on a parallel flat surface at ratios of total pressure to ambient pressure up to 250,000 has been reported in reference 8. Theoretical confirmation of the experimental program required extensive modifications to the characteristics method used in reference 18 to obtain meaningful calculations at large distances downstream of the nozzle exit for high pressure ratios. In view of the continued effort anticipated in the study of jet plumes and the complexity in setting up the computation procedure, the complete program for the characteristics method is included in this report.

SYMBOLS

d_j	nozzle-exit diameter
l	distance along jet axis from plane of nozzle exit to location of Riemann wave
M	Mach number
M_j	nozzle-exit Mach number
p_j	static pressure at nozzle exit
$p_{t,j}$	nozzle total pressure
p_∞	ambient static pressure
r	perpendicular distance from jet axis, equivalent to y in appendixes
r_j	radius of nozzle exit
S	diameter of Riemann wave
x	distance downstream from plane of nozzle exit measured parallel to jet axis
α_N	initial turning angle, measured between jet axis and tangent to jet boundary at the nozzle lip
γ	ratio of specific heats
θ	angle of flow, measured between direction of flow and jet center line
θ_N	nozzle half-angle, or angle of flow at nozzle lip, measured between direction of flow and jet center line
μ	Mach angle
ν	Prandtl-Meyer angle (angle through which a supersonic stream is turned to expand to a Mach number greater than 1)
ν_N	Prandtl-Meyer expansion angle from sonic velocity to nozzle-exit Mach number
ν_l	Prandtl-Meyer expansion angle from sonic velocity to jet-boundary Mach number

Subscript:

max maximum

APPARATUS FOR EXPERIMENTAL STUDIES

Test Setup and Procedure

The principal part of the experimental investigation to obtain schlieren observations of free-jet flow fields was conducted in the 41-foot-diameter vacuum sphere at the Langley Research Center with the test setup as shown in figure 1(a). Air from a tank farm pressurized to approximately 2,400 psia and 90° F, and of sufficient volume to maintain essentially a constant nozzle stagnation pressure during a test run, was supplied to the nozzles through a 3/4-inch-diameter supply pipe. An electrically operated solenoid valve located just upstream of the nozzle permitted a rapid start sequence. Over a total testing time of approximately 30 seconds the ratio of total pressure to ambient pressure was reduced from a value of approximately 250,000 down to about 20,000.

Nozzle stagnation pressures were measured by a 3,000-psia pressure transducer located between the electrically operated solenoid valve and the nozzle inlet bell. (See insert in fig. 1(a).) Initial pretest sphere pressures of approximately 0.4 mm Hg (0.0077 psia) were attained with vacuum pumps and measured with a McLeod gage. The change in sphere ambient pressure with time was measured by a pressure transducer calibrated from 0.005 to 0.100 psia. All pressure measurements were continually recorded on oscillograph paper. With the test nozzle in operation, the sphere pressure increased linearly with time; therefore, the ratio of total pressure to ambient pressure decreased inversely with time.

High-speed 16-mm motion pictures of the exhaust plume were obtained from a double-pass schlieren system. A 25-inch-diameter parabolic mirror was mounted about 4 feet behind the nozzle (as shown in fig. 1(a)), and both the camera and schlieren light source were located on the equator of the vacuum sphere in the monitoring room. The camera was synchronized with the flashing light source and operated at about 750 frames per second. Timing marks recorded on the edge of the film from a 60-cycle flashing light source permitted a correlation of the motion pictures with a plot of pressure ratio against time.

Supplementary experimental data were obtained in the low-pressure-ratio test facility shown in figure 1(b). This test setup permitted operation at a constant pressure ratio and adjustment of the single-frame schlieren system for maximum sensitivity. The larger nozzles tested in this facility improved the quality of the schlieren photographs of the free-jet flow fields. Supply air from a large-capacity tank farm was available at total pressures up to 400 psia and total temperatures of about 90° F. Stagnation pressure was measured by a total-pressure tube located at the outlet of a small settling chamber as shown in the figure. With a nozzle in operation, values of ambient pressure as low as 0.5 psia could be held constant over long periods of time by using a series of compressors as vacuum pumps. Ambient pressure in this facility was measured with a mercury manometer.

Test Nozzles

Sketches of the two nozzles used for the high-pressure-ratio tests in the 41-foot vacuum facility are shown in figure 2(a). The converging nozzle ($M_j = 1.0$) had an exit diameter of 0.125 inch, and the converging-diverging conical nozzle, having a nominal design Mach number of 5.0, based on inviscid flow, had an exit diameter of 0.625 inch, an area ratio of 25, and a half-angle of 15° . For some tests conducted with the nominal $M = 5.0$ nozzle, a static-pressure orifice installed in the diverging wall just upstream of the exit indicated an actual exit Mach number of 4.79.

The initial phase of this investigation (ref. 8) reported that measurements of the initial turning angle of the flow at the nozzle exit α_N , obtained from a series of photographic enlargements of the Mach 5 nozzle, indicated a substantially larger value of expansion half-angle θ_N than the inviscid design value. This comparison was performed by using an expression, $\alpha_N = \nu_1 - \nu_N + \theta_N$ (see, for example, ref. 19). With ν_N and ν_1 determined from the estimated exit Mach number of 4.79 and the experimental value of the ratio of ambient pressure to total pressure, respectively, the effective nozzle half-angle θ_N was computed to be 26.5° , or about 11.5° greater than the inviscid design value. The difference between the measured and calculated value of α_N , when correlated with a Reynolds number of about 13×10^6 based on nozzle-exit conditions and diffuser conical length, compares favorably with the results of reference 3. The larger effective nozzle half-angle is believed to be due to a combination of factors, including small-scale model size, sharp corners at the nozzle throat, boundary-layer growth, and a thinning of the boundary layer at the nozzle exit. It is evident that more research is needed in this area; and until experimental results indicate otherwise, it is believed that θ_N will correspond to the geometric angle for large-scale models.

The two large-scale models tested in the low-pressure-ratio facility are shown in figure 2(b). Both nozzles had smooth entrances and minimum throat diameters of 0.707 inch. The $M_j = 2.22$ contoured nozzle was designed by the method of characteristics for parallel flow at the exit. Nozzle coordinates are tabulated on the figure.

RESULTS AND DISCUSSION

Basic Considerations

Jet exhaust description.- Prior to a discussion of theoretical and experimental results, a few of the more basic fundamentals of jet exhaust plumes will be considered. Rocket nozzles are usually classified either as conical or contoured. The exhaust gases leave a conical nozzle in a radial direction whereas the contoured nozzle is designed for exhaust flow parallel with the axial center line. Regardless of the type of nozzle used the structure of the exhaust jets produced by operating these nozzles in a highly underexpanded condition is

basically similar, as shown by the illustration in figure 3. Some of the more important features of a typical exhaust plume consist of the leading characteristic line, internal shock, jet boundary, and normal shock.

The leading characteristic, or Mach line, as determined from the nozzle-exit Mach number, is a straight line for the contoured nozzle and forms the familiar Mach cone. All flow conditions along this Mach line and within the Mach cone, including M , θ , μ , and ν , are constant. For the conical nozzle the leading characteristic line is curved and flow conditions are different for each point downstream of the nozzle exit. A more detailed discussion of the leading characteristic line is contained in appendix A. For both nozzles, however, when operating at or above the design pressure ratio the leading characteristic serves as a dividing line between two different flow regions. The internal region (Mach cone or radial flow zone) bounded by this line consists of a zone of zero external influence in which flow properties are determined strictly from nozzle design criteria. In the region external of this line and bordered by the jet boundary, the ratio of stagnation pressure to ambient pressure is the controlling factor with respect to size and shape of the jet plume.

In the region bounded by the leading characteristic line, the axial center line, the normal shock, and the internal shock, the controlling factors are the corner expansion fan originating at the nozzle lip and the overall three-dimensional nature of the flow. The characteristic net comprising this region is made up entirely of an expansion network in which the flow is isentropic. Mach numbers within this area are therefore continually increasing, both with distance downstream of the nozzle exit and also in a direction perpendicular to the axial center line out to the position of the internal shock.

The internal shock is formed by the coalescence of infinitesimally weak compression waves reflected from the jet boundary. At pressure ratios slightly above the nozzle design value of 1.0 the internal-shock system forms the familiar diamond pattern. As pressure ratio increases a normal shock forms and the internal shock approaches the jet boundary. The internal shock originates near the nozzle exit and increases in strength with distance downstream of the nozzle. In traversing the internal shock in a direction perpendicular to the nozzle axial center line, a sharp Mach number discontinuity exists followed by a gradual decrease to the final boundary value. The jet boundary, as the name implies, defines the external shape of the exhaust plume and is the separation line between ambient conditions and flow from the exhaust nozzle. Mixing at the jet boundary is ignored in this presentation.

Factors affecting exhaust plume.- The primary parameters which influence exhaust plume size and shape are M_j , θ_N , γ , p_j , and p_∞ . Of these parameters M_j , θ_N , and p_j are constant and dependent only upon nozzle design parameters and chamber stagnation pressure. In real-gas flow the ratio of specific heats γ varies to some degree with the reduction in exhaust gas temperature produced in the expansion process, and the state of equilibrium of the flow. In order to prevent further complications of the calculation procedure, frozen equilibrium has been assumed; therefore, γ remains constant. The remaining parameter is ambient pressure p_∞ which varies with altitude and is expressed as nondimensional pressure ratio, p_j/p_∞ .

Highly underexpanded exhaust nozzles have an excess of pressure p_j at the nozzle exit, and, as a result, the exhaust gases leaving the nozzle exit must expand until the pressure is equal to the surrounding or ambient pressure. At near vacuum values of ambient pressure, even moderate nozzle-chamber pressures produce very large values of p_j/p_∞ . It is at these high pressure ratios that concern arises as to the maximum angle through which the exhaust gases expand and the overall size and shape of the plume.

Initial turning angle.- The method of calculating the initial turning angle at the nozzle lip is shown in figure 4 along with a sketch of the initial section of the jet boundary. Also listed are the controlling parameters previously discussed. Since the circumference of the nozzle exit can be considered to be made up of a large number of straight line segments, the flow just at the nozzle lip can be classified as two dimensional. Furthermore the absence of shocks at the nozzle exit indicates an isentropic expansion of the flow to the ambient pressure. The flow angle through which the flow will expand ($\Delta\nu = \nu_1 - \nu_N$) is the difference between the Prandtl-Meyer expansion angles corresponding to the jet-boundary Mach number and the nozzle-exit Mach number. Boundary Mach number, the only unknown in determining ν_1 , depends upon the altitude, with its corresponding ambient pressure p_∞ , and the nozzle total pressure $p_{t,j}$. Inclusion of the flow direction as imparted by the nozzle half-angle θ_N completes the equation for finding the initial turning angle:

$$\alpha_N = \nu_1 - \nu_N + \theta_N$$

An indication of the magnitude of the initial turning angle and the variation with pressure ratio is shown in figure 5 for two different nozzles. For a perfect gas ($\gamma = 1.4$) the maximum Prandtl-Meyer angle through which the flow might expand at an infinite pressure ratio is shown in reference 28 to be 130.45° . The expansion process may be either internal in which part of the expansion occurs within the nozzle proper to attain a given exit Mach number, or external in which the process is concluded by expanding to ambient conditions after the gas has left the nozzle. In order to achieve the maximum turning angle (130.45°) all of the expansion is required to occur external of the nozzle as is shown for the $M_j = 1.0$ case in figure 5; however, this situation is not desirable, since external expansion is synonymous with loss in thrust performance. From the standpoint of increasing propulsive efficiency, it is desirable to increase the Mach number of the nozzle in order to achieve as much internal expansion as possible. Structural and weight limitations, however, place a limit on the nozzle design Mach number, which in turn precludes having all internal expansion, particularly for high-altitude operations. As a result of these limitations, nozzles are usually designed for a moderate supersonic Mach number such as the $M_j = 5.0$ case shown in figure 5. The maximum turning angle for this particular design Mach number and nozzle half-angle is only about 69° .

If the $M_j = 5.0$ nozzle of figure 5 were contoured for axial flow at the exit, $\theta_N = 0^\circ$, the variation of initial turning angle with pressure ratio would be a curve originating at $\alpha_N = 0^\circ$, similar to the existing curve, and located 15° lower at any selected pressure ratio.

It would appear from the previous discussion that restrictions of the turning angles to moderate values might not be too difficult. When real-gas flows are encountered the initial turning angle may be much higher than those indicated in figure 5. As an example, initial turning angles with all external expansion reach maximum values as high as 243° for $\gamma = 1.15$, and 203° for $\gamma = 1.20$ (see ref. 29), in comparison with 130.45° for $\gamma = 1.4$. Although some of the expansion process will be internal, as has previously been shown, these numbers serve to illustrate that initial turning angles approaching and even exceeding 90° , depending upon the value of γ , should not be unexpected.

Theoretical Results

Method of calculations.- The method of characteristics used in calculating free-jet boundaries, by using three-dimensional irrotational equations of flow and the "foldback" procedure, has been well established in reference 18. However, certain limitations arise in using the foldback method as the pressure ratio increases. These limitations restrict the range of computations to a region close to the nozzle exit. In order to obtain complete contours of the jet boundary out to the maximum diameter of the jet plume at the higher pressure ratios, it became necessary to eliminate the foldback portion of the calculations and develop a procedure in which the outer region of the characteristic net would be developed similar to that of the actual flow. A description of the calculation procedure including equations and a complete FORTRAN (FORMula TRANslation) writeup is included in the appendixes. Consequently, only a brief description of the revised characteristic network obtained by eliminating the foldback is included here.

A segment of a typical characteristic network is shown in figure 6 and illustrates points of primary interest in the revised calculations procedure. The nozzle-exit center line is located at the top of the figure and flow from the nozzle is from left to right. The initial turning angle at the nozzle exit α_N is in excess of 90° and the greatly expanded abscissa scale permits improved visualization of the characteristic network. Three primary types of lines comprise the characteristic network and are identified in the figure as A, B, and C lines. Type A lines originate at the nozzle lip and comprise the corner expansion fan, whereas type B lines originate either on the leading characteristic or on the diametrically opposite lip. The type C lines are referred to as reflected rays due primarily to the fact that the B lines strike the boundary and then appear to reflect as though from a physical surface. The coalescence of these reflected rays, which are actually very weak compression waves, forms the internal shock previously discussed. As more of these waves coalesce, the strength of the internal shock increases.

Additional intersections of the corner expansion rays, A lines, with the internal shock, in addition to the reflected ray intersections, result in

obvious complications to the calculations in the region of the internal shock. In the foldback procedure the corner expansion rays are allowed to continue on past the location of the internal shock and hence no solution is required for intersecting lines; however, this situation does not simulate actual flow conditions. A reasonable approximation of actual flow conditions is to combine these rays at the point of intersection. In three-dimensional calculations rays are generally referred to as right-or-left-running characteristic lines (or members of opposite families), and by using the known flow conditions on two of these lines it is possible to compute a third point to complete the net. From the sketch in figure 6 it is observed that the intersections which must be handled are composed of members of the same family type of lines and must therefore be handled as such. Development of appropriate equations for the solution of flow conditions at these intersections is presented in appendix C.

Initially, in setting up the program for machine calculations, only two intersections were considered possible in between any two consecutive B lines. It is clear, however, that the spacing of these two consecutive characteristic lines determines to some extent the number of intersections that might occur. When more than two intersections occurred the reflected rays, which would produce the additional intersections, were skipped and the calculations proceeded as though these rays were nonexistent. Omitting these points amounted to increasing the size of the characteristic net at this particular location with a subsequent small decrease in accuracy. Some of these dropped points are shown in figure 6 as reflected rays that are terminated before intersecting the internal shock. The FORTRAN program as presented in appendix C has been revised, however, to permit any number of intersections to occur between two consecutive B lines.

Jet boundary coordinates for $M_j = 1$ as obtained from the revised calculations are compared in figure 7 with results obtained by using the foldback method of reference 18. Coordinates are presented in a nondimensional form, x/r_j and r/r_j , for pressure ratios p_j/p_∞ of 20 and 45,000. Agreement between the two methods is good at $p_j/p_\infty = 20$, but a decided deviation between the two curves occurs at large values of r/r_j for $p_j/p_\infty = 45,000$.

. Theoretical jet boundaries.- Results of the calculations of jet plume boundaries are shown in figures 8(a) to 8(g) for the following nozzles: $M_j = 1.0$, $\theta_N = 0^\circ$; $M_j = 5.0$, $\theta_N = 15^\circ$; $M_j = 4.79$, $\theta_N = 26.5^\circ$; and $M_j = 2.22$, $\theta_N = 0^\circ$. Two sets of curves are shown for some of the test nozzles - one set, such as in figure 8(a), at an expanded scale to show greater detail of the boundaries near the nozzle axis, and the second set showing the complete boundaries (fig. 8(b)). Symbols on some of the curves show point spacings on the boundaries but are omitted for the lower pressure ratios or where crowding of the curves would occur. Figure 8(b) indicates that the maximum radius of the jet exhaust plume will be about 450 nozzle radii for a pressure ratio of 45,000, with the location of the maximum radius occurring approximately 1,300 nozzle radii downstream. As a result of limitations of the initial program setup, boundaries for the two highest pressure ratios were terminated at a radius of approximately 350 nozzle radii. As additional boundaries were computed and

insight gained in the intricacies involved in the calculation procedure, these limitations have gradually been removed.

Similar boundaries computed for a $M_j = 5.0$ nozzle with $\theta_N = 15^\circ$ are shown in figures 8(c) and 8(d). In the calculations for this nozzle as well as all others, pressure ratios p_j/p_∞ were chosen from preselected values of initial turning angle α_N on the basis of maintaining a relatively uniform increase in α_N . The maximum angle through which the gas could expand for the $M_j = 5.0$ nozzle was only about one-half of that for the previous $M_j = 1.0$ nozzle; therefore, fewer boundaries were computed. At a pressure ratio of 8,143 the boundary reached a maximum radius of 225 nozzle radii at a distance of 1,050 radii downstream of the nozzle exit.

Boundary coordinates for a $M_j = 4.79$ nozzle with a half-angle θ_N of 26.5° are shown in figures 8(e) and 8(f) for pressure ratios ranging from about 29 up to 2,926. The maximum computed boundary at $p_j/p_\infty = 2,926$ corresponded to $r/r_j = 188$ at $x/r_j = 720$.

The two boundaries in figure 8(g) were computed for comparison with experimental results from a $M_j = 2.22$ nozzle having parallel exit flow at the two specific pressure ratios shown. Also given are the internal shock coordinates as obtained from the computer program. These shocks appear to originate at some distance downstream of the nozzle exit; however, if an infinitely small point spacing is selected, the shock would approach the nozzle exit.

Maximum jet boundary coordinates.- Rapid determination of the size of the exhaust jet at the maximum diameter of the exhaust plume may be obtained from figures 9(a) to 9(c) for three of the nozzles for which boundaries are presented. The maximum boundary coordinates, $(x/r_j)_{\max}$ and $(r/r_j)_{\max}$, are shown as a function of pressure ratio on logarithmic coordinates. From this figure the maximum size of the jet boundary may be obtained for any intermediate pressure ratio over the range of computed values. The nearly linear variation on log-log paper of the maximum boundary size with pressure ratio permits extrapolation to much higher pressure ratios with an expectancy of good accuracy.

Boundary contours from cross plots.- Construction of additional jet boundary contours at any intermediate pressure ratio, other than those specifically computed, may be obtained from the plots of figures 10(a) to 10(c) for nozzles with exit Mach numbers and half-angles as follows: $M_j = 1.0$, $\theta_N = 0^\circ$; $M_j = 5.0$, $\theta_N = 15^\circ$; and $M_j = 4.79$, $\theta_N = 26.5^\circ$. These plots were obtained by cross plotting figures 8(a) to 8(g) at constant values of x/r_j . The pressure ratios corresponding to the computed boundaries are indicated by the ticks at the bottom of each figure. It is noted that all curves of constant x/r_j fair asymptotically into a single curve which has been shown in figure 9 as the variation of $(r/r_j)_{\max}$ with pressure ratio.

The only calculated boundaries in which the jet expanded in excess of 90° were obtained for the $M_j = 1.0$ nozzles, and cross plots for this condition are shown in figure 10(a). The initial turning angle first reached 90° at a pressure ratio of 1,852, and this is indicated by the intersection of the line for $x/r_j = 0$ with the pressure-ratio axis. At higher pressure ratios double values of the boundary coordinate r/r_j exist for all negative values of x/r_j . The locus of maximum absolute negative values of x/r_j (in terms of r/r_j and pressure ratio), as defined by a line passing through the minimum pressure-ratio point for each different negative value of x/r_j , is shown to be an essentially linear variation on log-log paper. At pressure ratios p_j/p_∞ on the order of 10^7 , values of x/r_j in excess of -15 nozzle radii exist at values of r/r_j of about 150 nozzle radii.

Experimental Results

Comparisons of experimental and theoretical results.- One of the primary objectives of this investigation, in addition to computing the jet boundaries, was to provide experimental confirmation of the calculation procedure. Experimental results therefore consist of selected schlieren photographs of the free-jet flow field obtained at constant flow conditions and also individual enlargements from high-speed schlieren motion pictures in which flow conditions were continually varying. Photographs of the jet plume are shown in figures 11, 12, and 13 for the $M_j = 1.0$, $M_j = 2.22$, and nominal $M_j = 5.0$ nozzles, respectively. The computed jet boundaries, indicated by dots on the photographs, were obtained from the cross plots of figure 10 at the jet pressure ratios corresponding to those of the photographs. The series of photographs for the $M_j = 1.0$ nozzle in figures 11(a) to 11(h) and the $M_j = 2.22$ nozzle shown in figures 12(a) and 12(b) was taken in a test facility in which operating conditions could be held constant; consequently, the schlieren sensitivity could be adjusted for best results. Conversely, results obtained from the high-speed motion pictures required a presetting of the schlieren sensitivity, which did not always prove to be the correct setting. As a point of reference the grid wires shown in figures 11(a) to 11(h) and figures 12(a) and 12(b) were spaced for 3-inch squares; for the small-scale models, figures 11(i) to 11(p) and figure 13, a 6-inch spacing of the grid wires was used.

Comparisons of computed boundaries with experimental results for the $M_j = 1.0$ nozzle in the pressure-ratio range of $p_j/p_\infty = 11.5$ to $p_j/p_\infty = 194.2$ (figs. 11(a) to 11(h)) show that excellent agreement of the boundaries is achieved. In each of these photographs the last point on the theoretical curve corresponds to the location of the maximum diameter of the jet plume as obtained in the calculations. Downstream of the maximum plume diameter the main flow field appears to remain essentially constant in size; however, there is a considerable increase in the amount of turbulence along the edge of the jet.

For all pressure ratios for which photographs of the flow field are shown, the pressure ratios are sufficiently high that the familiar shock diamonds, or periodic chain-like jet structures, have been reduced to a single lobe with the accompanying normal shock. Downstream of the normal shock the jet plume appears to consist primarily of turbulent subsonic flow. That the flow is subsonic is evident by the lack of any additional shock structure or lobes typical of those generally associated with free jets at pressure ratios near the nozzle design value. The schlieren sensitivity and viewing distance downstream of the initial normal shock are believed to be sufficient for detection of other lobes or shock structure if they were present in the flow.

Photographic enlargements of individual frames from the motion-picture film, showing the free-jet discharge from the small-scale model, are shown in figures 11(i) to 11(p) for the $M_j = 1.0$ nozzle at pressure ratios ranging from $p_j/p_\infty = 9,190$ to $p_j/p_\infty = 102,180$. Again, good agreement exists between the computed and experimental jet boundaries. The distance over which the clearly defined boundary exists appears to be a function of pressure ratio; the higher the pressure ratio the greater the length of boundary definition. As shown in figure 11(p) the boundary definition extends out to the approximate location of the second grid wire, 12 inches or about 96 nozzle-exit diameters, where it begins to form a general fan shape and becomes less clearly defined with increasing distance from the nozzle. At the outer edge of the photograph the boundary is completely obscured. The fan region appears very unstable in the motion pictures with rather violent in-and-out fluctuations which increase with distance away from the nozzle. These violent fluctuations in the neighborhood of the jet boundary were also observed and reported in reference 10, described as a turbulent mixing region, in which motion pictures were made of the exhaust region from the rocket motor of a second-stage flight vehicle in the presence of an external flow field. Motion pictures of the current tests show considerable turbulence with the computed boundary defining the outermost edge of the fan region.

An additional point of interest concerns the location of the normal shock with respect to the location of the maximum jet plume diameter. At low pressure ratios the normal shock is located downstream of the maximum jet plume diameter, whereas at the higher pressure ratios the shock location occurs ahead of the maximum diameter. A comparison of figures 11(a) and 11(i) indicates these phenomena.

Schlieren photographs of free-jet flow from a $M_j = 2.22$ contoured nozzle are shown in figures 12(a) and 12(b) in which both the computed boundary and internal shock are indicated. A limiting minimum value of ambient pressure restricted the maximum pressure ratio to a relatively low value of $p_j/p_\infty = 37.7$. Good agreement is indicated for both the jet boundary and the location of the internal shock.

Theoretical and experimental jet plume boundaries for the nominal $M_j = 5.0$ nozzle are shown in figures 13(a) to 13(e). It should be emphasized here that the theoretical calculations were based on the actual exit Mach number of 4.79 and nozzle half-angle of 26.5° , which are both considerably different from the

inviscid design value. The good agreement between theoretical and experimental boundaries indicates that the method of obtaining the nozzle half-angle in the presence of a boundary layer of unknown thickness is an acceptable procedure for small-scale models.

Further details of the flow phenomena associated with exhaust jets, which were not readily apparent in the individual motion-picture frames (figs. 13(a) to 13(e)), were determined from the schlieren motion pictures. Boundary definition at $p_j/p_\infty = 85$, figure 13(a), extended about halfway between the end of the nozzle and the upper edge of the photograph ($x/r_j = 29$). Downstream of this approximate location severe turbulence exists on, and obliterates, the jet boundary. As pressure ratio increases the boundary definition extends further downstream of the nozzle exit and appears to delay the onset of the turbulence. The edge of the jet is again subject to violent in-and-out fluctuations, somewhat less severe than those described for the $M_j = 1.0$ jet. Vortices appear to form on the jet boundary at the approximate location of the fadeout in boundary definition with substantial growth occurring with increasing distance downstream of the nozzle exit. The theoretical boundary defines very closely the outer edge of both the visible boundary near the nozzle exit and also the turbulent region that exists further downstream.

Comparisons of characteristic and empirical solutions.- In view of the obvious complications and time involved in the characteristic calculations, an empirical method of computing jet boundaries proves to be extremely beneficial. Such a method was developed in reference 19 and permits both rapid and satisfactory calculations of the initial portion of jet boundaries for a wide range of nozzle Mach numbers, specific-heat ratios, and pressure ratios. A comparison of boundaries computed by the method of characteristics and by the empirical method of reference 19 is shown in figures 14(a) and 14(b) for the $M_j = 1.0$ and $M_j = 5.0$ nozzles, respectively, to determine to what extent the empirical solutions are in agreement.

Results are presented in figure 14(a) for the $M_j = 1.0$ nozzle at pressure ratios ranging from $p_j/p_\infty = 45$ to $p_j/p_\infty = 45,000$. In general, the empirical boundaries fall slightly below the characteristic curves near the nozzle exit but finally cross over and continually deviate in such a manner as to produce boundaries larger than those indicated for the characteristic solution. Satisfactory comparisons of the boundaries are obtained for values of r/r_j up to about 5 at the lowest pressure ratio and up to about 10 for $p_j/p_\infty = 45,000$. Thus, when interest in the jet boundary is restricted to a region relatively close to the nozzle exit, the empirical solution provides a rapid and relatively accurate method for approximating the boundary. Similar results are shown in figure 14(b) for the $M_j = 5.0$ nozzle at pressure ratios from $p_j/p_\infty = 20$ to $p_j/p_\infty = 2,000$. Correlation of the two methods of calculations is again good with the range of agreement extending over a somewhat greater range than the Mach 1.0 results.

Location and diameter of Riemann wave (normal shock).- The effects of jet pressure ratio on the nondimensional distance along the jet axis from the plane of the nozzle exit to the location of the Riemann wave (l/d_j) are shown in figure 15(a) for the $M_j = 1.0$ nozzle. Also shown for comparison are the results obtained from figure 8(a) of reference 18. With both the nondimensional distance l/d_j and pressure ratio p_j/p_∞ plotted on log coordinates the result is a near linear variation over the range of pressure ratios for which the shock position could be determined.

The schlieren photographs of figures 11(a) to 11(p) show that the thickness of the shock at times may be as much as several nozzle-exit diameters. However, this is probably a three-dimensional effect which produces an illusion of considerable shock thickness. The values shown in figure 15 are the average distances. It is of interest to note also that the motion pictures show a high-frequency pulsation of the Riemann wave along the nozzle axial center line with an amplitude roughly equivalent to the apparent shock thickness shown in the photographs. Instability at the outer edges of the Riemann wave diameter is even more pronounced with fluctuations in location occurring first on one side of the center line and then on the other. These fluctuations appear to be dependent on local pressure and become increasingly severe at the extremely low pressures and high Mach numbers within the exhaust plume.

Figure 15(b) presents results of the normal-shock location for a contoured nozzle with an exit Mach number of 2.22. Figure 15(c) presents previously unpublished data from a contoured $M_j = 2.63$ nozzle. Again on log-log paper, linear variations of the shock location with pressure ratio are shown, which indicate that extrapolations may be made to higher pressure ratios with a probability of fair accuracy. However, in these figures it is shown that ambient pressure has a definite effect on the shock location. At a given pressure ratio the lower the ambient pressure the less the distance from the nozzle exit to the location of the normal shock. Although the effect is small at the lower pressure ratios, in terms of nozzle diameters, slightly larger effects are indicated for the higher pressure ratios.

The effect of jet pressure ratio upon the nondimensional diameter of the normal shock (S/d_j) is shown in figure 16 for the sonic nozzle. The current data span the limited data included from figure 9(a) of reference 18 and extend the pressure-ratio range for which the shock diameter could be determined to p_j/p_∞ of about 30,000. In general, agreement of both sets of data is very good. Some uncertainty exists in measuring the shock diameter at the highest pressure ratios (see figs. 11(i) to 11(p)), resulting in the scatter of data points at the high-pressure-ratio end of the curve. The maximum scatter is on the order of approximately 15 nozzle diameters. The extension of data provided in the current tests indicates, for pressure ratios in excess of p_j/p_∞ of 10, that the variation in shock diameter is essentially a linear variation with pressure ratio on log-log paper. At a pressure ratio of 30,000 the shock has a diameter of approximately 100 nozzle diameters, which is equivalent to roughly 30 percent of the maximum jet plume diameter (see fig. 9(a) for jet plume size).

SUMMARY OF RESULTS

An experimental and theoretical investigation of highly underexpanded free-jet boundaries has been conducted. The experimental program, initiated to verify the theoretical calculations of the boundaries and internal-shock positions, was conducted with unheated air and consisted of obtaining schlieren photographs of exhaust jet boundaries from nozzles having design exit Mach numbers of 1.0, 2.22, and 5.

Extensive modifications to an existing characteristics-method computer program have been made which permit extension of the calculations of free-jet boundaries to high pressure ratios and large distances downstream of the nozzle exit. The calculations procedure has been incorporated into a computer program which facilitates rapid calculations of jet exhaust characteristics. A FORTRAN program for use on an IBM 7094 electronic data processing system is presented.

Based on the calculations using the method of characteristics and the experimental tests, the following results were obtained:

1. Theoretical jet boundaries have been calculated and contour plots developed which permit construction of jet boundaries for the following nozzles: Mach 1.0, Mach 5.0 (wall angle 15°), and Mach 4.79 (wall angle 26.5°). Partial or complete jet boundaries may be constructed at pressure ratios up to 10^7 , 10^6 , and 0.5×10^4 for the three nozzles, respectively.

2. For a given nozzle configuration it was found that the maximum jet boundary size varied almost linearly on logarithmic coordinates with the ratio of nozzle-exit pressure to ambient pressure. For the Mach 1.0, 5.0, and 4.79 nozzles the calculated maximum radius of the jet boundary was 450, 225, and 188 nozzle radii at a distance of 1,300, 1,050, and 720 nozzle radii downstream of the nozzle exit, respectively, at corresponding pressure ratios of 45,000, 8,143, and 2,926. Experimental results indicated an almost constant jet plume size downstream of the maximum plume diameter.

3. Comparisons of theoretical and experimental jet boundaries show good agreement over the complete range of pressure ratios investigated. Limited comparisons of the theoretical and experimental internal-shock location also showed very good correlation.

4. Experimental results at low pressure ratios show the Riemann wave (normal shock) to be positioned downstream of the maximum plume diameter, whereas at the higher pressure ratios the shock location occurs upstream of the maximum diameter. At the higher pressure ratios the familiar shock diamond structure reduces to a single lobe, or normal shock. The location of the shock downstream of the nozzle exit and also the maximum diameter of the shock have a near linear relationship on logarithmic coordinates with the ratio of nozzle-exit pressure to ambient pressure.

Langley Research Center,
National Aeronautics and Space Administration,
Langley Station, Hampton, Va., February 26, 1964.

APPENDIX A

DETERMINATION OF LEADING CHARACTERISTIC LINE

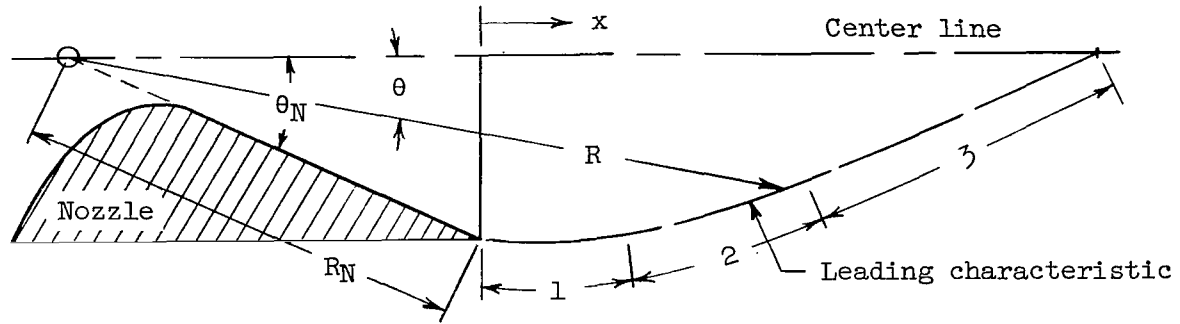
Input Data

Calculations of a characteristic network including the input quantities when computed by hand calculators are both lengthy and time consuming, particularly when large numbers of input points along the leading characteristic line are desired. A program has therefore been set up to machine compute and deliver the input data in punchcard form, which may be placed directly in the characteristic network program. Through additional processes the data may be indicated numerically on the cards or tabulated for visual inspection. The following paragraphs describe the important features of the leading characteristic line and give an example of the required input information.

Regardless of the type of nozzle, either contoured for parallel flow at the exit or conical with radial-exit flow, several initial conditions depending only on nozzle design are immediately known, namely: M_j , θ_N , μ , v_N , and γ . With these nozzle characteristics it is possible to determine the leading characteristic, or Mach, line which separates the nozzle flow from the external influence of ambient pressure. The only limitation is that the nozzle must be operating in an underexpanded condition such that the pressure ratio p_j/p_∞ is greater than 1.0.

Conical nozzle.- The inherent radial flow properties of a conical nozzle result in a curved leading characteristic line; therefore, all flow conditions along this line are continually varying. It is therefore necessary to determine for each x and y location along this line the flow properties required in the calculations. It should be pointed out that all phases of the characteristic program calculations are performed below the nozzle center line, and that all procedures are set up on this basis.

Point spacings along the leading characteristic are determined, for convenience, in terms of Mach number increments. At low pressure ratios large point spacings may be used whereas for higher pressure ratios a much closer spacing is required immediately downstream of the nozzle exit. No criterion for explicit point spacing, or Mach number increments, exists and, therefore, individual judgment must be used depending on the length of the leading characteristic and the Mach number change from the nozzle exit to the intersection of the leading characteristic with the nozzle center line. Several groups of Mach number increments are usually calculated; for example, the leading characteristic shown in sketch (A1) has been divided into three different groups of Mach number increments - small increments in group 1 and larger increments in groups 2 and 3. If the characteristic program terminates before reaching the maximum jet boundary, it may be necessary to use smaller Mach number increments in group 1.



Sketch (A1)

As an aid in selecting the Mach number increments along the leading characteristic line, the Mach number at the intersection of the leading characteristic with the nozzle axial center line is determined by the method of reference 18. The Prandtl-Meyer expansion angle at the center line is:

$$\nu_{\Phi} = \nu_N + 2\theta_N \quad (\text{A1})$$

The change in flow direction between the nozzle exit and end of the leading characteristic reduces to θ_N , since the flow direction is zero at the center line. The Mach number corresponding to the Prandtl-Meyer expansion angle ν_1 may be obtained from gas flow tables (refs. 29 and 30, for example) at the appropriate value of γ . Other parameters needed, in addition to the selected Mach number increments, are: M_j , θ_N , and γ . From the input data the computer program determines the flow properties at various points along the leading characteristic line until the nozzle axial center line is reached. Input data downstream of the end of the leading characteristic are not required since the characteristic network program (appendix C) contains provisions for computing these flow properties.

The end point of the leading characteristic (on the nozzle center line) may be obtained from the following expressions given in reference 18 for calculating the shape of the leading characteristic. (See sketch (A1).)

$$R = C \left[1 + \frac{2}{\gamma - 1} \left(\frac{1}{M^2} \right) \right]^{\frac{\gamma+1}{4(\gamma-1)}} \frac{1}{M^{\gamma-1}} \quad (\text{A2})$$

$$x = R \cos \theta - R_N \cos \theta_N \quad (\text{A3})$$

From the initial flow properties just at the nozzle exit, M_j , μ , γ , and θ_N , the constant C may be determined. By using this constant and the Mach number

obtained from expression (A1) and gas flow tables, with its corresponding value of μ , the expressions (A2) and (A3) yield the desired x location.

Other basic equations used in this program, in addition to (A2) and (A3), are as follows:

$$\mu = \tan^{-1} \frac{1}{\sqrt{M^2 - 1}} \quad (A4)$$

$$\nu = \sqrt{\frac{\gamma + 1}{\gamma - 1}} \tan^{-1} \sqrt{\frac{\gamma - 1}{\gamma + 1} (M^2 - 1)} - \tan^{-1} \sqrt{M^2 - 1} \quad (A5)$$

$$y = -R |\sin \theta| \quad (A6)$$

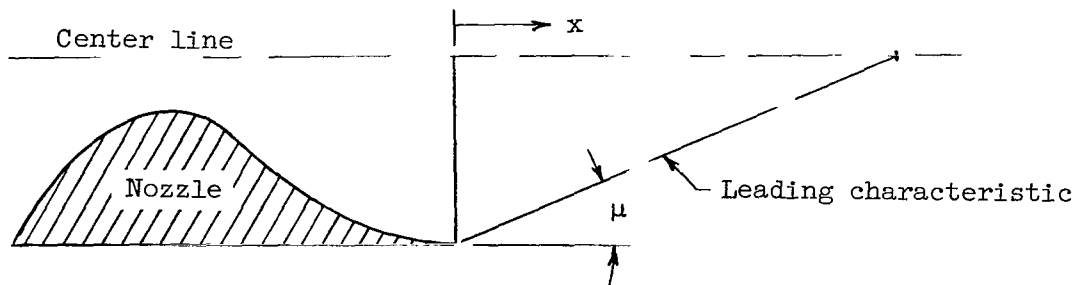
Example of input data for a conical nozzle.- For a nozzle with the known exit conditions of $M_j = 5.0$, $\theta_N = 15^\circ$, and $\gamma = 1.4$, the additional required engineering input is obtained in the following manner. From the known exit conditions and equation (A1) the values of ν_ϕ and M at the point of intersection of the leading characteristic with the axial center line are found to be $\nu_\phi = 106.92^\circ$ and $M = 12.02$. The Mach number increments are arbitrarily chosen as follows:

ΔM	M_{limit}
0.05	7.0
.10	10.0
.15	12.1

The final Mach number of 12.1 was chosen slightly larger than the computed value of 12.02 in order to allow the program to determine a more accurate final Mach number. Since three different Mach number increments were selected, there will be three input cards - each containing the known exit conditions and one of the Mach number increments with its corresponding final Mach number. The computer program uses the data contained on the three input cards and calculates the coordinates and other flow conditions required for the characteristic network calculations.

Contoured nozzle.- In contrast to the conical nozzles, the leading characteristic associated with contoured nozzles designed for parallel exit flow is a straight line as shown in sketch (A2). As a result, all flow conditions

along this line are constant. The inclination of this line with respect to the nozzle axial center line is equivalent to the Mach angle μ corresponding to the nozzle-exit Mach number. Closely spaced points near the nozzle exit,



Sketch (A2)

similar to the point spacing discussed for the conical nozzle, are again recommended.

Sonic nozzle.- The leading-characteristic input conditions for a sonic nozzle are similar to those for the contoured nozzle. However, if M_j is exactly equal to 1.0, the slope of the leading characteristic is infinite and the characteristic program will not function under these conditions. For this reason, the initial conditions of $M_j = 1.0038$ and $\mu = 85^\circ$ were selected for the current program. Reference 18 showed that a similar selection resulted in negligible effects upon the free-jet boundary shape.

Computer Program

A computer program has been developed for calculating the leading characteristic line of a conical nozzle. This program, written in FORTRAN language (see ref. 31), may be used on the IBM 7094 electronic data processing system.

The input requirements for this program consist of: (1) the nozzle-exit Mach number M_j , (2) the flow direction at the nozzle lip θ_N , (3) the ratio of specific heats γ , (4) the Mach number increments ΔM , and (5) the limiting Mach number for each Mach number increment for which the flow conditions are to be determined. From these input data a series of points defining the leading characteristic line are calculated, and cards are punched to be used as input for a computer program that calculates the characteristic network of a free-jet boundary (see appendix C).

This particular program is capable of computing the leading characteristic for several different Mach number increments during one machine run. The program output for each computed point is x , y , θ , and M and is as follows:

```

C P-5432 LEADING CHARACTERISTIC LINE PROGRAM
C PUNCHES INPUT CARDS FOR FREE JET INVESTIGATION (P-5430)
C
C INPUT FOR A CASE
C
C THETA, MACH NO., LIMITING MACH NO., DELTA MACH, GAMMA
C
C DEG=57.29578
C WRITE (6,50)
50 FORMAT(1H1/28HLEADING CHARACTERISTIC LINE,4X6HP-5432)
C
C INPUT A CARD
C
C 7 READ (5,15)FTH,FMACH,EMACH,DEL,GAMMA
15 FORMAT (5F7.0)
WRITE (6,55)GAMMA
55 FORMAT (///7H0GAMMA=1F7.3///
15X4HMACH16X1HX19X1HY19X11HTHETA, DEG,9X8HMU, DEG,///)
DU=0.0
XC=0.0
FTH=FTH/DEG
C1=GAMMA-1.0
C2=GAMMA+1.0
C3=FMACH**2
C4=C3-1.0
C5=SQRT(C4)
C EQUATION A4
FMUC=ATAN(1.0/C5)
A=2.0/C1
B=C2/(4.0*C1)
D=1.0/C1
SA=SQRT(C2/C1)
SA1=1.0/SA
SB=SA*ATAN(SA1*C5)
C EQUATION A5
U=SB-ATAN(C5)
RN=1.0/SIN(FTH)
C=RN/(((1.0+A*(1.0/C3))**B)*(FMACH**D))
R=RN
GO TO 8
2 IF (THETC)6,7,6
6 FMACH=FMACH+DEL
C
C EXIT IF MACH GREATER THAN LIMITING VALUE
C
C IF (EMACH-FMACH) 7,75,75
75 C3=FMACH**2
C4=C3-1.0
C5=SQRT(C4)
FMUC=ATAN(1.0/C5)
SB=SA*(ATAN(SA1*C5))
U2=SB-ATAN(C5)
DU=U2-U
C EQUATION A2
R=C*((1.0+A*(1.0/C3))**B)*(FMACH**D)
8 DTH=-.5*DU
TH2=FTH+DTH
THETC=-TH2*DEG
IF (THETC)4,7,4
4 X1=XC
C EQUATION A1
U2L=2.0*FTH+U
C EQUATION A3
XC=R*COS(TH2)-(RN*COS(FTH))
C EQUATION A6
YC=-R*SIN(TH2)
IF (THETC)11,11,12
11 U21=U2
FMUC=FMUC*DEG
C
C PUNCH AND PRINT
C
C PUNCH 17,XC,YC,THETC,FMUC
17 FORMAT (4E16.8)
WRITE (6,60)FMACH,XC,YC,THETC,FMUC
60 FORMAT (5E20.8)
GO TO 2
12 UR=(U2L-U21)/(U2-U21)
FMACH=UR*DEL+(FMACH-DEL)
XC=UR*(XC-X1)+X1
FMUC=ATAN(1.0/SQRT(FMACH**2-1.0))
THETC=0.0
YC=0.0
GO TO 11
END

```



APPENDIX B

DETERMINATION OF CORNER EXPANSION FAN

Input Data

An additional input requirement for computing a characteristic network is the corner expansion fan just at the nozzle exit. A computer program has been developed for a high-speed digital computer to provide these data in suitable form to be used directly in the characteristic program. Primary consideration was directed toward expediency by limiting the amount of engineering input required.

Two-dimensional flow can be assumed to exist at the nozzle lip. A further assumption of instantaneous expansion permits evaluation of all flow conditions at the coordinates $x/r_j = 0$ and $y/r_j = -1.0$. The initial consideration consists of determining the change in Mach angle μ between that for the design exit Mach number and the final value as fixed by the particular pressure ratio $p_\infty/p_{t,j}$ for which a characteristic net is to be computed. This change in Mach angle μ is then divided into a number of increments, which determines the value of $\Delta\mu$ to be used in the input data.

The following table illustrates the general procedure for supplying the input data:

	Initial	Final
M	4.9987008	7.2756624
θ , deg	15.000000	30.462664
μ , deg	11.539999	7.8999996
ν , deg	76.908041	92.370705
γ , deg	1.3999999	

For the known initial conditions at the nozzle exit it is desired to find the final conditions for $p_j/p_\infty = 10.095$ in order to compute the input data. From the nozzle-exit pressure ratio $p_j/p_{t,j}$ at $\gamma = 1.4$ and the static-pressure ratio p_j/p_∞ the boundary Mach number corresponding to the pressure ratio $p_\infty/p_{t,j}$ is found to be 7.2756624. The corresponding values of μ and ν at the boundary Mach number are obtained from flow tables (ref. 28, for example). The final flow direction θ_{final} is synonymous with the initial turning angle α_N and is found from the expression

$$\theta_{\text{final}} = \alpha_N = \nu_1 - \nu_N + \theta_N \quad (B1)$$

The value of $\Delta\mu$, although selected somewhat arbitrarily, may then be determined by the number of rays desired for the variation in θ . Thus, if θ changes by approximately 15.5° and one expansion ray is desired for each 1° change in θ , then the change in Mach angle μ between the initial and final values should be divided into increments of 0.23° (i.e., $\Delta\mu = 0.23^\circ$). The number of significant figures for which $\Delta\mu$ is given is unimportant since the computer program assumes this is an absolute number and gives results for other parameters out to eight significant figures. However, the initial and final values of μ should be determined as accurately as possible. The required input to the computer program utilizing the change in Mach angle μ between the initial and final conditions is listed as follows:

γ	1.4
x/r_j	0.0
y/r_j	-1.0
θ_N , deg	15.0
μ_{initial} , deg	11.539999
$\Delta\mu$, deg	0.23
μ_{final} , deg	7.8999996

Computer Program

A computer program has been developed for calculating the corner expansion rays to be used as input data in the characteristic network calculation procedure and is applicable to either conical or contoured nozzles. Input requirements for this program consist of initial flow conditions at the nozzle exit, μ , θ_N , and γ , a value for Mach angle increments $\Delta\mu$, and the value of μ corresponding to the boundary conditions. The Mach angle increment is determined from the fineness desired in the characteristic network. The program computes the various flow conditions corresponding to the designated Mach angles and cards are punched, which may be placed directly in the characteristic program (appendix C). This program is written in FORTRAN language for the IBM 7094 electronic data processing system and contains equations (or versions of) (A4), (A5), and (B1). It is as follows:

```

C P-5433 CORNER EXPANSION RAY PROGRAM
C PUNCHES INPUT CARDS FOR FREE JET INVESTIGATION (P-5430)
C
C INPUT FOR A CASE
C
C 1ST DATA CARD
C FIRST MU, FIRST THETA, GAMMA
C DATA CARDS 2,3,4,.....
C MU VALUE, DELTA MU, STOPPING MU VALUE
C
C CON=.17453292E-01
C XA=0.0
C YA=-1.0
C WRITE (6,2)
2 FORMAT(1H1/21H0CORNER EXPANSION RAY4X6HP-5433)
C
C READ 1ST DATA CARD
C
C READ (5,4)FMUA,THETA,GAMMA
4 FORMAT(1F9.0,2F7.0)
C THETA=-THETA
C WRITE (6,6)GAMMA
6 FORMAT(///7H0GAMMA=F7.3///
15X4HMACH16X1HX19X1HY19X11HTHETA, DEG.9X
28HMU, DEG.12X7HV, DEG.///)
C TH2=THETA*CON
C FMU2=FMUA*CON
C H=(GAMMA-1.0)/(GAMMA+1.0)
C H1=SQRT((GAMMA+1.0)/(GAMMA-1.0))
C
C COMPUTE STARTING VALUES
C EQUATION A4
C
C FMACH=1.0/SIN(FMU2)
C ABCD=FMACH**2-1.0
C VPAR=H1*ATAN(SQRT(H*ABCD))
C EQUATION A5
C V2=VPAR-ATAN(SQRT(ABCD))
C VPR=V2/CON
C
C PUNCH AND PRINT
C
C PUNCH 10,XA,YA,THETA,FMUA
10 FORMAT(4E16.8)
C WRITE (6,15)FMACH,XA,YA,THETA,FMUA,VPR
15 FORMAT(6E20.8)
C
C SAVE THETA AND V
C
C V1=V2
C TH1=TH2
C
C INPUT DATA CARD
C
C 20 READ (5,4)FMUA,DEL,ENDMU
30 FMU2=FMUA*CON
C FMACH=1.0/SIN(FMU2)
C ABCD=FMACH**2-1.0
C VPAR=H1*ATAN(SQRT(H*ABCD))
C V2=VPAR-ATAN(SQRT(ABCD))
C EQUATION B1
C TH2=V1-V2+TH1
C THETA=TH2/CON
C VPR=V2/CON
C
C PUNCH AND PRINT
C
C PUNCH 10,XA,YA,THETA,FMUA
C WRITE (6,15)FMACH,XA,YA,THETA,FMUA,VPR
C
C SAVE THETA AND V
C
C V1=V2
C TH1=TH2
C
C DECREMENT MU
C
C FMUA=FMUA-DEL
C
C CHECK STOPPING MU
C
C IF(ENDMU-FMUA)30,30,20
C END

```

APPENDIX C

CHARACTERISTIC METHOD FOR CALCULATING FREE-JET BOUNDARIES

General Description of Characteristic Network

The calculation of free-jet boundaries by the method of characteristics makes use of three-dimensional irrotational equations of flow. The characteristic net describing the flow field, a lattice point-type structure requiring no iteration, is machine computed in a point-to-point calculation procedure. Computations begin with a set of given conditions on the leading characteristic plus the conditions for a series of two-dimensional expansion rays originating at the nozzle lip. The existing program, permitting calculations to high pressure ratios and large distances downstream of the nozzle exit, is the result of extensive modifications and refinement of the program used in reference 18.

The general assumptions concerning the characteristic network are:

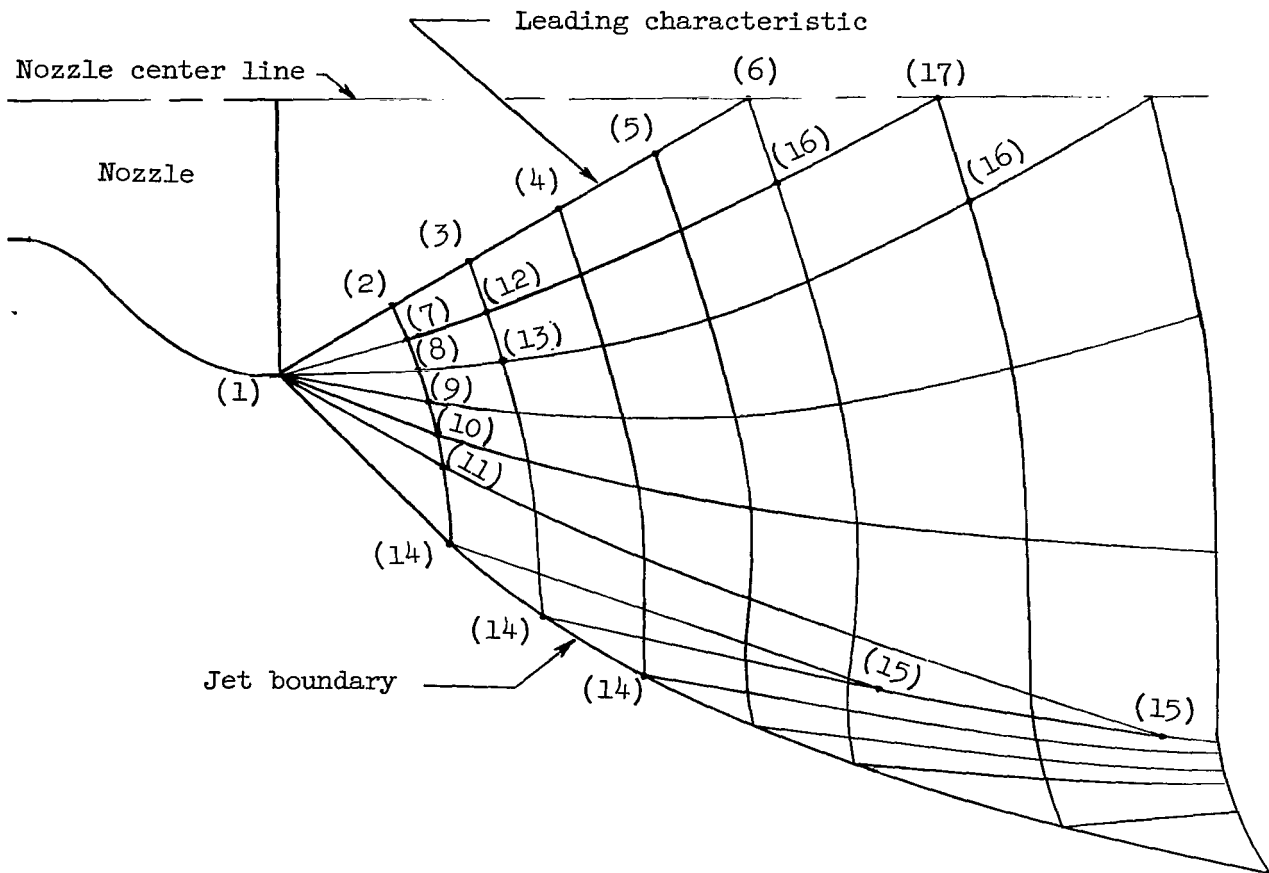
- (1) The characteristic solution assumes a constant ambient pressure and hence constant Mach number boundary.
- (2) The ratio of specific heats γ remains constant in all calculations.
- (3) Isentropic flow is assumed to exist throughout the flow field.

Various sections of a typical characteristic net require different equations to determine the local flow properties. These sections are listed as follows in order of their probable occurrence during the calculation procedure:

- (1) Solutions for general points.
- (2) Solutions for points on the jet boundary.
- (3) Solution for the intersection of characteristic lines of the same family indicating the presence of an internal shock.
- (4) Solution for a point adjacent to the nozzle axial center line.
- (5) Solution for points on the center line.

Each of these topics is discussed in the following sections.

An expanded view of a typical characteristic net is shown in sketch (C1).



Sketch (C1)

The types of points in sketch (C1) are identified as follows:

- (1) nozzle lip, source for a series of given two-dimensional expansion rays
- (2),(3),(4),(5) input data points on leading characteristic line
- (6) last leading characteristic input data point (also first point on center line)
- (7),(8),(9),(10),(11),(12),(13) general points
- (14) boundary points
- (15) same family points (internal shock)

- (16) points adjacent to center line
- (17) center-line point

Symbols

M	Mach number
T	temperature, °R
V	velocity, ft/sec
V_L	limiting velocity, ft/sec
W	ratio of local velocity to limiting velocity
x,y	Cartesian coordinates, referred to nozzle radius
γ	ratio of specific heats
θ	flow angle between velocity vector and X-axis (positive in first quadrant and negative in fourth quadrant), radians
μ	Mach angle, $\sin^{-1} \frac{1}{M}$, radians
ρ	density, slugs/cu ft

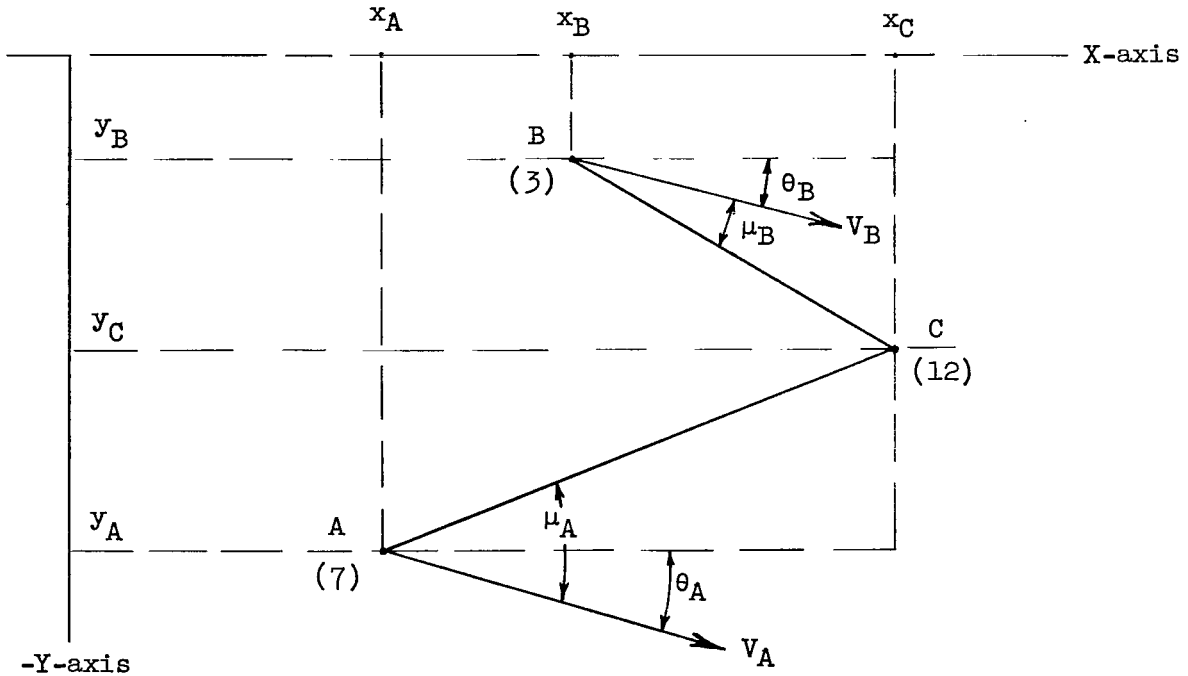
Subscripts:

A	points of first family
B	points of second family
C	points calculated from A and B
t	stagnation conditions

General-Point Solution

In supersonic flow if the flow conditions at two points near each other are known, the flow conditions at some point C, which is the intersection of two characteristic lines of different families starting from the two known points, can be determined. In sketch (C1) calculations begin with the given conditions at points (1) and (2) and proceed along the line containing points (2) and (14) with use of the general-point solutions to find points (7) to (11) and the boundary-point solution to find point (14). The procedure is then repeated beginning with the given point (3) and the conditions as computed for point (7) to find point (12); the points (12) and (8) are used to find (13), and so forth.

An enlargement of points (3) and (7) as used in obtaining the general solution for point (12) is shown in sketch (C2).



Sketch (C2)

With all conditions known for points A and B, the flow conditions at point C remain to be found. The upward sloping line AC, a characteristic of the first family, is defined as

$$\frac{dy}{dx} = \frac{y_C - y_A}{x_C - x_A} = \tan(\theta_A + \mu_A) \quad (C1)$$

The slope of line BC, a second-family characteristic, is defined as

$$\frac{dy}{dx} = \frac{y_C - y_B}{x_C - x_B} = \tan(\theta_B - \mu_B) \quad (C2)$$

A simultaneous solution of equations (C1) and (C2) yields

$$x_C = \frac{x_A \tan(\theta_A + \mu_A) - y_A + y_B - x_B \tan(\theta_B - \mu_B)}{\tan(\theta_A + \mu_A) - \tan(\theta_B - \mu_B)} \quad (C3)$$

Now that x_C is known, equation (C1) may be solved for the y coordinate, y_C , from

$$y_C = (x_C - x_A) \tan(\theta_A + \mu_A) + y_A \quad (C4)$$

First- and second-family equations in terms of velocity are as follows (from ref. 32, p. 264):

For the first family

$$\frac{dV_A}{V_A} - d\theta_A \tan \mu_A - l_A \frac{dx_A}{y_A} = 0 \quad (C5)$$

For the second family

$$\frac{dV_B}{V_B} + d\theta_B \tan \mu_B - m_B \frac{dx_B}{y_B} = 0 \quad (C6)$$

For definitions of l_A and m_B , see equations (C9) and (C10). The velocity terms may be reduced to the nondimensional ratio form of W by dividing through by the limiting velocity V_L .

$$W = \frac{V}{V_L}$$

Therefore, in equations (C5) and (C6)

$$d\left(\frac{V_A}{V_L}\right) = W_C - W_A$$

$$d\left(\frac{V_B}{V_L}\right) = W_C - W_B$$

and

$$d\theta_B = d\theta_A + \theta_A - \theta_B$$

Substituting these expressions into equations (C5) and (C6) and solving simultaneously results in

$$\left(\tan \mu_B + \frac{W_A}{W_B} \tan \mu_A \right) d\theta_A = 1 - \frac{W_A}{W_B} - (\theta_A - \theta_B) \tan \mu_B + m_B \frac{dx_B}{y_B} - \lambda_A \frac{dx_A}{y_A} \frac{W_A}{W_B} \quad (C7)$$

which is similar to the form in reference 32. By substituting

$$d\theta_A = (\theta_C - \theta_A)$$

$$dx_A = (x_C - x_A)$$

and

$$dx_B = (x_C - x_B)$$

equation (C7) is reduced to the following form with only one unknown:

$$\theta_C = \frac{-W_A - W_A \left[-\theta_A \tan \mu_A + \frac{\lambda_A}{y_A} (x_C - x_A) \right] + W_B + W_B \left[\theta_B \tan \mu_B + \frac{m_B}{y_B} (x_C - x_B) \right]}{(W_A \tan \mu_A + W_B \tan \mu_B)} \quad (C8)$$

where

$$\lambda_A = \frac{\sin \mu_A \sin \theta_A \tan \mu_A}{\cos(\theta_A + \mu_A)} \quad (C9)$$

and

$$m_B = \frac{\sin \mu_B \sin \theta_B \tan \mu_B}{\cos(\theta_B - \mu_B)} \quad (C10)$$

Now that θ_C is known, equation (C5) is used to obtain

$$W_C = W_A + W_A \left[\tan \mu_A (\theta_C - \theta_A) + \frac{\lambda_A}{y_A} (x_C - x_A) \right] \quad (C11)$$

The remaining parameters to be determined at point C are

$$\mu_C = \sin^{-1} \sqrt{\frac{\gamma - 1}{2} \left(\frac{1}{W_C^2} - 1 \right)} \quad (C12)$$

$$M_C = \frac{1}{\sin \mu_C} \quad (C13)$$

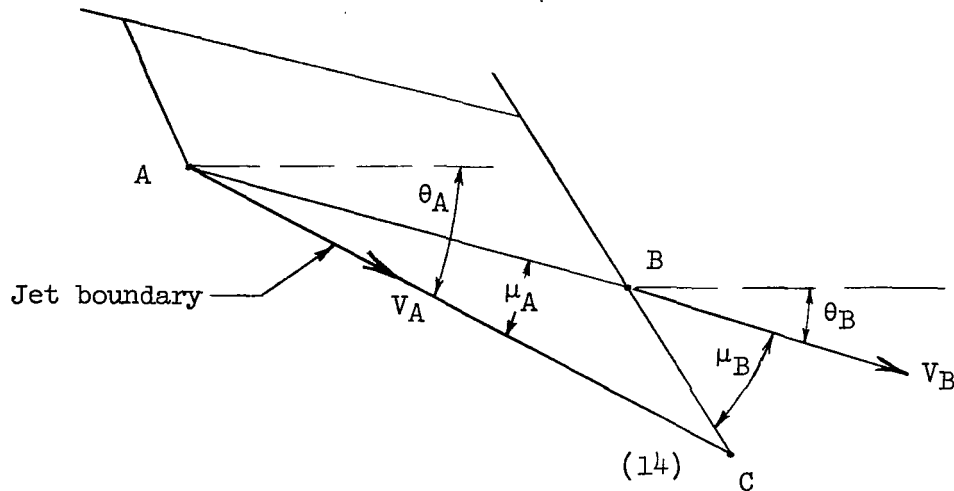
$$\frac{T}{T_t} = \frac{1}{1 + \left(\frac{\gamma - 1}{2}\right)M^2} \quad (C14)$$

and

$$\frac{\rho}{\rho_t} = \frac{1}{\left[1 + \left(\frac{\gamma - 1}{2}\right)M^2\right]^{\frac{1}{\gamma-1}}} \quad (C15)$$

Jet Boundary Point

Boundary-point calculations, although still dependent upon the basic first- and second-family relationship, require a different form of the equations for determining the conditions and location of the unknown boundary point C. As in previous calculations it is necessary to adhere strictly to the signs associated with the various angles. For these calculations (see sketch (C3)) it is noted



Sketch (C3)

that the line AC is actually a streamline, where previously the line AC has been a characteristic line. The slopes of the streamline AC (first family) and characteristic line BC (second family) are

$$\frac{dy}{dx} = \frac{y_C - y_A}{x_C - x_A} = \tan \theta_A \quad (C16)$$

$$\frac{dy}{dx} = \frac{y_C - y_B}{x_C - x_B} = \tan(\theta_B - \mu_B) \quad (C17)$$

The x location as determined from a simultaneous solution of equations (C16) and (C17) is

$$x_C = \frac{x_A \tan \theta_A - y_A + y_B - x_B \tan(\theta_B - \mu_B)}{\tan \theta_A - \tan(\theta_B - \mu_B)} \quad (C18)$$

and from equation (C16)

$$y_C = (x_C - x_A) \tan \theta_A + y_A \quad (C19)$$

Since the boundary Mach number is constant, $\mu_C = \mu_A$ and $W_C = W_A$; the flow direction at point C is obtained from the basic second-family form of equation (C6). In equation (C6)

$$d\theta_B = \theta_C - \theta_B$$

and

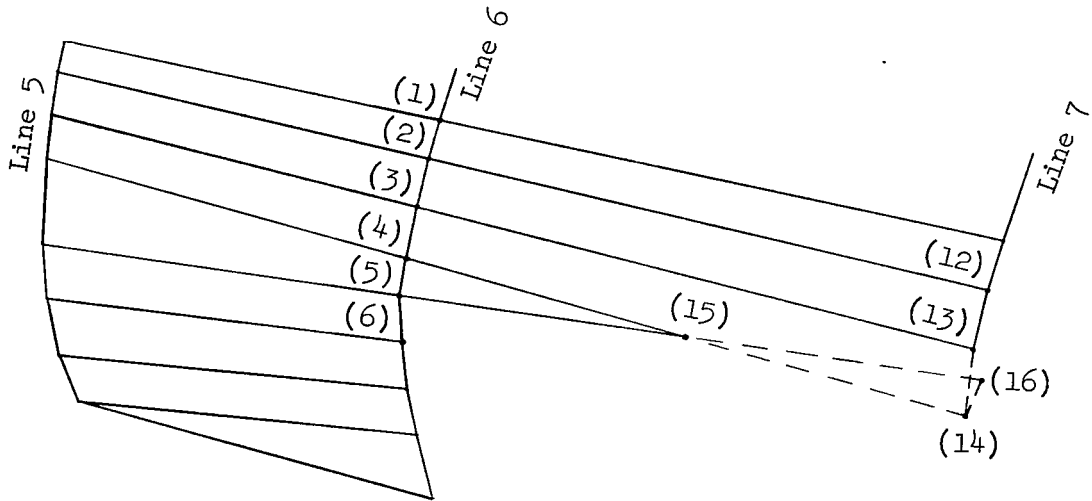
$$\theta_C = \theta_B + \frac{\left(-\frac{W_C - W_B}{W_B} + m_B \frac{x_C - x_B}{y_B} \right)}{\tan \mu_B} \quad (C20)$$

where m_B is as defined in equation (C10).

Intersection of Same Family Characteristic Lines

The presence of a finite ambient pressure requires a turning of the jet boundary in a downstream direction which in turn introduces a series of weak

compression waves. These waves, which are shown in sketch (C4) and are members of the first-family type of characteristic lines (see sketch (C1)), eventually intersect with the expansion rays originating at the nozzle exit or with each other and form the internal shock. The intersecting characteristic lines, both members of the first-family type of lines, are shown in sketch (C4). Prior to the occurrence of this intersection at point (15), calculations progressing along line 7 in sketch (C4) (arbitrarily identified lines and points) have involved members of different families. The normal procedure of using points (4) and (13) as A and B, respectively, to find (14) as C, and then using (5) and (14) as new values of A and B to find point (16), results in a foldback



Sketch (C4)

of the characteristic net (see ref. 18). Once the foldback has begun it becomes progressively more severe and eventually a point is reached where the program can no longer continue. In order to eliminate the foldback, flow conditions must be found for the point of intersection (15); once these are found, then points (15) and (13) may be used as A and B points, respectively, in the general-point equations.

An enlargement of the two intersecting rays is shown in sketch (C5). Since μ is always considered to be positive and strict observance must be made of the sign associated with the angle θ , the characteristic lines are both members of the first family and the slopes are $\tan(\theta + \mu)$; therefore,

$$\left(\frac{dy}{dx}\right)_A = \frac{y_C - y_A}{x_C - x_A} = \tan(\theta_A + \mu_A) \quad (C21)$$

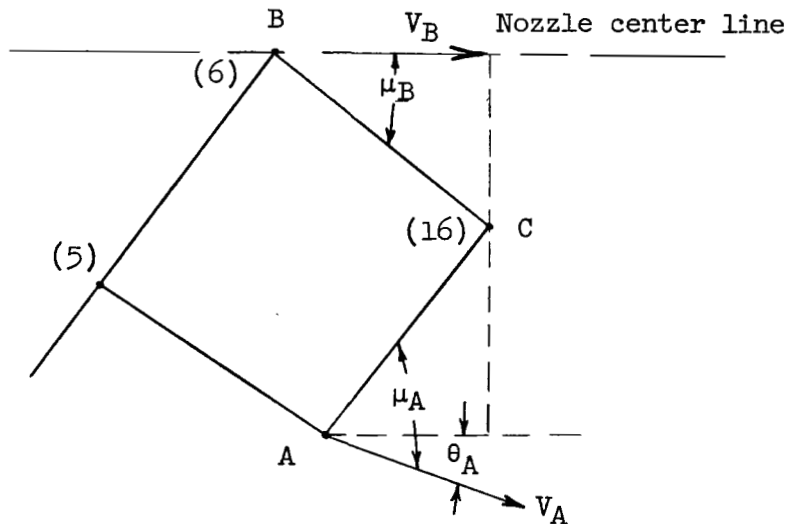
The equation for θ_C is the same as equation (C8) except that

$$m_B = \frac{\sin \mu_B \sin \theta_B \tan \mu_B}{\cos(\theta_B + \mu_B)} \quad (C24)$$

All other terms are identical to those of the general-point solution.

Point Adjacent to the Center Line

The characteristic lines used in defining flow conditions of a point adjacent to the axial center line involve a point on the center line, point B in sketch (C6), for which the flow direction is $\theta_B = 0^\circ$. The general-point equations (C3) and (C4) provide solutions for both x and y coordinates of



Sketch (C6)

point C; however, complications arise in determining θ_C since the term

$m_B \frac{dx_B}{y_B}$ used in the second-family equation (C6) becomes indeterminate $\left(\frac{0}{0}\right)$ at the

axis. Reference 32 makes several simplifying assumptions and derives an equation for the second-family characteristic line BC which is:

$$\frac{\Delta W}{W_B} - \Delta \theta \tan \mu_B - \frac{\Delta \theta \tan \mu_B \sin \mu_B}{\cos \mu_B} \frac{\Delta x}{y_C} = 0 \quad (C25)$$

Equation (C25), written for a point above the center line, conforms to conditions below the center line in this report by changing the minus (-) sign in front of the term $(\Delta\theta \tan \mu_B)$ to a plus (+) sign. An equation now exists for a second-family characteristic line similar in form to the second-family line in equation (C6). However, in equation (C25)

$$\frac{\Delta x}{y_C} = \frac{x_C - x_B}{y_C} = - \frac{1}{\tan \mu_B}$$

and

$$\frac{\sin \mu_B}{\cos \mu_B} = \tan \mu_B$$

Substitution of these terms into equation (C25) along with the required sign change produces

$$\frac{w_C - w_B}{w_B} + 2(\theta_C - \theta_B) \tan \mu_B = 0 \quad (C26)$$

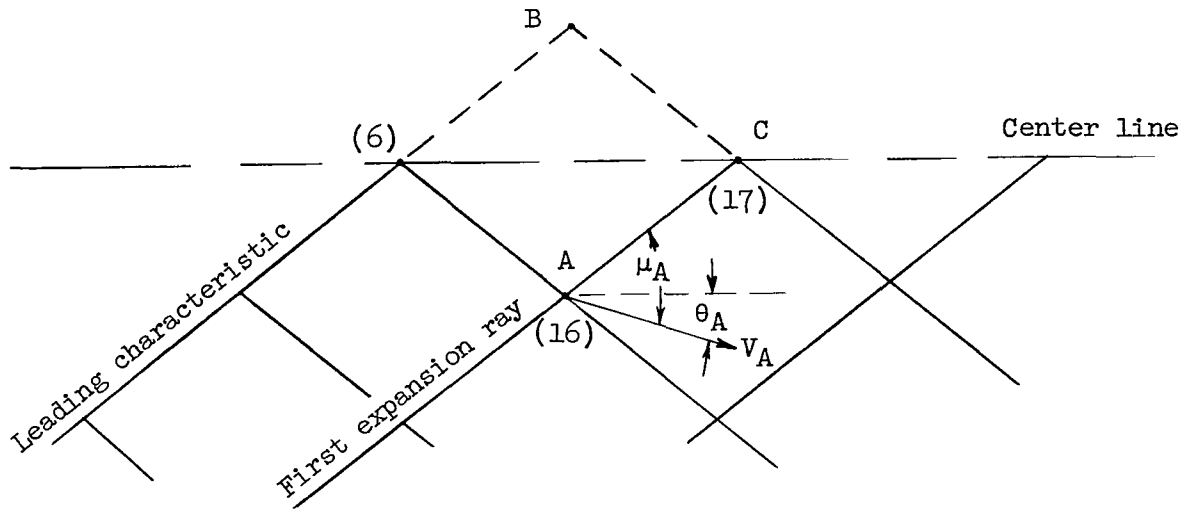
The simultaneous solution of the first-family equation (C5) and the second-family equation (C26) yields

$$\theta_C = \frac{-w_A - w_A \left(-\theta_A \tan \mu_A + \lambda_A \frac{x_C - x_A}{y_A} \right) + w_B + 2w_B \theta_B \tan \mu_B}{w_A \tan \mu_A + 2w_B \tan \mu_B} \quad (C27)$$

The velocity ratio w_C and Mach angle μ_C may now be found by using the general-point solutions.

Center-Line Point

The procedure for finding flow conditions at points along the nozzle axial center line is simplified in that both y_C and θ_C are zero. The intersection of the leading characteristic with the center line is the last given point in the input data; therefore, the intersection of the first expansion ray with the center line is the first point of this type which must be calculated and is shown in sketch (C7). An identical expansion originating at the opposite side of the nozzle results in point B which is a mirror image of point A. As a result of this similarity only the first-family characteristic line AC is needed



Sketch (C7)

to determine the location of point C. With y_C and θ_C equal to zero equation (C1) reduces to

$$x_C = x_A - \frac{y_A}{\tan(\theta_A + \mu_A)} \quad (C28)$$

Other parameters such as W_C , μ_C , and M_C may be found with the general-point equations.

Computer Program

A computer program has been developed for calculating the characteristic network of a jet boundary using three-dimensional irrotational equations of flow. This program is written in FORTRAN language (ref. 31) and is presented at the end of this appendix.

A set of initial conditions, x , y , θ , and μ , defining a series of points along the leading characteristic line is supplied to the computer in addition to the conditions defining the point origins of a series of two-dimensional expansion rays originating at the nozzle lip. The number of rays given, for any given exit Mach number, depends upon the fineness of the characteristic net desired and the pressure ratio in question. Computer programs have been written that may be used to supply the initial conditions for the leading characteristic line (see appendix A) and the conditions for the corner rays (see appendix B).



Points are computed along a downward sloping characteristic line from each given point on the leading characteristic line until the boundary point is computed. When the leading characteristic line is ended, points are computed along the nozzle axial center line with two new points being computed by interpolation between normal successive center-line points. Additional characteristic lines are computed originating at these center-line points. When $|y|$ has reached a maximum on the boundary, computation of points along characteristic lines continues until x on the center line or on the leading characteristic line has reached the value of x at the maximum boundary.

The following program has been used on the IBM 7094 electronic data processing system at the Langley Research Center to obtain the results presented herein.

```

C P-5430      FREE JET INVESTIGATION - CHARACTERISTIC METHOD
C
C          INPUT FOR A CASE
C
C      1ST CARD IDENTIFICATION, COL.1-80
C      2ND CARD NO. OF CORNER RAY CARDS, COL.1-3
C      NO. OF LEADING CHARACTERISTIC CARDS, COL.4-6
C      VALUE OF LAST Y(RAY) READ IN, COL.7-13
C      GAMMA, COL.14-20
C      DATA CARDS 3,4,.....
C      1ST GROUP
C      EACH CARD (NO. OF CARDS GIVEN BY COL.1-3 ON CARD 2)
C      DESCRIBES A POINT ON THE CORNER RAY AND CONTAINS
C      4 VALUES (X,-Y,-THETA,MU)
C
C      2ND GROUP
C      EACH CARD (NO. OF CARDS GIVEN BY COL.4-6 ON CARD 2)
C      DESCRIBES A POINT ON THE LEADING CHARACTERISTIC
C      LINE AND CONTAINS 4 VALUES (X,-Y,-THETA,MU)
C
C      DIMENSION CASE(14),XA(400),YA(400),THETA(400),FMUA(400),
C      IWA(400),CHARAC(6,700),XC(400),YC(400),THETC(400),
C      FMUC(400),WC(400),FMACHC(400)
C      COMMON CASE,XA,YA,THETA,FMUA,WA,
C      FMACHC,XC,YC,THETC,FMUC,WC,CHARAC,
C      GM1,GM12,XP,LINE,NA,NC,NRAY,NREFL
C
C          INITIALIZATION SECTION
C
C          EQUATION (C13)
C      FMU(X)=1./SIN(X)
C      DEG=57.29578
C      WRITE (6,1)
C      1 FORMAT(1H1///23HOFREE JET INVESTIGATION#X6HP-5430///)
C      2 CALL SLITE (0)
C      NREFL=0
C      CALL DVCHK (K000FX)
C      GO TO(4,4),K000FX
C
C      READ IN CASE
C      READ 1ST 2 CARDS
C
C      4 READ (5,5)CASE,LINE,NCHAR,YPREV,GAMMA
C      5 FORMAT (13A6,A2/2I3,2F7.0)
C      NRAY=LINE-1
C
C      READ CORNER RAY CARDS
C
C      READ (5,7)(XC(I),YC(I),THETC(I),FMUC(I),I=1,LINE)
C      7 FORMAT(4E16.0)
C
C      READ LEADING CHARACTERISTIC CARDS
C
C      READ (5,7)((CHARAC(I,J),I=1,4),J=1,NCHAR)
C
C      PRINT ID AND GAMMA
C
C      WRITE (6,9)CASE,GAMMA
C      9 FORMAT (1X13A6,A2//7HOGAMMA=F7.3///)
C
C      SET READ TO DETERMINE LAST CHARACTERISTIC POINT GIVEN
C
C      I=NCHAR-1
C      DO 10 J=1,I
C      10 CHARAC(6,J)=0.0
C      CHARAC(6,NCHAR)=1.0
C      WRITE(6,11)
C      11 FORMAT(6H0 MACH13X1HX16X1HY16X5HTHETA
C      111X2HMU14X1HW15X4HT/TO12X8HRHO/RHO0//)
C
C      GM1=GAMMA-1.0
C      GM12=GM1/2.0
C      XP=1.0/GM1
C
C      CHANGE THETA AND MU TO RADIANS
C      COMPUTE WC AND MACHC FROM INPUT MUC
C
C      DO 19 I=1,LINE
C      THETC(I)=THETC(I)/DEG
C      FMUC(I)=FMUC(I)/DEG
C      EQUATION (C12)
C      WC(I)=SQRT(GM1/(2.*SIN(FMUC(I))*2+GM1))
C      FMACHC(I)=FMU(FMUC(I))
C      19 CONTINUE
C
C      PRINT CORNER RAY
C
C      DO 22 I=1,LINE
C      CALL PRINT(FMACHC(I),XC(I),YC(I),THETC(I),
C      1FMUC(I),WC(I))
C      22 CONTINUE
C      CALL PREND
C
C      MOVE C ARRAY
C
C      DO 23 I=1,LINE
C      XA(I)=XC(I)
C      YA(I)=YC(I)

```

```

      THETA(I)=THETC(I)
      FMUA(I)=FMUC(I)
23  WA(I)=WC(I)
C
C      CHANGE CHARACTERISTIC THETA AND MU TO RADIANS
C      COMPUTE ALL W FOR LEADING CHARACTERISTICS
C
      DO 26 I=1,NCHAR
24  CHARAC(3,I)=CHARAC(3,I)/DEG
      CHARAC(4,I)=CHARAC(4,I)/DEG
C      EQUATION (C12)
      CHARAC(5,I)=SQRT(GM1/(2.*SIN(CHARAC(4,I))*2+GM1))
26  CONTINUE
C
C      COMPUTE 1ST LINE-NO REFLECTION
C
28  ICELL=2
      LEADC=1
      LINE=NRAY-1
      NA=1
      NC=1
C
C      MOVE 1ST LEADING CHARACTERISTIC TO 1ST C POINT
C
32  XC=CHARAC(1,1)
      YC=CHARAC(2,1)
      THETC=CHARAC(3,1)
      FMUC=CHARAC(4,1)
      WC=CHARAC(5,1)
      WRITE(6,11)
      FMACHC=FMU(FMUC)
      CALL PRINT(FMACHC,XC,YC,THETC,FMUC,WC)
35  NA=NA+1
      NC=NC+1
      CALL GENL(XA(NA),YA(NA),THETA(NA),FMUA(NA),WA(NA),
1XC(NC-1),YC(NC-1),THETC(NC-1),FMUC(NC-1),WC(NC-1),
2XC(NC),YC(NC),THETC(NC),FMUC(NC),WC(NC))
      FMACHC(NC)=FMU(FMUC(NC))
      CALL PRINT(FMACHC(NC),XC(NC),YC(NC),THETC(NC),
1FMUC(NC),WC(NC))
      LINE=LINE-1
      IF(LINE)998,40,35
40  NA=NA+1
      NC=NC+1
      CALL BNDRY(XA(NA),YA(NA),THETA(NA),FMUA(NA),WA(NA),
1XC(NC-1),YC(NC-1),THETC(NC-1),FMUC(NC-1),WC(NC-1),
2XC(NC),YC(NC),THETC(NC),FMUC(NC),WC(NC))
      FMACHC(NC)=FMU(FMUC(NC))
      CALL PRINT(FMACHC(NC),XC(NC),YC(NC),THETC(NC),
1FMUC(NC),WC(NC))
      LINE=NRAY-1
      CALL PRENO
C
C      MOVE C ARRAY
C
      DO 45 I=1,LINE
      XA(I)=XC(I)
      YA(I)=YC(I)
      THETA(I)=THETC(I)
      FMUA(I)=FMUC(I)
45  WA(I)=WC(I)
      NREFL=1
C
C
C      MODE 1 - SL2 OFF, READ=0
C      MAX BOUNDARY NOT REACHED, USE CHARAC LINE
C
100  MODE=1
102  LINE=NRAY+NREFL-1
      LEADC=LEADC+1
      NA=1
      NC=1
C
C      MOVE LEADING CHARACTERISTIC TO 1ST C POINT
C
104  XC=CHARAC(1,LEADC)
      YC=CHARAC(2,LEADC)
      THETC=CHARAC(3,LEADC)
      FMUC=CHARAC(4,LEADC)
      WC=CHARAC(5,LEADC)
108  READ=CHARAC(6,LEADC)
      WRITE(6,11)
      FMACHC=FMU(FMUC)
      CALL PRINT(FMACHC,XC,YC,THETC,FMUC,WC)
C
C      TEST FOR 1ST CENTERLINE
C
      IF(READ)998,110,109
109  NA=2
      NC=2
      CALL OFCNT(XA(2),YA(2),THETA(2),FMUA(2),WA(2),
1XC,FMUC,WC,XC(2),YC(2),THETC(2),FMUC(2),WC(2))
      FMACHC(2)=FMU(FMUC(2))
      CALL PRINT(FMACHC(2),XC(2),YC(2),THETC(2),
1FMUC(2),WC(2))
      LINE=LINE-1
110  NA=NA+1
      NC=NC+1
      CALL GENL(XA(NA),YA(NA),THETA(NA),FMUA(NA),WA(NA),
1XC(NC-1),YC(NC-1),THETC(NC-1),FMUC(NC-1),WC(NC-1),
2XC(NC),YC(NC),THETC(NC),FMUC(NC),WC(NC))

```

```

      IF(LINE-4)112,112,111
111 CALL TEST
      NA=NA
112 CALL TEST2(1SIG)
      NC=NC
113 GO TO (114,123), 1SIG
114 FMACHC(NC)=FMMU(FMUC(NC))
      CALL PRINT(FMACHC(NC),XC(NC),YC(NC),THETC(NC),
1FMUC(NC),WC(NC))
      LINE=LINE-1
      IF (LINE)99B,120,110
120 NC=NC+1
122 CALL BNDRY(XA(NA),YA(NA),THETA(NA),FMUA(NA),WA(NA),
1XC(NC-1),YC(NC-1),THETC(NC-1),FMUC(NC-1),WC(NC-1),
2XC(NC),YC(NC),THETC(NC),FMUC(NC),WC(NC))
      FMACHC(NC)=FMMU(FMUC(NC))
      CALL PRINT(FMACHC(NC),XC(NC),YC(NC),THETC(NC),
1FMUC(NC),WC(NC))
123 LINE=NRAY+NREFL+1
      CALL PREND
C
C      MOVE ARRAYS
C
      DO 125 I=1,LINE
      XA(I)=XC(I)
      YA(I)=YC(I)
      THETA(I)=THETC(I)
      FMUA(I)=FMUC(I)
      WA(I)=WC(I)
125 CONTINUE
C
C      TEST FOR NEXT MODE
C
      IF(YPREV-YC(NC))130,150,150
130 CALL SLITE(2)
      XMAX=XC(NC)
      IF(READ)99B,300,132
132 ICELL=3
      GO TO 400
150 YPREV=YC(NC)
      IF(READ)99B,152,151
151 ICELL=3
      GO TO 200
152 NREFL=NREFL+1
      GO TO 102
C
C
C      MODE II - SL2 OFF, READ NOT 0
C      MAX BOUNDARY NOT REACHED, CENTERLINE POINTS COMPUTED
C
200 MODE=2
201 GO TO (760,740,700), ICELL
202 LINE=NRAY+NREFL-2
204 NA=NA+1
      NC=NC+1
      CALL GENL(XA(NA),YA(NA),THETA(NA),FMUA(NA),WA(NA),
1XC(NC-1),YC(NC-1),THETC(NC-1),FMUC(NC-1),WC(NC-1),
2XC(NC),YC(NC),THETC(NC),FMUC(NC),WC(NC))
      IF(LINE-4)206,206,205
205 CALL TEST
      NA=NA
206 CALL TEST2(1SIG)
      NC=NC
207 GO TO (208,212), 1SIG
208 FMACHC(NC)=FMMU(FMUC(NC))
      CALL PRINT(FMACHC(NC),XC(NC),YC(NC),THETC(NC),
1FMUC(NC),WC(NC))
      LINE=LINE-1
      IF (LINE)99B,210,204
210 NC=NC+1
      CALL BNDRY(XA(NA),YA(NA),THETA(NA),FMUA(NA),WA(NA),
1XC(NC-1),YC(NC-1),THETC(NC-1),FMUC(NC-1),WC(NC-1),
2XC(NC),YC(NC),THETC(NC),FMUC(NC),WC(NC))
      FMACHC(NC)=FMMU(FMUC(NC))
      CALL PRINT(FMACHC(NC),XC(NC),YC(NC),THETC(NC),
1FMUC(NC),WC(NC))
212 LINE=NRAY+NREFL+1
      CALL PREND
C
C      MOVE ARRAYS
C
      DO 215 I=1,LINE
      XA(I)=XC(I)
      YA(I)=YC(I)
      THETA(I)=THETC(I)
      FMUA(I)=FMUC(I)
      WA(I)=WC(I)
215 CONTINUE
C
C      TEST FOR NEXT MODE
C
      IF(YPREV-YC(NC))230,220,220
220 YPREV=YC(NC)
      GO TO 201
230 CALL SLITE(2)
      XMAX=XC(NC)
      GO TO 400
C
C
C      MODE III - SL2 ON, READ=0
C      MAX BOUNDARY REACHED, USE CHARAC LINE

```

```

C
C
300 MODE=3
302 LINE=NRAY+NREFL-1
   LEADC=LEADC+1
   NA=1
   NC=1
C
C      MOVE CHARAC TO 1ST C POINT
C
304 XC=CHARAC(1,LEADC)
   YC=CHARAC(2,LEADC)
   THETC=CHARAC(3,LEADC)
   FMUC=CHARAC(4,LEADC)
   WC=CHARAC(5,LEADC)
   READ=CHARAC(6,LEADC)
   IF(XC-XMAX)307,307,789
305 WRITE(6,11)
   FMACHC=FMUC(FMUC)
   CALL PRINT(FMACHC,XC,YC,THETC,FMUC,WC)
C
C      TEST FOR 1ST CENTERLINE
C
   IF(READ)998,310,306
306 NA=2
   NC=2
   CALL OFCNT(XA(2),YA(2),THETA(2),FMUA(2),WA(2),
   IXC,FMUC,WC,XC(2),YC(2),THETC(2),FMUC(2),WC(2))
   IF(XC(2)-XMAX)307,307,789
307 FMACHC(2)=FMUC(FMUC(2))
   CALL PRINT(FMACHC(2),XC(2),YC(2),THETC(2),
   IFMUC(2),WC(2))
   LINE=LINE-1
310 NA=NA+1
   NC=NC+1
   CALL GENL(XA(NA),YA(NA),THETA(NA),FMUA(NA),WA(NA),
   IXC(NC-1),YC(NC-1),THETC(NC-1),FMUC(NC-1),WC(NC-1),
   2XC(NC),YC(NC),THETC(NC),FMUC(NC),WC(NC))
C
C      TEST FOR MAX BOUNDARY X
C
   IF(XC(NC)-XMAX)320,320,350
320 IF(LINE=4)330,330,329
329 CALL TEST
   NA=NA
330 CALL TEST2(1SIG)
   NC=NC
331 GO TO(335,370),1SIG
335 FMACHC(NC)=FMUC(FMUC(NC))
   CALL PRINT(FMACHC(NC),XC(NC),YC(NC),THETC(NC),
   IFMUC(NC),WC(NC))
   LINE=LINE-1
   IF(LINE)998,370,310
C
C      COMPUTE RAYS AND REFLECTIONS
C
350 LOOK=NC-1
   IF(LOOK-NRAY)352,353,356
352 NRAY=LOOK
353 NREFL=0
   GO TO 370
356 NREFL=LOOK-NRAY
370 LINE=NRAY+NREFL
   CALL PREND
C
C      EXIT TEST
C
   IF(NRAY-1)990,990,375
C
C      MOVE ARRAYS
C
375 DO 380 I=1,LINE
   XA(I)=XC(I)
   YA(I)=YC(I)
   THETA(I)=THETC(I)
   FMUA(I)=FMUC(I)
   WA(I)=WC(I)
380 CONTINUE
C
C      TEST FOR NEXT MODE
C
   IF(READ)998,302,382
382 ICELL=3
C
C      MODE IV - SL2 ON, READ NOT 0
C      MAX BOUNDARY REACHED, CENTERLINE POINTS COMPUTED
C
400 MODE=4
402 GO TO(760,740,700),ICELL
404 LINE=NRAY+NREFL-2
   IF(LINE)998,470,408
408 NA=NA+1
   NC=NC+1
   CALL GENL(XA(NA),YA(NA),THETA(NA),FMUA(NA),WA(NA),
   IXC(NC-1),YC(NC-1),THETC(NC-1),FMUC(NC-1),WC(NC-1),
   2XC(NC),YC(NC),THETC(NC),FMUC(NC),WC(NC))
C
C      TEST FOR MAX BOUNDARY X
C
   IF(XC(NC)-XMAX)420,420,458

```

```

420 IF(LINE=4)430,430,429
429 CALL TEST
    NA=NA
430 CALL TEST2 (ISIG)
    NC=NC
431 GO TO (445,470), ISIG
445 FMACHC(NC)=FMMU(FMUC(NC))
    CALL PRINT(FMACHC(NC),XC(NC),YC(NC),THETC(NC),
1FMUC(NC),WC(NC))
    LINE=LINE-1
    IF (LINE)998,470,408
C
C      COMPUTE RAYS AND REFLECTIONS
C
450 LOOK=NC-1
    IF(LOOK=NRAY)452,453,456
452 NRAY=LOOK
453 NREFL=0
    GO TO 470
456 NREFL=LOOK-NRAY
470 LINE=NRAY+NREFL
    CALL PREND
C
C      MOVE ARRAYS
C
475 DO 480 I=1,LINE
    XA(I)=XC(I)
    YA(I)=YC(I)
    THETA(I)=THETC(I)
    FMUA(I)=FMUC(I)
    WA(I)=WC(I)
480 CONTINUE
    GO TO 402
C
C
C      INTERPOLATION SECTION FOR CENTERLINE POINTS
C
C      FOR ICELL=3
C
700 ICELL=2
    NA=2
    NC=2
    CALL CENTL(XA(2),YA(2),THETA(2),FMUA(2),WA(2),
1TX,TMU,TW)
C
C      COMPUTE DELTAS AND SAVE
C
    DELX=(TX-XA)/3.
    DELMU=(TMU-FMUA)/3.
    DELW=(TW-WA)/3.
C
C      COMPUTE 1/3 DISTANCE FOR NEW C
C
    XC=DELX+XA
    FMUC=DELMU+FMUA
    WC=DELW+WA
C
C      SENSE LIGHT TEST
C
712 CALL SLITET(2,K000FX)
    GO TO(715,720),K000FX
715 CALL SLITE (2)
    IF(XC-XMAX)720,720,990
720 WRITE(6,11)
    FMACHC=FMMU(FMUC)
    CALL PRINT(FMACHC,XC,YC,THETC,FMUC,WC)
C
C      COMPUTE 1 PT OFF CENTERLINE
C
    CALL OFCNT(XA(2),YA(2),THETA(2),FMUA(2),WA(2),
1XC,FMUC,WC,
2XC(2),YC(2),THETC(2),FMUC(2),WC(2))
    CALL SLITET(2,K000FX)
    GO TO(725,730),K000FX
725 CALL SLITE (2)
    IF(XC(2)-XMAX)727,727,728
727 FMACHC(2)=FMMU(FMUC(2))
    CALL PRINT(FMACHC(2),XC(2),YC(2),THETC(2),
1FMUC(2),WC(2))
    GO TO 404
728 NRAY=1
    NREFL=0
    LINE=1
    CALL PREND
    GO TO 990
730 FMACHC(2)=FMMU(FMUC(2))
    CALL PRINT(FMACHC(2),XC(2),YC(2),THETC(2),
1FMUC(2),WC(2))
    NREFL=NREFL+1
    GO TO 202
C
C      FOR ICELL=2
C
740 ICELL=1
    NA=2
    NC=2
    XC=XA+DELX
    FMUC=FMUA+DELMU
    WC=WA+DELW
    GO TO 712
C
C      FOR ICELL=1

```

```

C
760 ICELL=3
    NA=3
    NC=2
    CALL CENTL(XA(2),YA(2),THETA(2),FMUA(2),WA(2),
1XC,FMUC,WC)
    CALL SLITET(2,K000FX)
    GO TO(770,780),K000FX
770 CALL SLITE(2)
    IF(XC-XMAX)780,780,990
780 WRITE(6,11)
    FMACHC=FMU(FMUC)
    CALL PRINT(FMACHC,XC,YC,THETC,FMUC,WC)
    CALL OFCNT(XA(3),YA(3),THETA(3),FMUA(3),WA(3),
1XC,FMUC,WC,XC(2),YC(2),THETC(2),FMUC(2),WC(2))
    CALL SLITET(2,K000FX)
    GO TO(785,790),K000FX
785 CALL SLITE(2)
    IF(XC(2)-XMAX)787,787,789
787 FMACHC(2)=FMU(FMUC(2))
    CALL PRINT(FMACHC(2),XC(2),YC(2),THETC(2),
1FMUC(2),WC(2))
    NRAY=NRAY-1
    GO TO 404
789 NRAY=1
    NREFL=0
    LINE=1
    CALL PREND
    GO TO 990
790 NREFL=NREFL+1
    FMACHC(2)=FMU(FMUC(2))
    CALL PRINT(FMACHC(2),XC(2),YC(2),THETC(2),
1FMUC(2),WC(2))
    NRAY=NRAY-1
    GO TO 202
C
C      EXIT
C
990 CALL DVCHK(JJ)
    GO TO (992,995),JJ
992 WRITE (6,993)
993 FORMAT(34HODIVIDE CHECK ON WHEN EXIT REACHED/1H1)
    CALL EXIT
995 WRITE (6,996)
996 FORMAT(12HOEND OF CASE/1H1)
997 LINE=0
    CALL PREND
    CALL EXIT
C
C      ERROR
C
998 WRITE (6,999)MODE
999 FORMAT(22HOPROGRAM ERROR IN MODE,12/1H1)
    GO TO 997
    END

```

```

SUBROUTINE GENL(GXA,GYA,GTA,GMUA,GWA,GBX,GBY,GTB,
1GMUB,GBW,GXC,GYC,GTC,GMUC,GWC)
C
C      GENERAL POINT SUBROUTINE
C
    DIMENSION CASE(14),XA(400),YA(400),THETA(400),FMUA(400),
1WA(400),CHARAC(6,700),XC(400),YC(400),THETC(400),
2FMUC(400),WC(400),FMACHC(400)
    COMMON CASE,XA,YA,THETA,FMUA,WA,
1FMACHC,XC,YC,THETC,FMUC,WC,CHARAC,
2GM1,GM12,XP,LINE,NA,NC,NRAY,NREFL
    ASIN(X)=ATAN2(X,5QRT(1.-X**2))
    B1=SIN(GMUB)
    B2=COS(GTB-GMUB)
    B3=SIN(GMUA)
    B4=COS(GTA+GMUA)
    D1=SIN(GTA+GMUA)/B4
    D2=SIN(GTB-GMUB)/B2
    D4=B3/COS(GMUA)
    D5=B1/COS(GMUB)
C
    EQUATION (C3)
    GXC=(GXA*D1-GYA+GBY-GXB*D2)/(D1-D2)
    D3=GXC-GXA
    D6=D3/GYA
C
    EQUATION (C4)
    B GYC=D3*D1+GYA
C
    EQUATION (C10)
    FMB=(B1*SIN(GTB)*D5)/B2
C
    EQUATION (C9)
    FLA=(B3*SIN(GTA)*D4)/B4
    C1=-GTA*D4+D6*FLA
    C2=GTB*D5+(GXC-GXB)*FMB/GBY
C
    EQUATION (C8)
    GTC=(-GWA-GWA*C1+GBW+GBW*C2)/(GWA*D4+GBW*D5)
C
    EQUATION (C11)
    GWC=GWA+GWA*(D4*(GTC-GTA)+D6*FLA)
    C1=GM12*(1.0/GWC**2-1.0)
C
    EQUATION (C12)
    GMUC=ASIN(SQRT(C1))
28 RETURN
    END

```

```

SUBROUTINE CENTL(GXA,GYA,GTA,GMUA,GWA,
1GXC,GMUC,GWC)
C
C
C      CENTERLINE POINT SUBROUTINE
C
DIMENSION CASE(14),XA(400),YA(400),THETA(400),FMUA(400),
1WA(400),CHARAC(6,700),XC(400),YC(400),THETC(400),
2FMUC(400),WC(400),FMACHC(400)
COMMON CASE,XA,YA,THETA,FMUA,WA,
1FMACHC,XC,YC,THETC,FMUC,WC,CHARAC,
2GM1,GM12,XP,LINE,NA,NC,NRAY,NREFL
ASIN(X)=ATAN2(X,SQRT(1.-X**2))
B1=SIN(GMUA)
B2=COS(GTA+GMUA)
1 D1=SIN(GTA+GMUA)/B2
D2=B1/COS(GMUA)
C
C      EQUATION (C28)
GXC=GXA-GYA/D1
C
C      EQUATION (C9)
FLA=(B1*SIN(GTA)*D2)/B2
C
C      EQUATION (C11)
GWC=GWA+GWA*(-GTA*D2+(GXC-GXA)*FLA/GYA)
C1=GM12*(1.+0/GWC**2-1.0)
C
C      EQUATION (C12)
GMUC=ASIN(SQRT(C1))
18 RETURN
END

```

```

SUBROUTINE OFCNT(GXA,GYA,GTA,GMUA,GWA,GXB,
1GMUB,GWB,GXC,GYC,GTC,GMUC,GWC)
C
C
C      1 POINT OFF CENTERLINE SUBROUTINE
C
DIMENSION CASE(14),XA(400),YA(400),THETA(400),FMUA(400),
1WA(400),CHARAC(6,700),XC(400),YC(400),THETC(400),
2FMUC(400),WC(400),FMACHC(400)
COMMON CASE,XA,YA,THETA,FMUA,WA,
1FMACHC,XC,YC,THETC,FMUC,WC,CHARAC,
2GM1,GM12,XP,LINE,NA,NC,NRAY,NREFL
ASIN(X)=ATAN2(X,SQRT(1.-X**2))
B1=SIN(GMUA)
B2=COS(GTA+GMUA)
1 D1=B1/COS(GMUA)
D2=SIN(GMUB)/COS(GMUB)
D4=SIN(GTA+GMUA)/B2
D5=SIN(-GMUB)/COS(-GMUB)
C
C      EQUATION (C3)
GXC=(GXA*D4-GYA-GXB*D5)/(D4-D5)
D3=GXC-GXA
C
C      EQUATION (C4)
GYC=D3*D4+GYA
C
C      EQUATION (C9)
FLA=(B1*SIN(GTA)*D1)/B2
C1=-GTA*D1+D3*FLA/GYA
C
C      EQUATION (C27)
GTC=(-GWA-GWA*C1+GWB)/(GWA*D1+2.*GWB*D2)
C
C      EQUATION (C11)
GWC=GWA+GWA*(D1*(GTC-GTA)+D3*FLA/GYA)
C1=GM12*(1.+0/GWC**2-1.0)
C
C      EQUATION (C12)
14 GMUC=ASIN(SQRT(C1))
18 RETURN
END

```

```

SUBROUTINE BNDY (BXA,BYA,BTA,BMUA,BWA,BXB,BYB,BTB,BMUB,
1BWB,BXC,BYC,BTC,BMUC,BWC)
C
C
C      BOUNDARY POINT SUBROUTINE
C
B1=COS(BTB-BMUB)
B2=SIN(BMUB)
1 D1=SIN(BTA)/COS(BTA)
D2=SIN(BTB-BMUB)/B1
D3=SIN(BMUB)/COS(BMUB)
C
C      EQUATION (C18)
BXC=(BXA*D1-BYA+BYB-BXB*D2)/(D1-D2)
C
C      EQUATION (C19)
BYC=(BXC-BXA)*D1+BYA
BMUC=BMUA
BWC=BWA
C
C      EQUATION (C10)
FMB=(B2*SIN(BTB)*D3)/B1
C
C      EQUATION (C20)
BTC=BTB+(-BWC-BWB)/BWB+((BXC-BXB)/BYB)*FMB/D3
12 RETURN
END

```

```

SUBROUTINE SAMFM (SXB,SYB,STB,SMUB,SWB,
1SXA,SYA,STA,SMUA,SWA,SXC,SYC,STC,SMUC,SWC)
C
C
C      SAME FAMILY POINT SUBROUTINE
C
DIMENSION CASE(14),XA(400),YA(400),THETA(400),FMUA(400),
1WA(400),CHARAC(6,700),XC(400),YC(400),THETC(400),
2FMUC(400),WC(400),FMACHC(400)
COMMON CASE,XA,YA,THETA,FMUA,WA,

```

```

1FMACHC,XC,YC,THETC,FMUC,WC,CHARAC,
2GM1,GM12,XP,LINE,NA,NC,NRAY,NREFL
ASIN(X)=ATAN2(X,SQRT(TTT))
B1=SIN(SMUB)
B2=COS(STB+SMUB)
B3=SIN(SMUA)
B4=COS(STA+SMUA)
D1=SIN(STA+SMUA)/B4
D2=SIN(STB+SMUB)/B2
D4=B3/COS(SMUA)
D5=B1/COS(SMUB)
C EQUATION (C23)
SXC=(SXA*D1-SYA+SYB-SXB*D2)/(D1-D2)
D3=SXC-SXA
C EQUATION (C4)
SYC=D3*D1+SYA
C EQUATION (C24)
FMB=(B1*SIN(STB)*D5)/B2
C EQUATION (C9)
FLA=(B3*SIN(STA)*D4)/B4
C1=-STA*D4+D3*FLA/SYA
C2=STB*D5+((SXC-SXB)*FMB)/SYB
C EQUATION (C8)
STC=(-SWA-SWA*C1+SWB+SWB*C2)/(SWA*D4+SWB*D5)
C EQUATION (C11)
SWC=SWA+SWA*(D4*(STC-STA)+D3*FLA/SYA)
C1=GM12*(1.0/SWC*2-1.0)
IF(C1)97,24,24
24 TTT=SQRT(C1)
TTT=1.-TTT**2
IF(TTT)97,26,26
C EQUATION (C12)
26 SMUC=ASIN(TTT)
GO TO 28
97 WRITE(6,98)
98 FORMAT(37H SORT ERROR IN SAMFM POINT SUBROUTINE)
28 RETURN
END

```

```

SUBROUTINE TEST
C
C SUBROUTINE TO TEST FOR CROSSINGS
C USES 3 SAME FAMILY POINTS
C
DIMENSION CASE(14),XA(400),YA(400),THETA(400),FMUA(400),
1WA(400),CHARAC(6,700),XC(400),YC(400),THETC(400),
2FMUC(400),WC(400),FMACHC(400)
COMMON CASE,XA,YA,THETA,FMUA,WA,
1FMACHC,XC,YC,THETC,FMUC,WC,CHARAC,
2GM1,GM12,XP,LINE,NA,NC,NRAY,NREFL
500 CONV=57.29578
CON=THETC(INC-1)-FMUC(INC-1)
SLOPE=SIN(CON)/COS(CON)
CB=YC(INC-1)-XC(INC-1)*SLOPE
XASAV=XA(NA+1)
NASAV=NA
GO TO 515
C
C COMPUTE NEW GENL
C
510 CALL GENL(XA(NA),YA(NA),THETA(NA),FMUA(NA),WA(NA),
1XC(INC-1),YC(INC-1),THETC(INC-1),FMUC(INC-1),WC(INC-1),
2XC(INC),YC(INC),THETC(INC),FMUC(INC),WC(INC))
C
C COMPUTE 1 PT
C
515 CALL SAMFM(XA(NA),YA(NA),THETA(NA),FMUA(NA),WA(NA),
1XA(NA+1),YA(NA+1),THETA(NA+1),FMUA(NA+1),WA(NA+1),
2X1,Y1,THET1,FMU1,W1)
C
C COMPUTE 2 PT
C
520 CALL SAMFM(XA(NA+1),YA(NA+1),THETA(NA+1),FMUA(NA+1),WA(NA+1),
1XA(NA+2),YA(NA+2),THETA(NA+2),FMUA(NA+2),WA(NA+2),
2X2,Y2,THET2,FMU2,W2)
C
C COMPUTE 3 PT
C
CALL SAMFM(XA(NA+2),YA(NA+2),THETA(NA+2),FMUA(NA+2),WA(NA+2),
1XA(NA+3),YA(NA+3),THETA(NA+3),FMUA(NA+3),WA(NA+3),
2X3,Y3,THET3,FMU3,W3)
C
C FIND X AND Y MIN AND MAX FOR BOX
C
525 XMIN=AMINI(XC(INC),XA(NA),XA(NA+1),XA(NA+2),XA(NA+3))
526 XMAX=AMAXI(XC(INC),XA(NA),XA(NA+1),XA(NA+2),XA(NA+3))
527 YMIN=AMINI(YC(INC),YA(NA),YA(NA+1),YA(NA+2),YA(NA+3))
528 YMAX=AMAXI(YC(INC),YA(NA),YA(NA+1),YA(NA+2),YA(NA+3))
C
C CHECK 1 PT FOR CROSSING
C
CALL CROSS(X1,Y1,XMAX,XMIN,YMAX,YMIN,
1THETA(NA),FMUA(NA),THETA(NA+1),FMUA(NA+1),
2SLOPE,CB,IT)
IT=IT
GO TO(530,535),IT
530 KODE=2
GO TO 538
535 KODE=1
C

```

```

C          CHECK 2 PT FOR CROSSING
C
538 CALL CROSS(X2,Y2,XXMAX,XMIN,YYMAX,YMIN,
1THETA(NA+1),FMUA(NA+1),THETA(NA+2),FMUA(NA+2),
2SLOPE,CB,IT)
IT=IT
GO TO(540,545),IT
540 GO TO(542,544),KODE
542 KODE=3
GO TO 545
544 KODE=4
C
C          CHECK 3 PT FOR CROSSING
C
545 CALL CROSS(X3,Y3,XXMAX,XMIN,YYMAX,YMIN,
1THETA(NA+2),FMUA(NA+2),THETA(NA+3),FMUA(NA+3),
2SLOPE,CB,IT)
IT=IT
GO TO(550,560),IT
C
C          FIND COMBINATION OF CROSSINGS TO CHECK
C
550 GO TO(750,760,770,780),KODE
560 GO TO(710,720,730,740),KODE
C
C          NO CROSSING
C
710 LINE=LINE-(NA-NASAV)
RETURN
C
C          1 PT IS CROSSING TO USE
C
720 TPR=THET1*CONV
FMUPR=FMU1*CONV
WRITE (6,722)X1,Y1,TPR,FMUPR,W1
722 FORMAT(6H **1**11X,3E17.8,2E16.8)
IF(NC-NRAY)725,725,724
724 NREFL=NREFL-1
GO TO 726
725 NRAY=NRAY-1
726 NA=NA+1
XA(NA)=X1
YA(NA)=Y1
THETA(NA)=THET1
FMUA(NA)=FMU1
WA(NA)=W1
GO TO 510
C
C          2 PT IS CROSSING TO USE
C
730 TPR=THET2*CONV
FMUPR=FMU2*CONV
WRITE (6,732)X2,Y2,TPR,FMUPR,W2
732 FORMAT(6H **2**11X,3E17.8,2E16.8)
IF(NC-NRAY)735,735,734
734 NREFL=NREFL-1
GO TO 736
735 NRAY=NRAY-1
736 XA(NA+1)=XA(NA)
YA(NA+1)=YA(NA)
THETA(NA+1)=THETA(NA)
FMUA(NA+1)=FMUA(NA)
WA(NA+1)=WA(NA)
NA=NA+1
XA(NA+1)=X2
YA(NA+1)=Y2
THETA(NA+1)=THET2
FMUA(NA+1)=FMU2
WA(NA+1)=W2
GO TO 515
C
C          BOTH 1 AND 2 ARE CROSSINGS, SELECT ONE TO USE
C
740 DIFF1=ABS(X1-XASAV)
DIFF2=ABS(X2-XASAV)
IF(DIFF1-DIFF2)720,720,730
C
C          3 PT IS CROSSING TO USE
C
750 TPR=THET3*CONV
FMUPR=FMU3*CONV
WRITE (6,752)X3,Y3,TPR,FMUPR,W3
752 FORMAT(6H **3**11X,3E17.8,2E16.8)
IF(NC-NRAY)755,755,754
754 NREFL=NREFL-1
GO TO 756
755 NRAY=NRAY-1
756 XA(NA+2)=XA(NA+1)
YA(NA+2)=YA(NA+1)
THETA(NA+2)=THETA(NA+1)
FMUA(NA+2)=FMUA(NA+1)
WA(NA+2)=WA(NA+1)
XA(NA+1)=XA(NA)
YA(NA+1)=YA(NA)
THETA(NA+1)=THETA(NA)
FMUA(NA+1)=FMUA(NA)
WA(NA+1)=WA(NA)
NA=NA+1
XA(NA+2)=X3
YA(NA+2)=Y3
THETA(NA+2)=THET3
FMUA(NA+2)=FMU3

```

```

      WA(NA+2)=W3
      GO TO 420
C
C      BOTH 1 AND 3 ARE CROSSINGS, SFLECT ONE TO USE
C
760 DIFF1=ABS(X1-XASAV)
      DIFF3=ABS(X3-XASAV)
      IF(DIFF1-DIFF3)720,720,750
C
C      BOTH 2 AND 3 ARE CROSSINGS, SELECT ONE TO USE
C
770 DIFF2=ABS(X2-XASAV)
      DIFF3=ABS(X3-XASAV)
      IF(DIFF2-DIFF3)730,730,750
C
C      1, 2, AND 3 ARE CROSSINGS, SELECT ONE TO USE
C
780 DIFF1=ABS(X1-XASAV)
      DIFF2=ABS(X2-XASAV)
      DIFF3=ABS(X3-XASAV)
      IF(DIFF1-DIFF2)782,782,785
782 IF(DIFF1-DIFF3)720,720,750
785 IF(DIFF2-DIFF3)730,730,750
      END

      SUBROUTINE TEST2(ISIG)
C
C      MERGES 2 CHARACTERISTIC LINES IF THEY CROSS
C      ISIG=1 FOR NO CROSSING
C      ISIG=2 FOR CROSSING FOUND
C
      DIMENSION CASE(14),XA(400),YA(400),THETA(400),FMUA(400),
1 WA(400),CHARAC(6,700),XC(400),YC(400),THETC(400),
2 FMUC(400),WC(400),FMACHC(400)
      COMMON CASE,XA,YA,THETA,FMUA,WA,
1 FMACHC,XC,YC,THETC,FMUC,WC,CHARAC,
2 GM1,GM12,XP,LINE,NA,NC,NRAY,NREFL
      ANGLE=-1,5707963
      1 IF (THETA(NA)+FMUA(NA)-ANGLE) 3,2,2
      2 IF(XC(NC)-XA(NA)) 6,5,5
      3 IF(XC(NC)-XA(NA)) 5,5,6
C
C      NO CROSSING
C
      5 ISIG=1
      RETURN
C
C      CROSSING FOUND
C
      6 CALL SLITET(2,K000FX)
      GO TO(8,10),K000FX
      8 CALL SLITE (2)
      GO TO 15
      10 NREFL=NREFL-1
C
C      MOVE REMAINING A ARRAY TO C ARRAY AND PRINT
C
      15 NARNA+1
      NC=NC+1
      20 XC(NC-1)=XA(NA-1)
      YC(NC-1)=YA(NA-1)
      THETC(NC-1)=THETA(NA-1)
      FMUC(NC-1)=FMUA(NA-1)
      WC(NC-1)=WA(NA-1)
      FMACHC(NC-1)=1./SIN(FMUC(NC-1))
      CALL PRINT(FMACHC(NC-1),XC(NC-1),YC(NC-1),THETC(NC-1),
1 FMUC(NC-1),WC(NC-1))
      LINE=LINE-1
      IF (LINE) 998,25,15
      25 ISIG=2
      NC=NC-1
      RETURN
      998 WRITE (6,999)
      999 FORMAT (20H0ERROR IN TEST2 SUBR/1H1)
      CALL EXIT
      END

      SUBROUTINE CROSS(X,Y,XMAX,XMIN,YMAX,YMIN,
1 T1,FM1,T2,FM2,SLOPE,CB,IT)
C
C      CHECKS A PARTICULAR POINT TO SEE IF A CROSSING
C      IT=1, CROSSING FOUND
C      IT=2, CROSSING NOT FOUND
C
C      CHECK LIMIT BOX
C
      IF(Y-YMIN)25,25,2
      2 IF(Y-YMAX)4,25,25
      4 IF(X-XMIN)25,25,6
      6 IF(X-XMAX)8,25,25
C
C      CHECK CONVERGING LINES
C
      8 IF((T1+FM1)-(T2+FM2))10,10,25
C
C      CHECK IF PAST LINE B
C
      10 CSF=Y-SLOPE*X

```

```

12 IF(SLOPE)14;16;16
C
C      NEGATIVE SLOPE
C
14 IF(CSF-CB)18;18;25
C
C      POSITIVE SLOPE
C
16 IF(CSF-CB)25;18;18
C
C      CROSSING FOUND
C
18 IT=1
RETURN
C
C      NO CROSSING FOUND
C
25 IT=2
RETURN
END

SUBROUTINE PRINT(PM,PX,PY,PT,PMU,PW)
C
C      PRINTS A POINT IN THE NETWORK
C
DIMENSION CASE(14),XA(400),YA(400),THETA(400),FMUA(400),
1WA(400),CHARAC(6,700),XC(400),YC(400),THETC(400),
2FMUC(400),WC(400),FMACHC(400)
COMMON CASE,XA,YA,THETA,FMUA,WA,
1FMACHC,XC,YC,THETC,FMUC,WC,CHARAC,
2GM1,GM12,XP,LINE,NA,NC,NRAY,NREFL
DEG=57.29578
TEMP=1.+GM12*PM**2
C      EQUATION (C14)
TTZ=1./TEMP
C      EQUATION (C15)
RRZ=1./TEMP**XP
TPR=PT*DEG
FMUPR=PMU*DEG
WRITE(6,10)PM,PX,PY,TPR,FMUPR,PW,TTZ,RRZ
10 FORMAT(4E17.8,4E16.8)
RETURN
END

SUBROUTINE PREND
C
C      MARKS END OF A CHARACTERISTIC LINE AND
C      WRITES A TAPE FOR OPTIONAL PLOTTING
C
DIMENSION CASE(14),XA(400),YA(400),THETA(400),FMUA(400),
1WA(400),CHARAC(6,700),XC(400),YC(400),THETC(400),
2FMUC(400),WC(400),FMACHC(400)
COMMON CASE,XA,YA,THETA,FMUA,WA,
1FMACHC,XC,YC,THETC,FMUC,WC,CHARAC,
2GM1,GM12,XP,LINE,NA,NC,NRAY,NREFL
IF(LINE)2,2,4
2 WRITE(9)LINE
END FILE 9
RETURN
4 WRITE(6,8)NRAY,NREFL
8 FORMAT(1H0,2I6/1H1)
C
C      WRITE PLOTTING TAPE
C
WRITE(9)LINE
WRITE(9)(FMACHC(I),XC(I),YC(I),I=1,LINE)
RETURN
END

ENTRY      UN09.
UN09. PZE  UN109
UN109 FILE  B(1),OUTPUT,BLOCK=256,BIN,HOLD
END

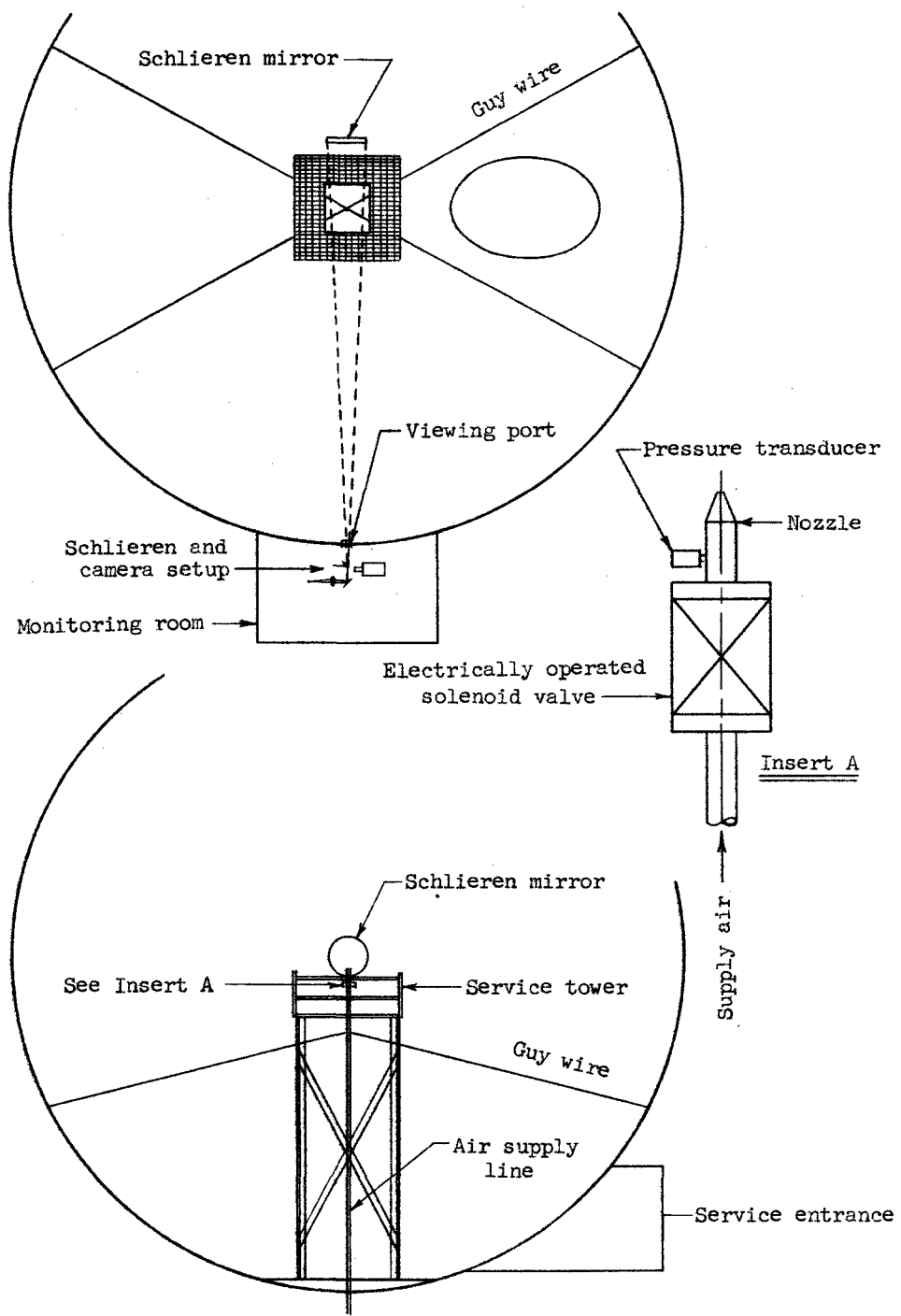
```

REFERENCES

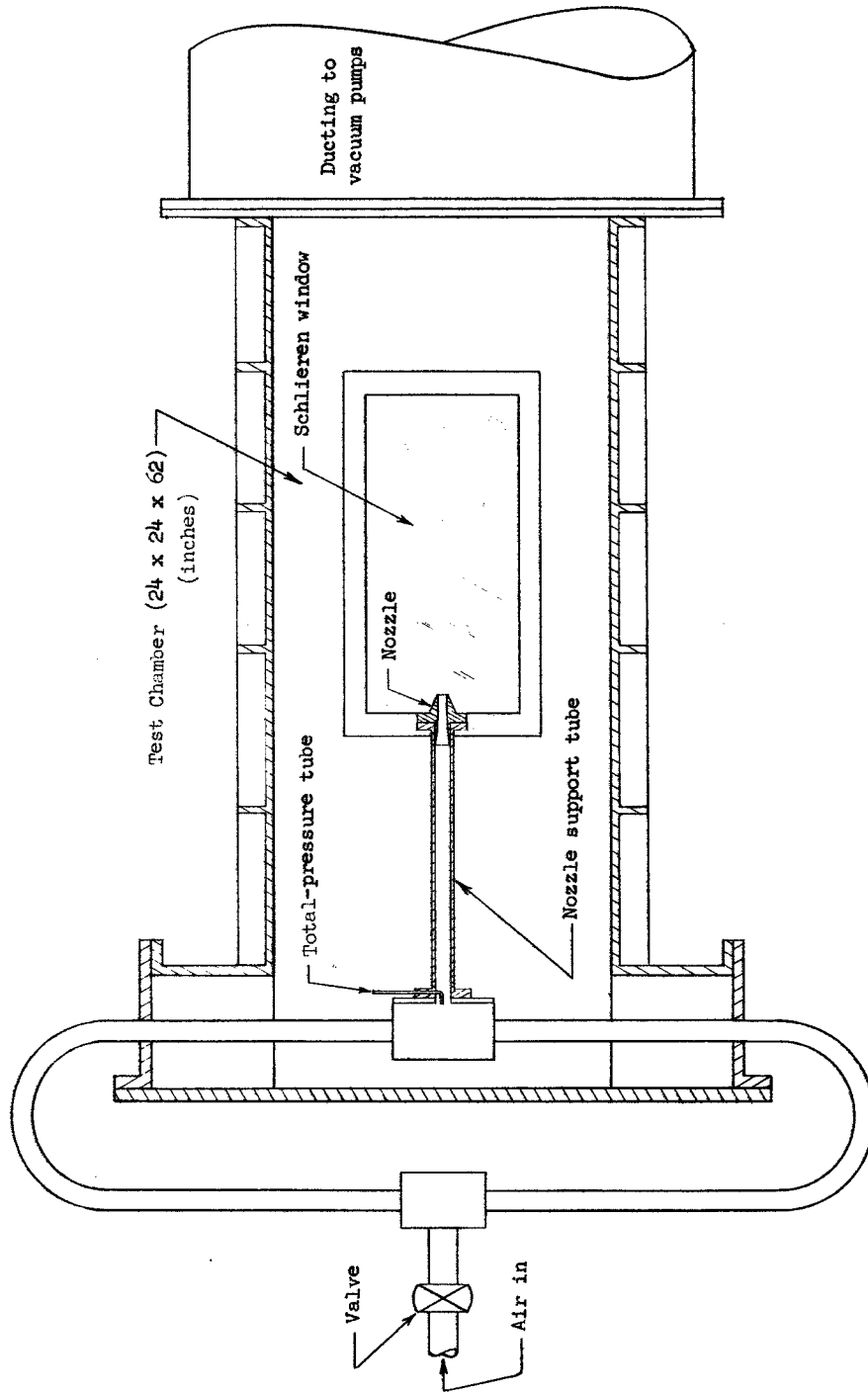
1. Fetterman, David E., Jr.: Effects of Simulated Rocket-Jet Exhaust on Stability and Control of a Research-Type Airplane Configuration at a Mach Number of 6.86. NASA TM X-127, 1959.
2. Salmi, Reino J.: Effects of Jet Billowing on Stability of Missile-Type Bodies at Mach 3.85. NASA TN D-284, 1960.
3. Falanga, Ralph A., Hinson, William F., and Crawford, Davis H.: Exploratory Tests of the Effects of Jet Plumes on the Flow Over Cone-Cylinder-Flare Bodies. NASA TN D-1000, 1962.
4. Hinson, William F., and Falanga, Ralph A.: Effect of Jet Plumbing on the Static Stability of Cone-Cylinder-Flare Configurations at a Mach Number of 9.65. NASA TN D-1352, 1962.
5. Peters, Tom, Christenson, R. J., and Dawson, J. G., Jr.: Impingement Effects of a Model SLV-5 Second-Stage Jet Plume on the First-Stage Booster Cases at Altitudes From 65,000 to 91,000 Ft. AEDC-TDR-63-7, Arnold Eng. Dev. Center, Mar. 1963.
6. Bauer, R. C., and Schlumpf, R. L.: Experimental Investigation of Free Jet Impingement on a Flat Plate. AEDC-TN-60-223. (Contract No. AF 40(600)-800 S/A 11(60-110)), Arnold Eng. Dev. Center, Mar. 1961.
7. Margolin, E. L., and Welch, Eugene: Final Report - Single Nozzle Jet Plume Test in the Rocket Nozzle Test Facility. SID 63-426, North American Aviation, Inc., May 6, 1963.
8. Vick, Allen R., and Andrews, Earl H., Jr.: An Experimental Investigation of Highly Underexpanded Free Jets Impinging Upon a Parallel Flat Surface. NASA TN D-2326, 1964.
9. Balwanz, W. W., and Weston, J. P.: The Prediction of Rocket Exhaust Interference With Radio Signals. [Preprint] 2591-62, American Rocket Soc., Oct. 1962.
10. McIver, Duncan E., Jr.: Study of the Effects of a Rocket Exhaust on Radio Frequency Signal Attenuation by the Use of a Recoverable Camera on the NASA Scout Vehicle. NASA TM X-888, 1963.
11. Calcote, H. F., and Silla, H.: Radar Attenuation in Solid Propellant Rocket Exhausts. Bull. 18th Meeting JANAF-ARPA-NASA Solid Propellant Group, Vol. III, June 1962, pp. 3-50.
12. Tuthill, C. M., Jr.: Altitude Evaluation of Radio Frequency Attenuation in the Exhaust Jet of the XLR91-AJ-5 Engine. AEDC-TDR-62-160 (Contract No. AF 40(600)-1000), Arnold Eng. Dev. Center, Aug. 1962.

13. Stitt, Leonard E.: Interaction of Highly Underexpanded Jets With Simulated Lunar Surfaces. NASA TN D-1095, 1961.
14. Stitt, Leonard E., and Latto, William T., Jr.: Highly Underexpanded Exhaust Jets Against Adjacent Surfaces. *Astronautics and Aerospace Eng.*, vol. 1, no. 1, Feb. 1963, pp. 107-110.
15. Spady, Amos A., Jr.: An Exploratory Investigation of Jet-Blast Effects on a Dust-Covered Surface at Low Ambient Pressure. NASA TN D-1017, 1962.
16. Roberts, Leonard: The Action of a Hypersonic Jet on a Dust Layer. Paper No. 63-50, *Inst. Aerospace Sci.*, Jan. 1963.
17. Eastman, Donald W., and Radtke, Leonard P.: Flow Field of an Exhaust Plume Impinging on a Simulated Lunar Surface. *AIAA Jour. (Tech. Notes and Comments)*, vol. 1, no. 6, June 1963, pp. 1430-1431.
18. Love, Eugene S., Grigsby, Carl E., Lee, Louise P., and Woodling, Mildred J.: Experimental and Theoretical Studies of Axisymmetric Free Jets. NASA TR R-6, 1959. (Supersedes NACA RM L54L31 by Love and Grigsby, RM L55J14 by Love, RM L56G18 by Love, Woodling, and Lee, and TN 4195 by Love and Lee.)
19. Latvala, E. K.: Spreading of Rocket Exhaust Jets at High Altitudes. AEDC-TR-59-11, ASTIA Doc. No. AD-215866 (Contract No. AF 40(600)-700 S/A 13(59-1)), Arnold Eng. Dev. Center, June 1959.
20. Wang, C. J., and Peterson, J. B.: Spreading of Supersonic Jets From Axially Symmetric Nozzles. [Preprint] 462-57, *American Rocket Soc.*, June 1957.
21. Henson, J. R., and Robertson, J. E.: Methods of Approximating Inviscid Jet Boundaries for Highly Underexpanded Supersonic Nozzles. AEDC-TDR-62-7 (Contract No. AF 40(600)-800 S/A 24(61-73)), Arnold Eng. Dev. Center, May 1962.
22. Tempelmeyer, K. E., and Dicks, J. B.: Some Gas Dynamic Characteristics of Argon Plasma - Application to Jet Spreading. AEDC-TDR-62-88 (Contract No. AF 40(600)-1000), Arnold Eng. Dev. Center, July 1962.
23. Owen, P. L., and Thornhill, C. K.: The Flow in an Axially-Symmetric Supersonic Jet From a Nearly-Sonic Orifice into a Vacuum. R. & M. No. 2616, *British A.R.C.*, 1952.
24. Woodley, J. G.: Measurement of the Flow Field of an Underexpanded Jet in a Hypersonic External Stream ($M_{\infty} = 6.8$). Tech. Note No. Aero. 2733, *British R.A.E.*, Dec. 1960.
25. Sergeant, R. J.: Scale Atlas Vernier Rocket Flame Expansion Studies. Rep. RT 59-105, CONVAIR, June 30, 1960.

26. Bowyer, J. M., Jr.: Determination of the Envelopes and the Lines of Constant Mach Number for an Axially Symmetric Free Jet. ZJ-7-054 (Contract No. AF 04(645)-4), Convair-Astronautics, Mar. 14, 1958.
27. Tjonneland, Elling: Graphical Presentation of Constant Mach Lines and Envelopes of the Exhaust Jet From a Rocket Engine With a Conical 5:1 Nozzle and a Chamber Pressure of 346 psia, Expanding into a Quiescent, Supersonic or Hypersonic Coaxial Free Stream of Various Altitudes. AA-E-117, Convair/Astronautics, Nov. 6, 1958.
28. Ames Research Staff: Equations, Tables, and Charts for Compressible Flow. NACA Rep. 1135, 1953. (Supersedes NACA TN 1428.)
29. Wang, C. J., Peterson, J. B., and Anderson, R.: Gas Flow Tables. GM-TR-154, Space Tech. Labs., Inc., Mar. 14, 1957. (Available from ASTIA as AD No. 221012.)
30. Tempelmeyer, K. E., and Sheraden, G. H.: Compressible Flow Tables for Gases With Specific Heat Ratios From 1.10 to 1.28. AEDC-TN-58-9, ASTIA Doc. No. AD-152041, Arnold Eng. Dev. Center, Mar. 1958.
31. McCracken, Daniel D.: A Guide to FORTRAN Programming. John Wiley & Sons, Inc., c.1961.
32. Ferri, Antonio: Elements of Aerodynamics of Supersonic Flows. The Macmillan Co., 1949.

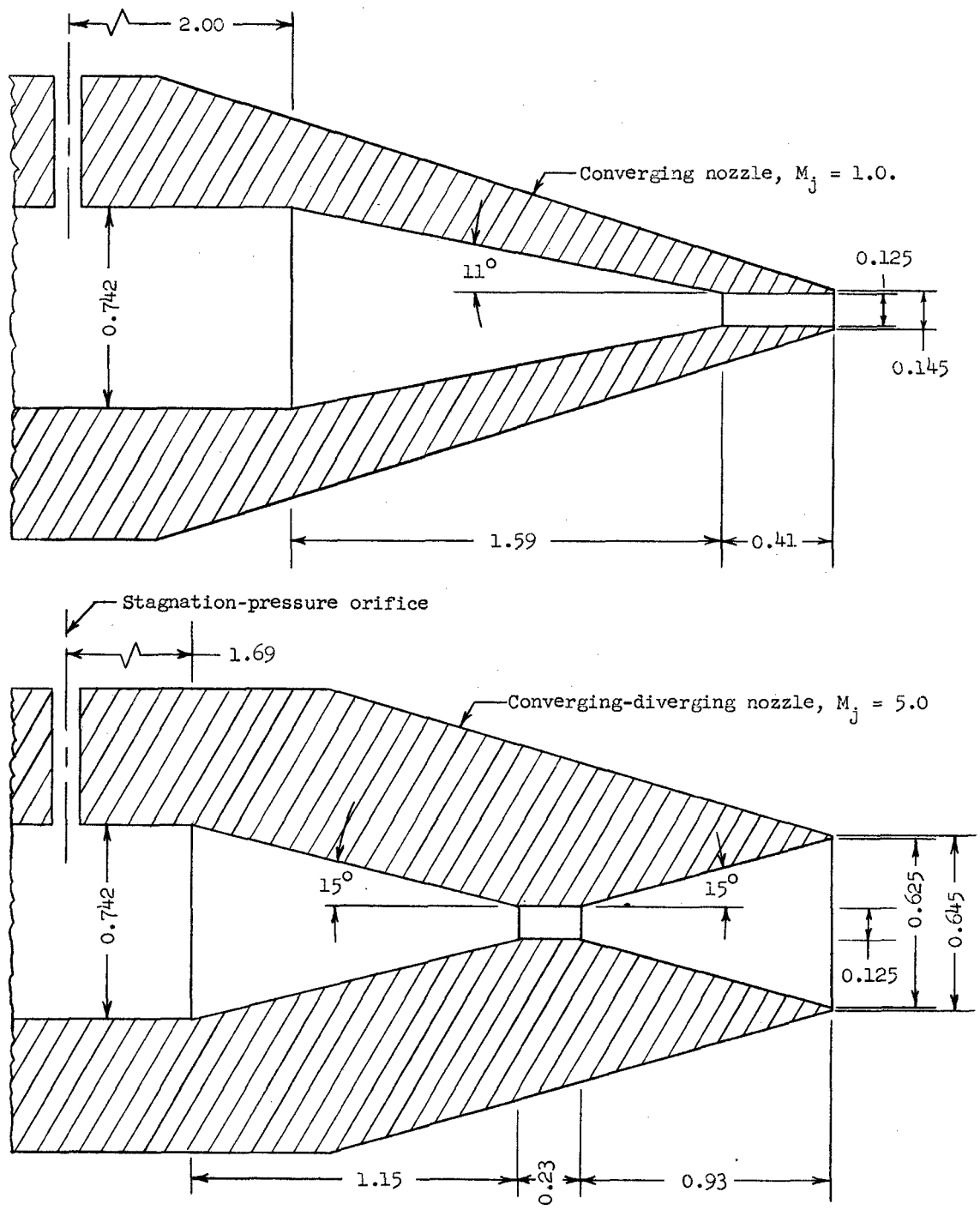


(a) Test setup in 41-foot vacuum sphere.
 Figure 1.- Schematics of test facilities.



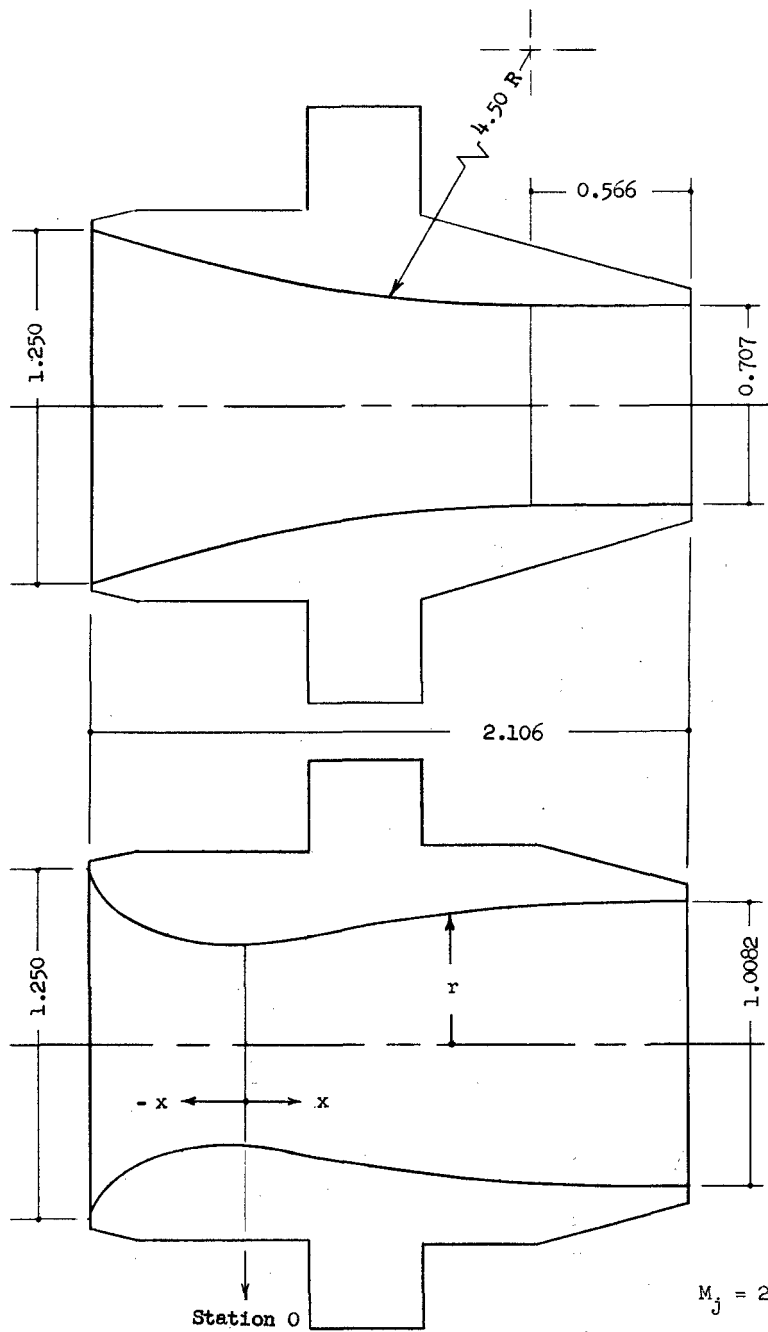
(b) Test chamber for low-pressure-ratio tests.

Figure 1.- Concluded.



(a) $M_j = 1.0$ and $M_j = 5.0$.

Figure 2.- Test nozzles.



$M_j = 1.0$

Nozzle coordinates

$M_j = 2.22$

x	r (Radius)
-.5430	.6250
-.5200	.5469
-.4900	.5080
-.4500	.4724
-.3000	.3987
-.1500	.3640
0.0000	.3535
.0354	.3570
.0707	.3623
.1414	.3747
.2828	.3995
.4242	.4242
.5656	.4461
.7070	.4638
.9191	.4850
1.1312	.4977
1.3433	.5027
1.5625	.5041

$M_j = 2.22$

(b) Contoured nozzles. All dimensions in inches.

Figure 2.- Concluded.

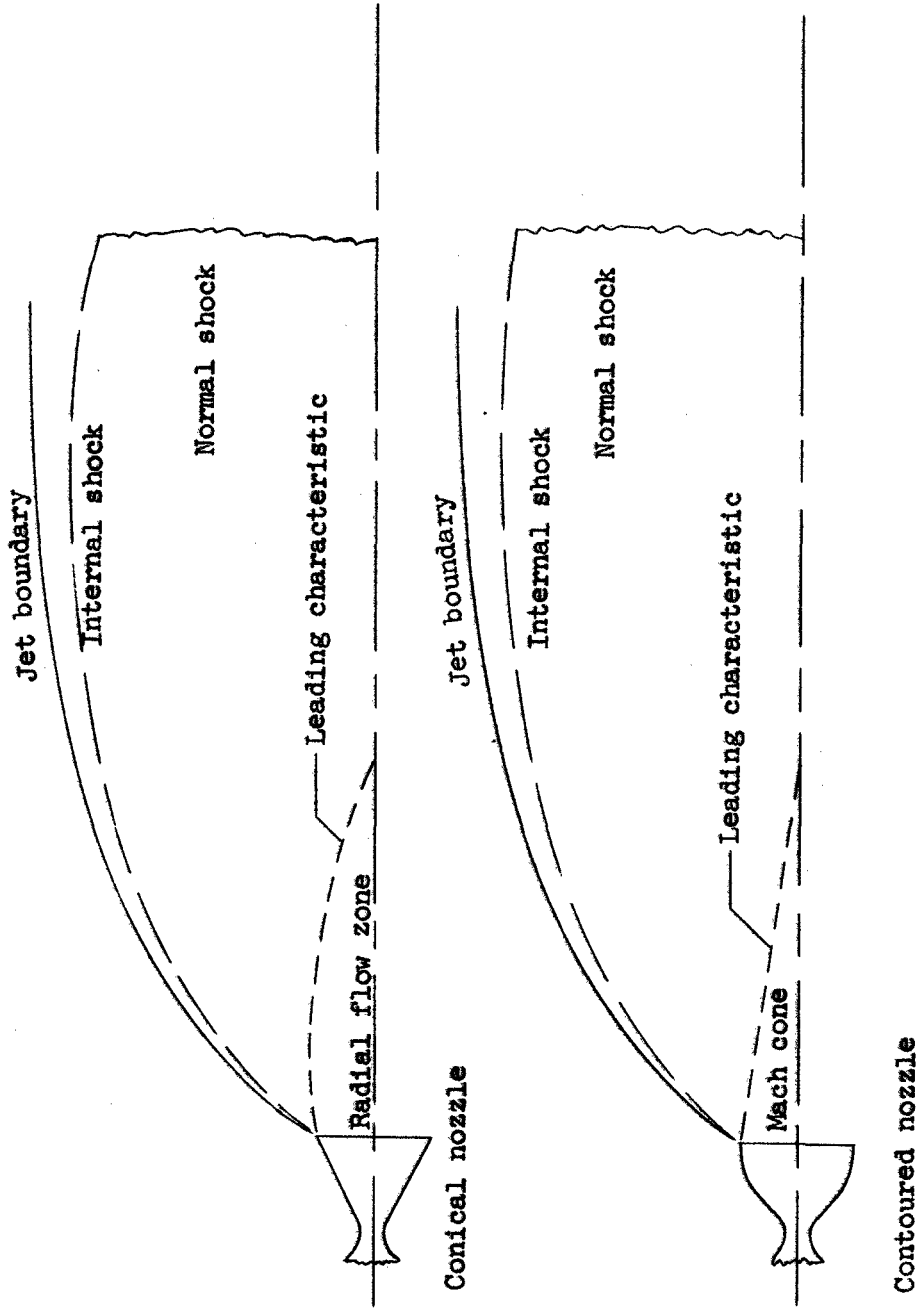
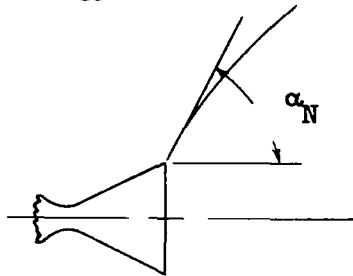


Figure 3.-- General description of exhaust jet.

FACTORS AFFECTING ROCKET EXHAUST SIZE AND SHAPE

- M_j Nozzle-exit Mach number
- θ_N Nozzle half-angle
- γ Ratio of specific heats
- p_j Static pressure at nozzle exit
- p_{∞} Ambient static pressure



$$\alpha_N = \nu_1 - \nu_N + \theta_N$$

where

- ν_1 Prandtl-Meyer expansion angle for boundary Mach number
- ν_N Prandtl-Meyer expansion angle for nozzle-exit Mach number

Figure 4.- Method of calculating initial turning angle of jet boundary at the nozzle lip.

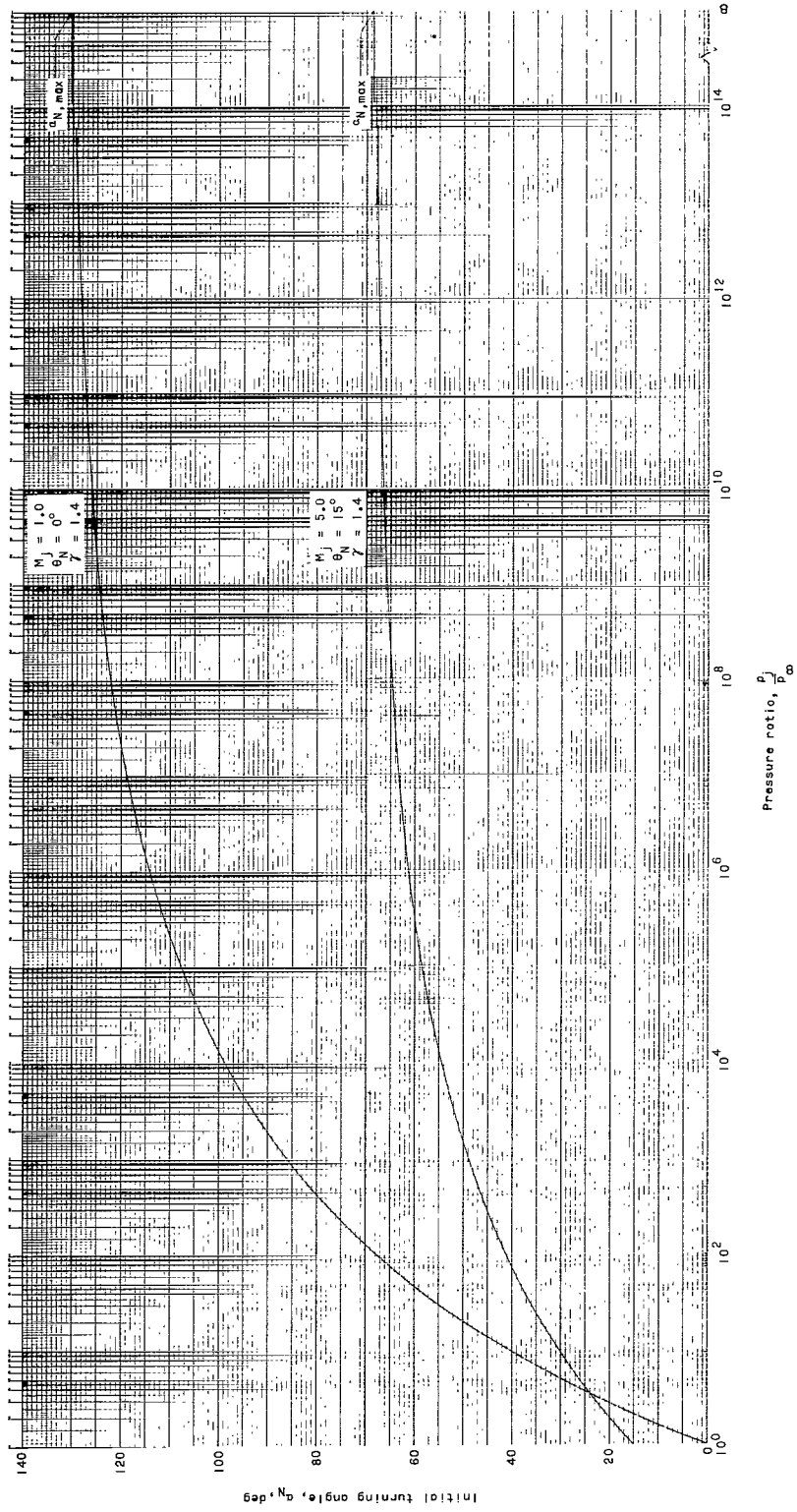


Figure 5.- Variation of initial turning angle with pressure ratio.

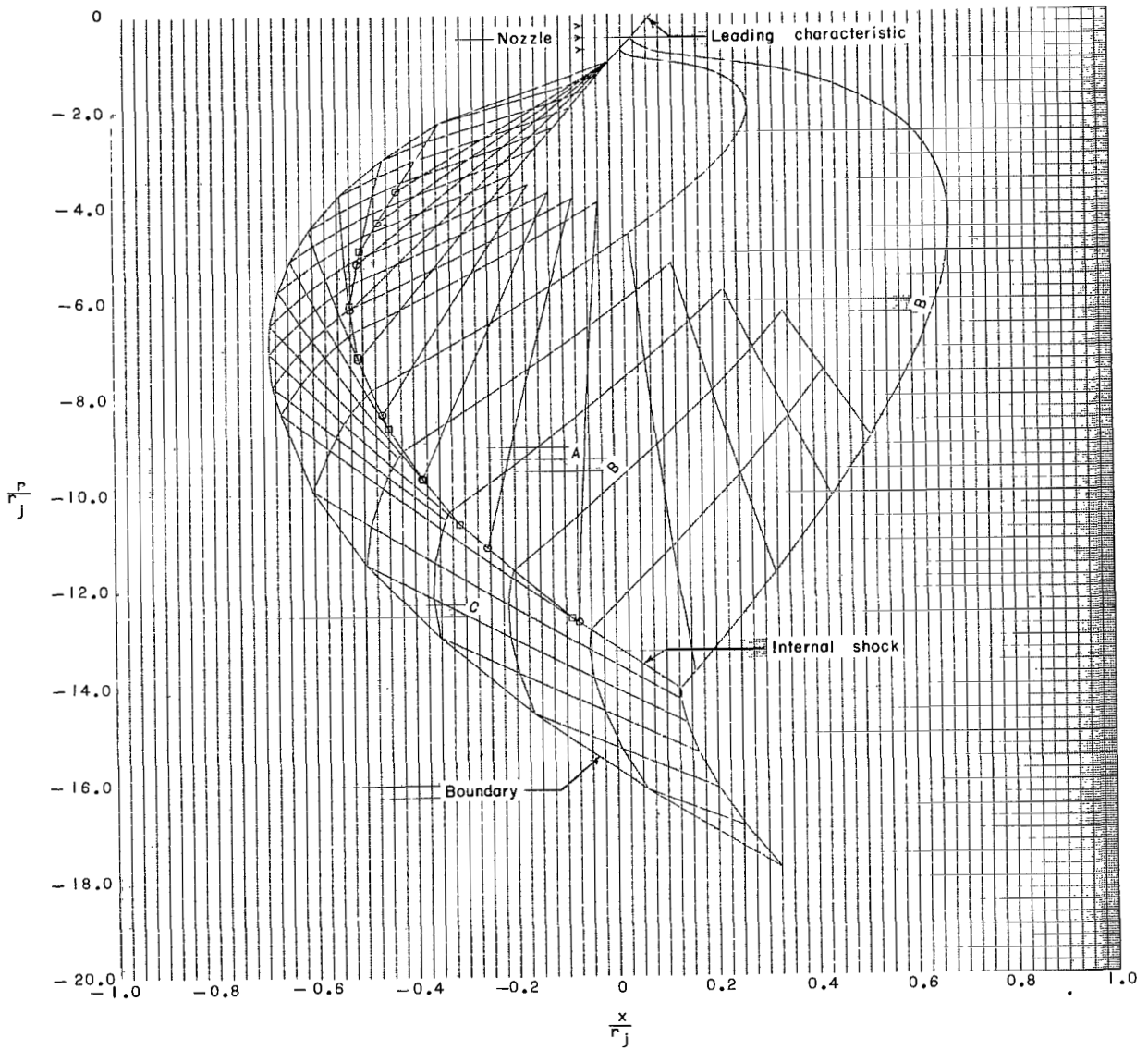


Figure 6.- Sketch of modified characteristic network obtained by eliminating foldback.

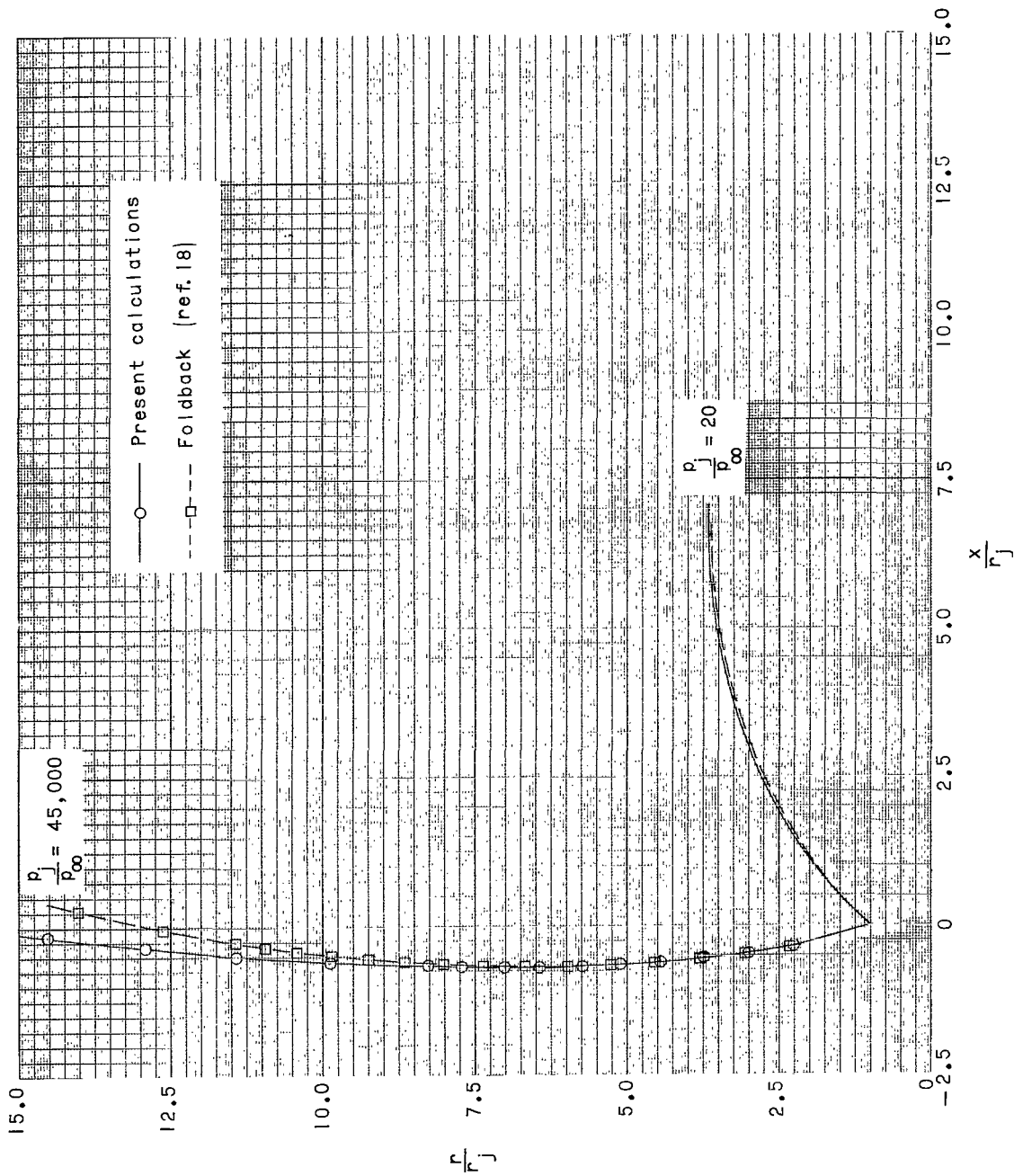
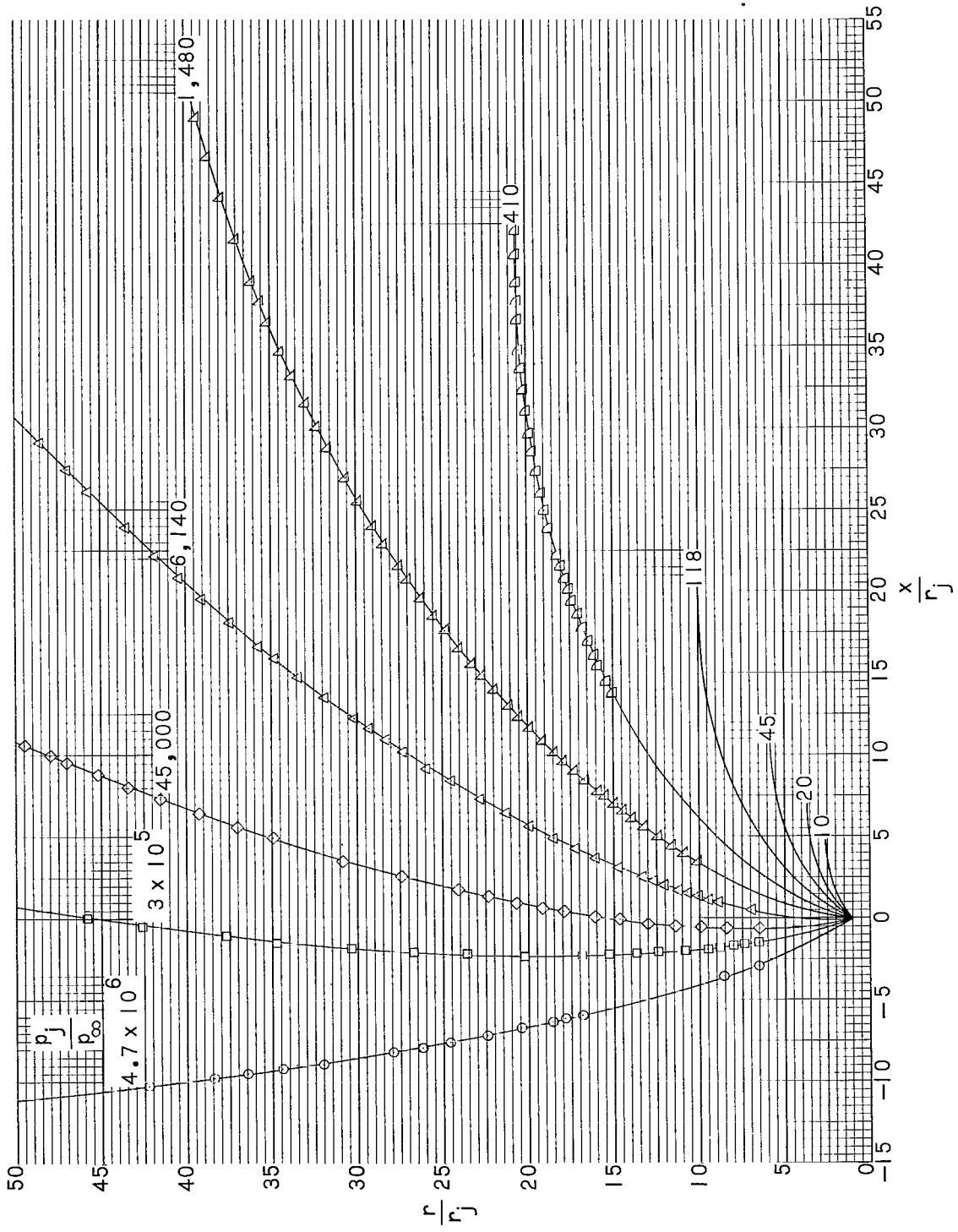
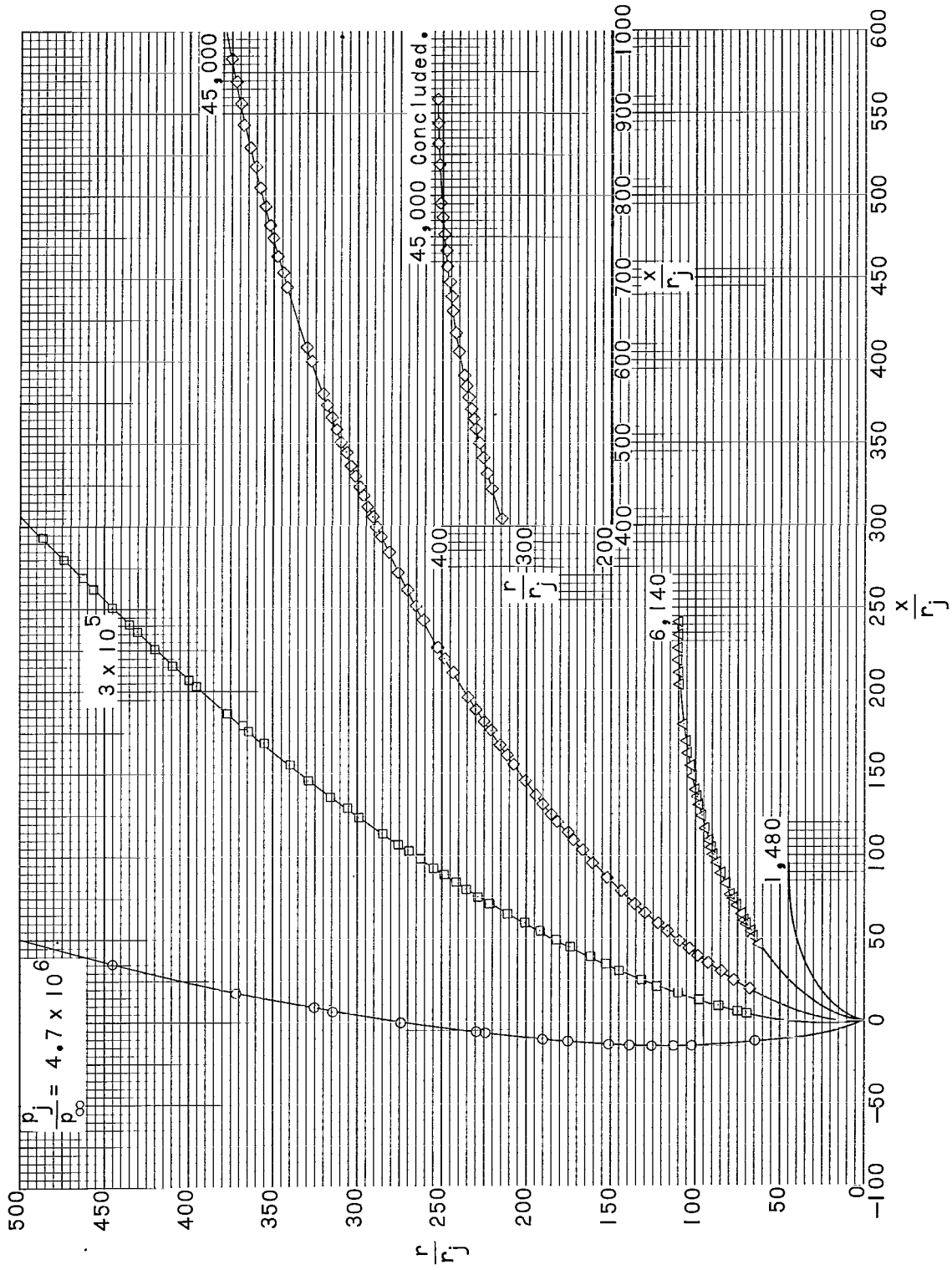


Figure 7.- Comparison of jet boundary coordinates for foldback procedure with those for modified method in which foldback is eliminated. $M_j = 1.0$.



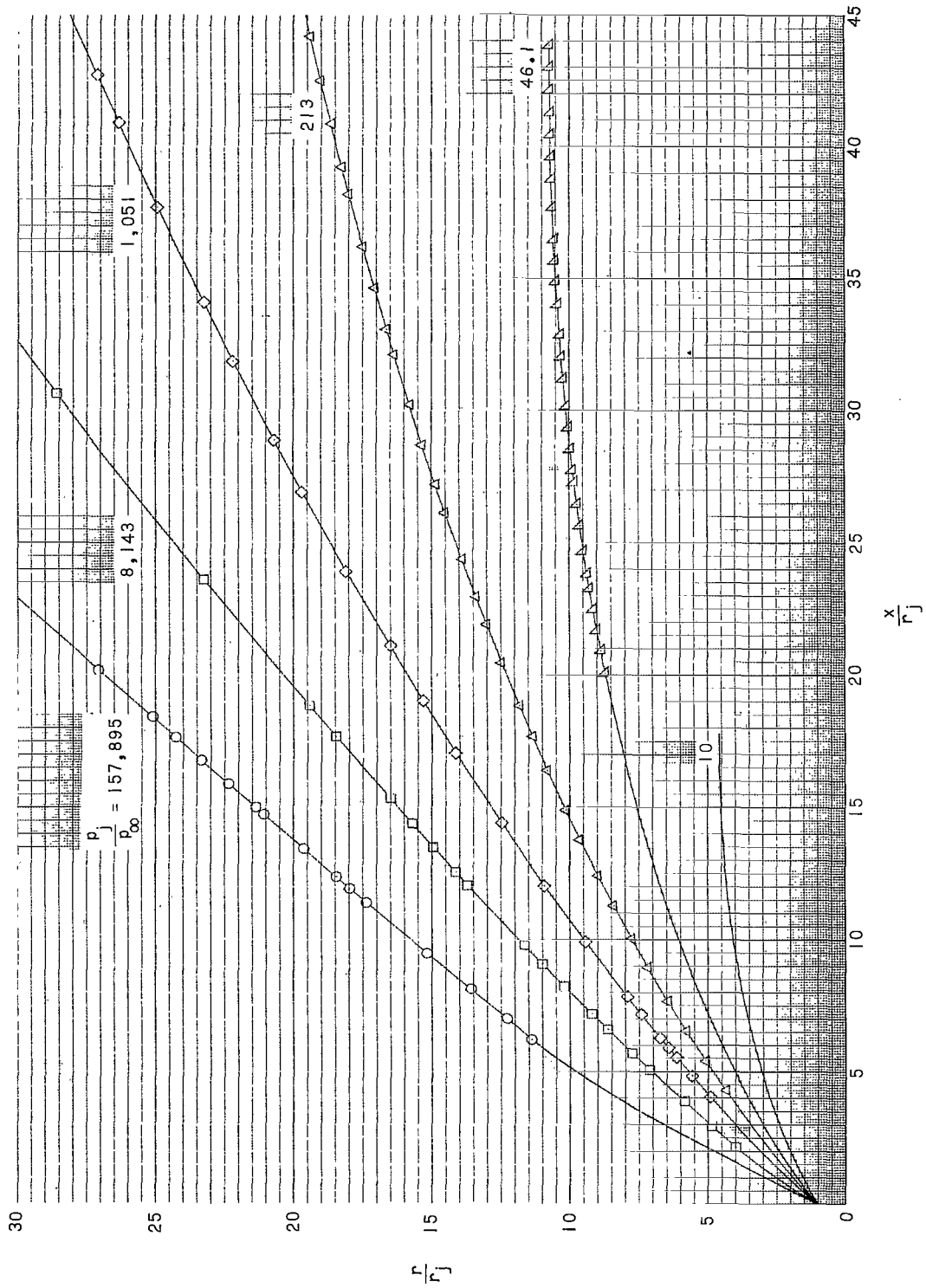
(a) Expanded scale showing boundaries near nozzle exit for $M_j = 1.0$, $\theta_N = 0^\circ$.

Figure 8.- Jet boundary coordinates calculated by characteristic method for various pressure ratios.



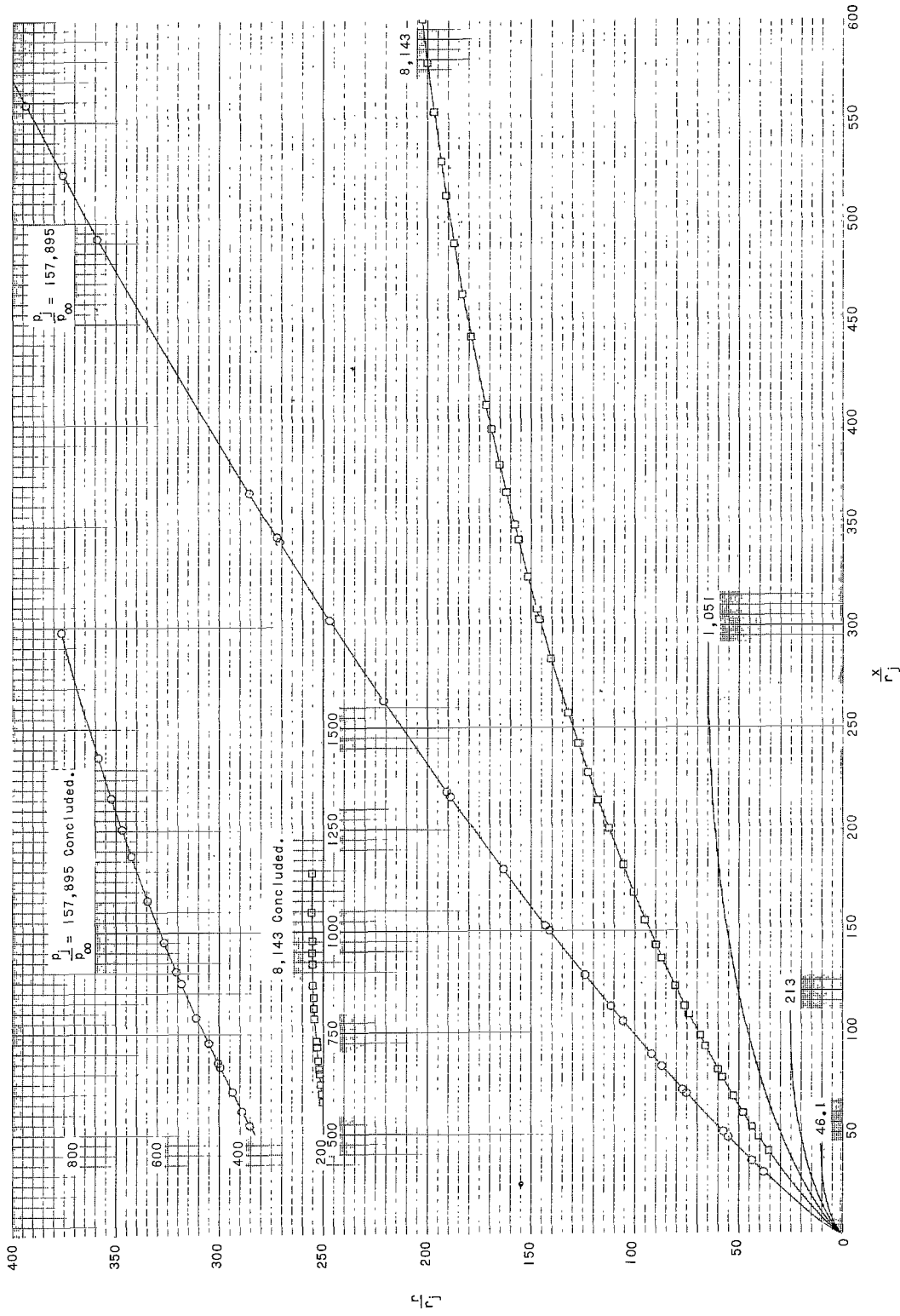
(b) Complete boundaries for $M_j = 1.0$, $\theta_W = 0^\circ$.

Figure 8.- Continued.



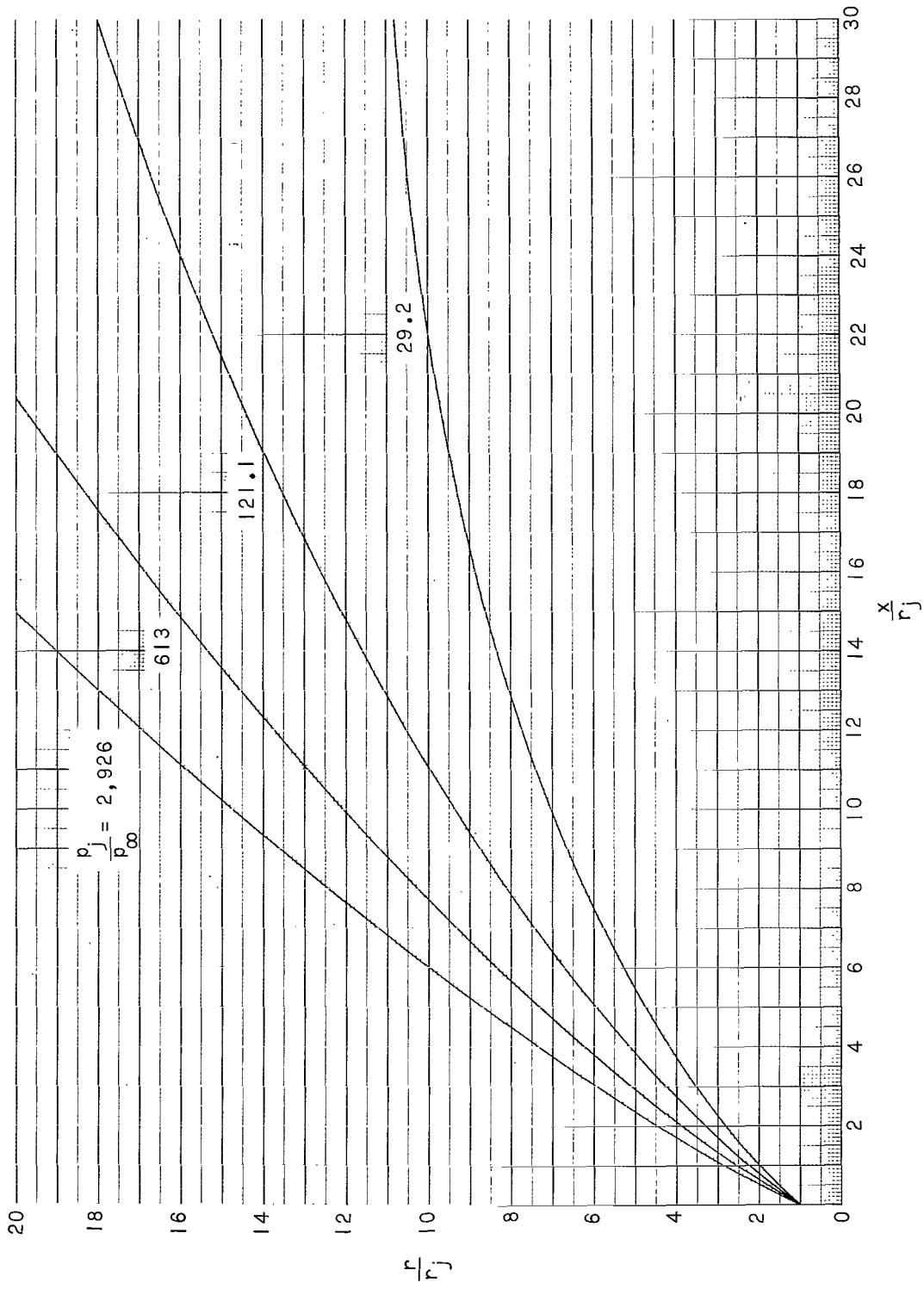
(c) Expanded scale showing boundaries near nozzle exit for $M_j = 5.0$. $\theta_N = 15^\circ$.

Figure 8.- Continued.



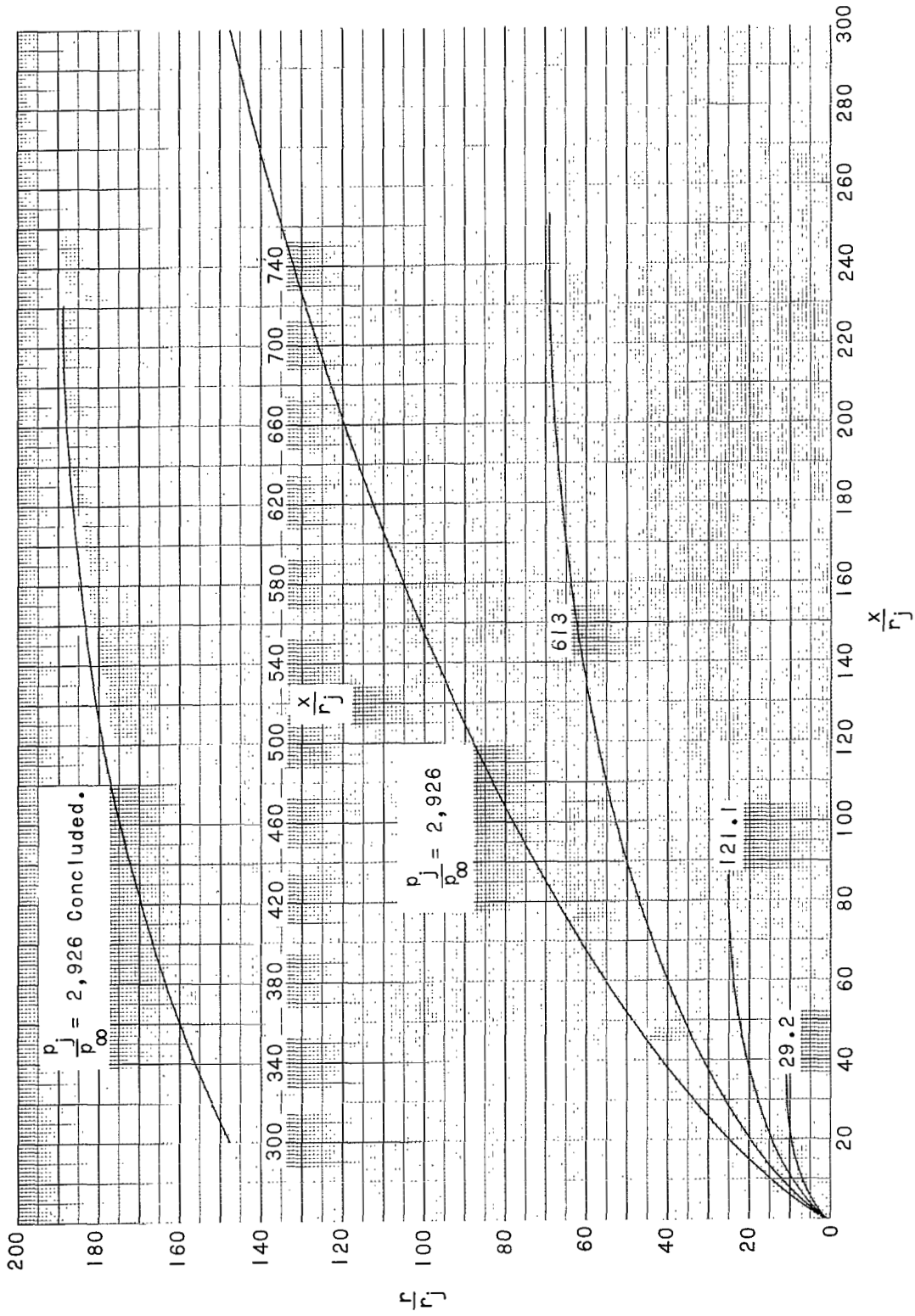
(d) Complete boundaries for $M_j = 5.0$. $\theta_N = 15^\circ$.

Figure 8.- Continued.



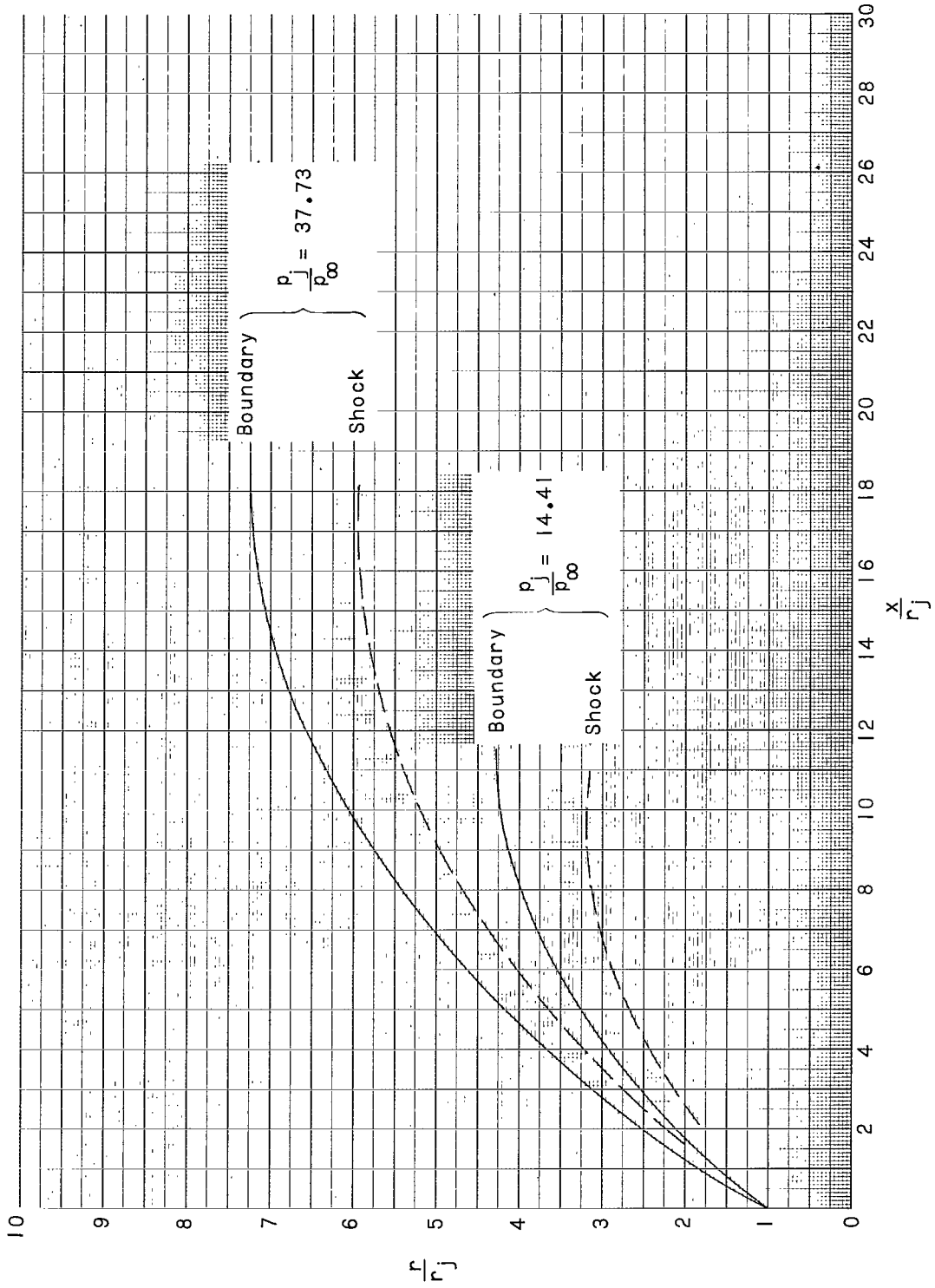
(e) Expanded scale near nozzle exit for $M_j = 4.79$. $\theta_N = 26.5^\circ$.

Figure 8.- Continued.



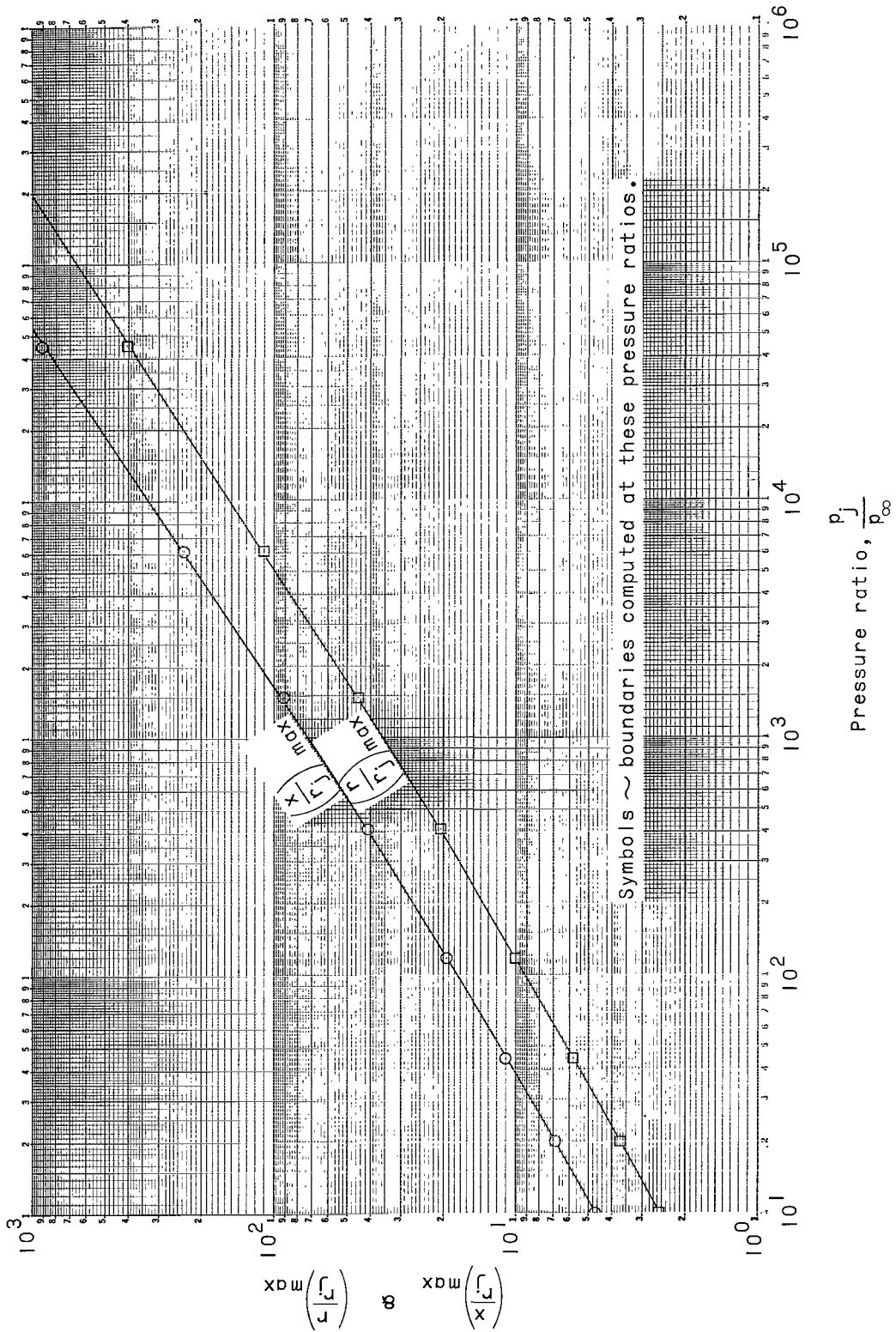
(f) Complete boundaries for $M_j = 4.79$. $\theta_N = 26.5^\circ$.

Figure 8.- Continued.



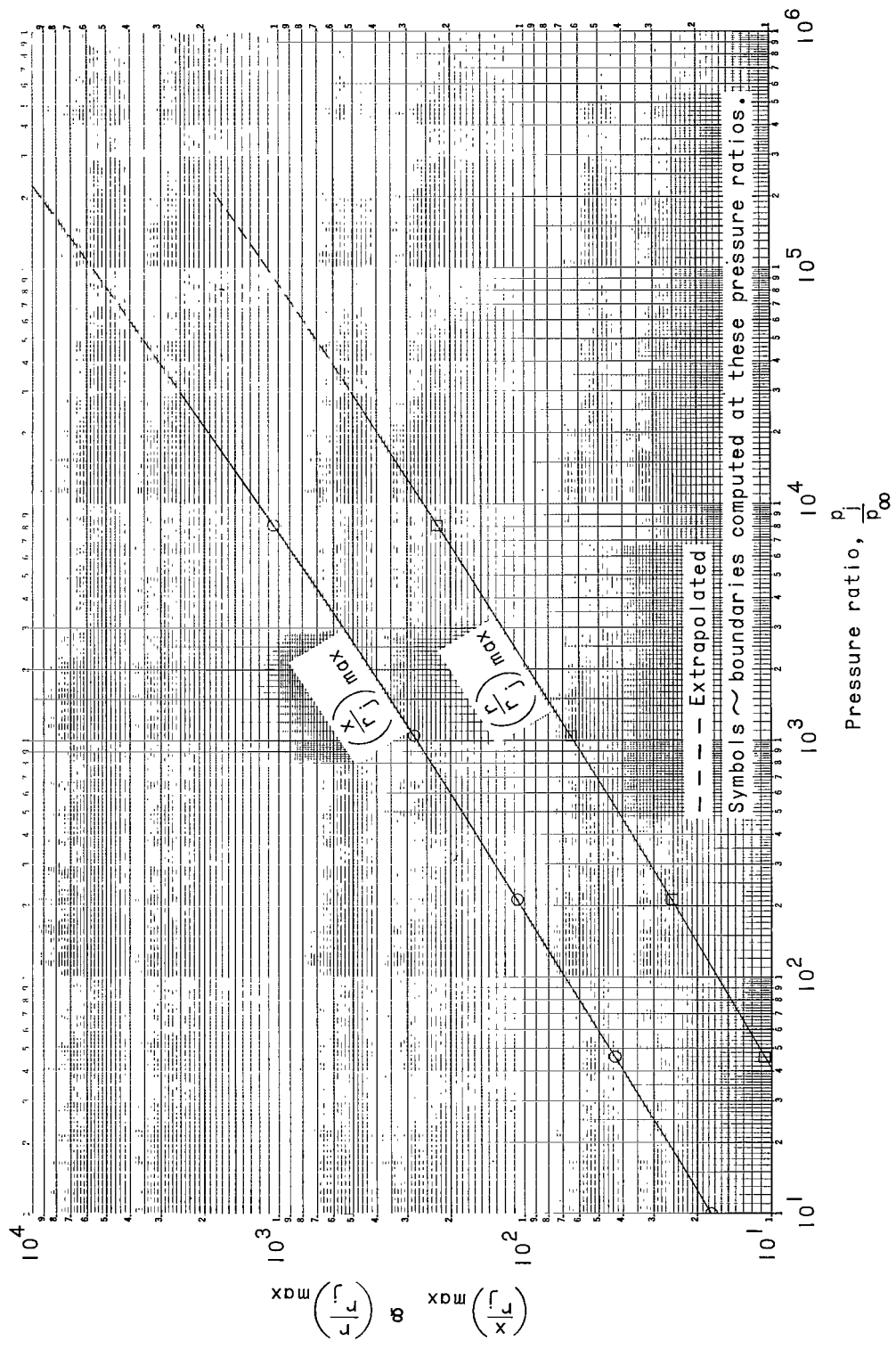
(g) Jet boundaries and internal shocks for $M_j = 2.22$, $\theta_N = 0^\circ$.

Figure 8.- Concluded.



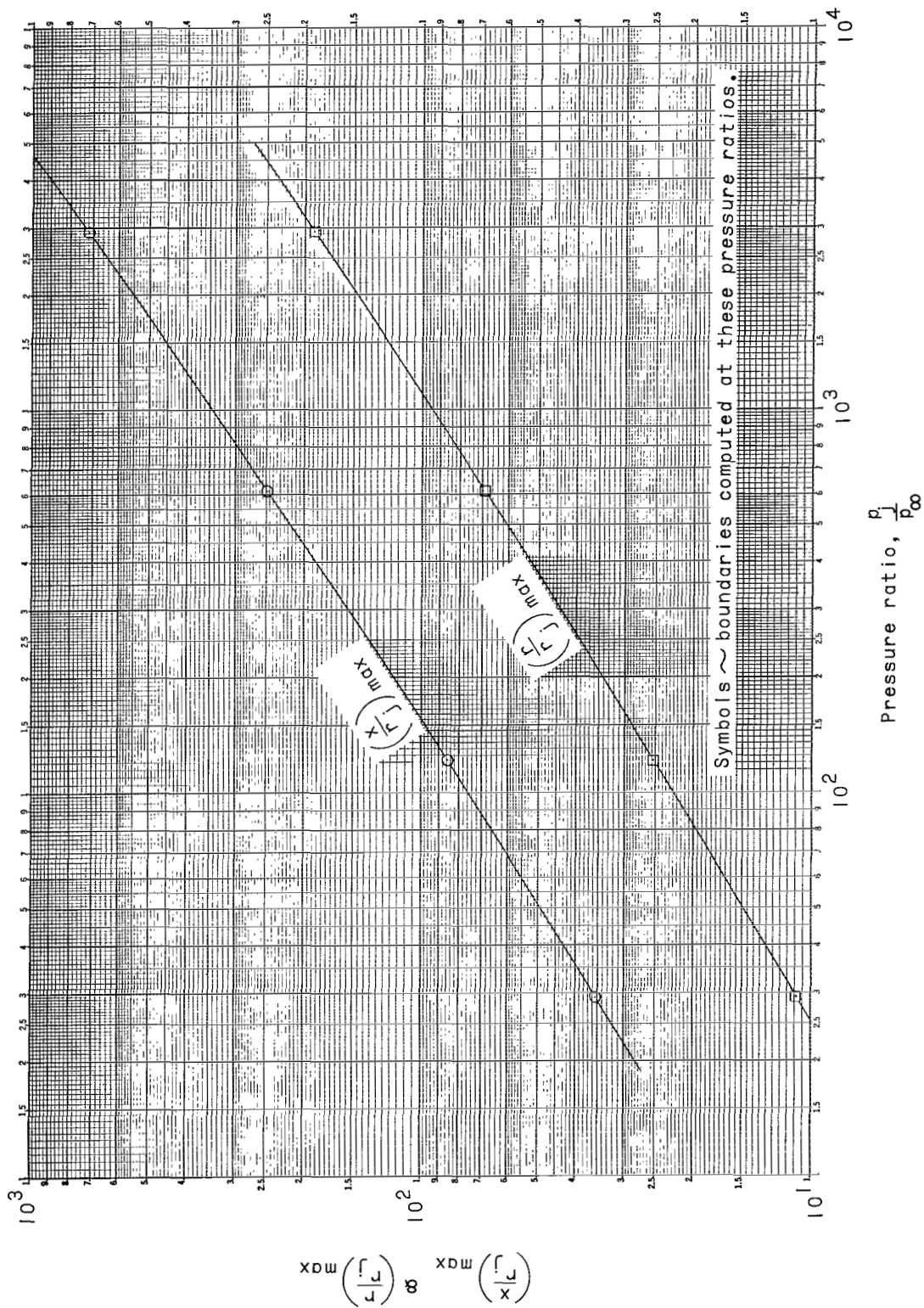
(a) $M_j = 1.0$; $\theta_N = 0^\circ$; $\gamma = 1.4$.

Figure 9.- Location of maximum jet exhaust boundary coordinates in terms of nozzle radius.



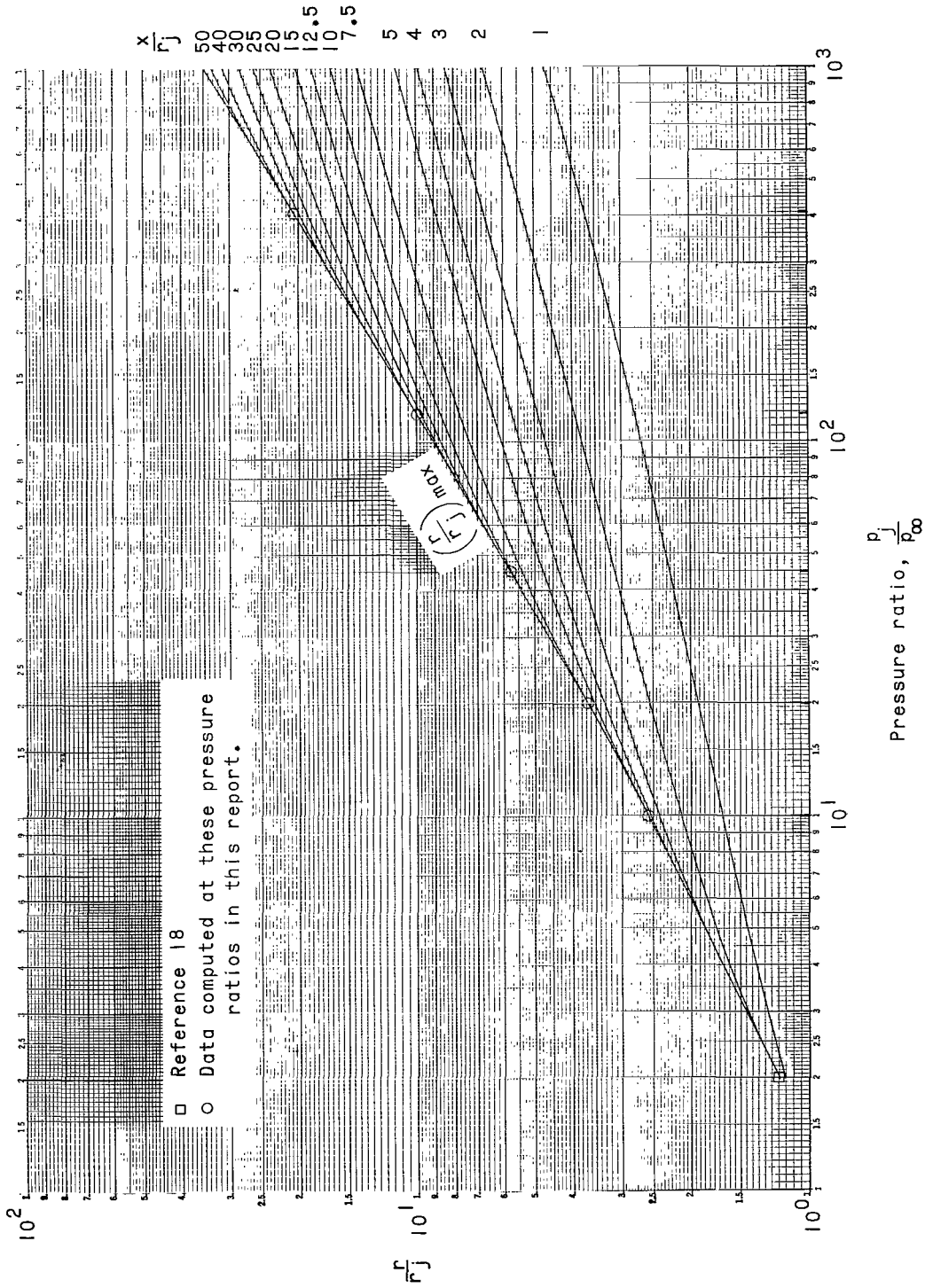
(b) $M_j = 5.0$; $\theta_N = 15^\circ$; $\gamma = 1.4$.

Figure 9.- Continued.



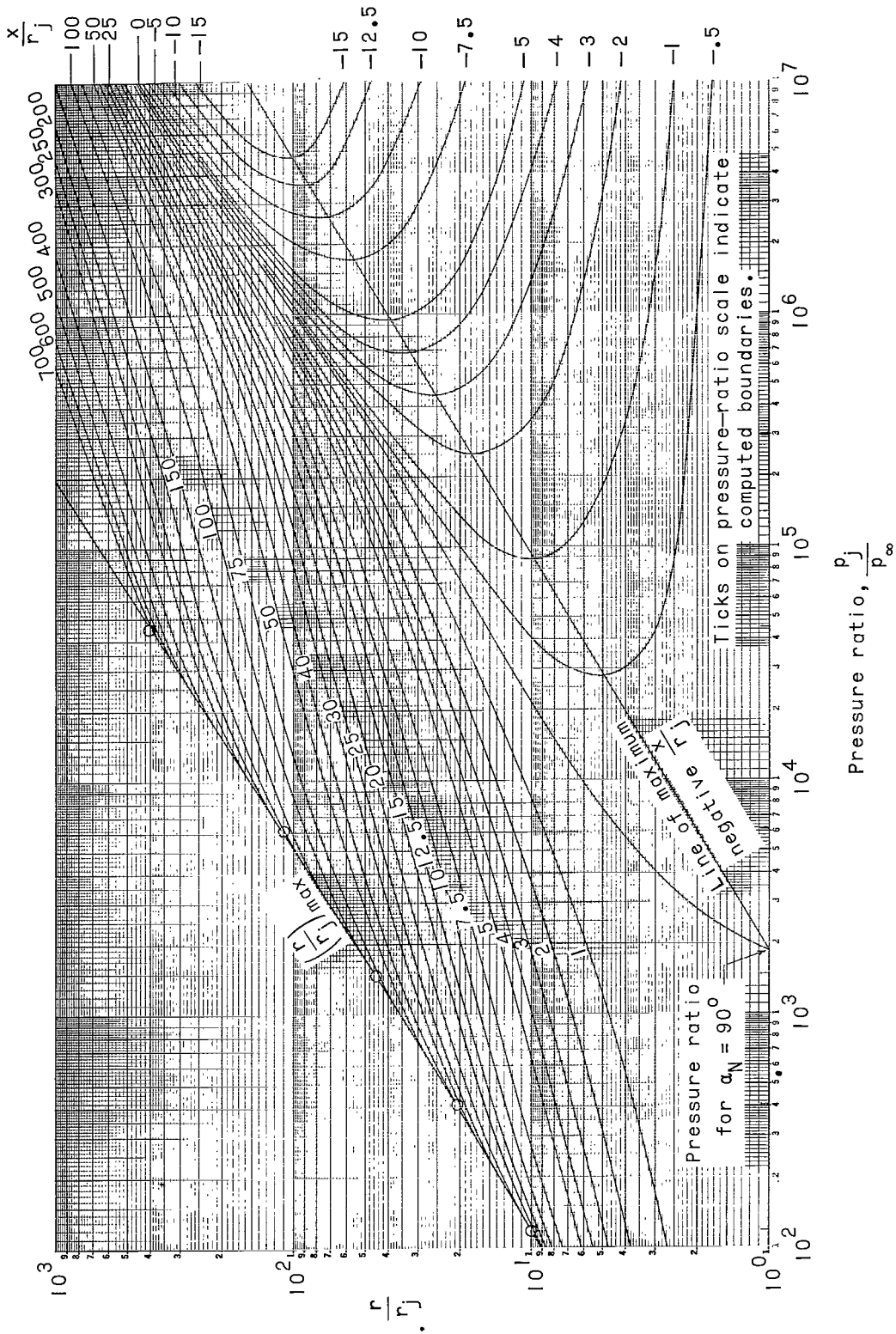
(c) $M_j = 4.79$; $\theta_N = 26.5^\circ$; $\gamma = 1.4$.

Figure 9.- Concluded.



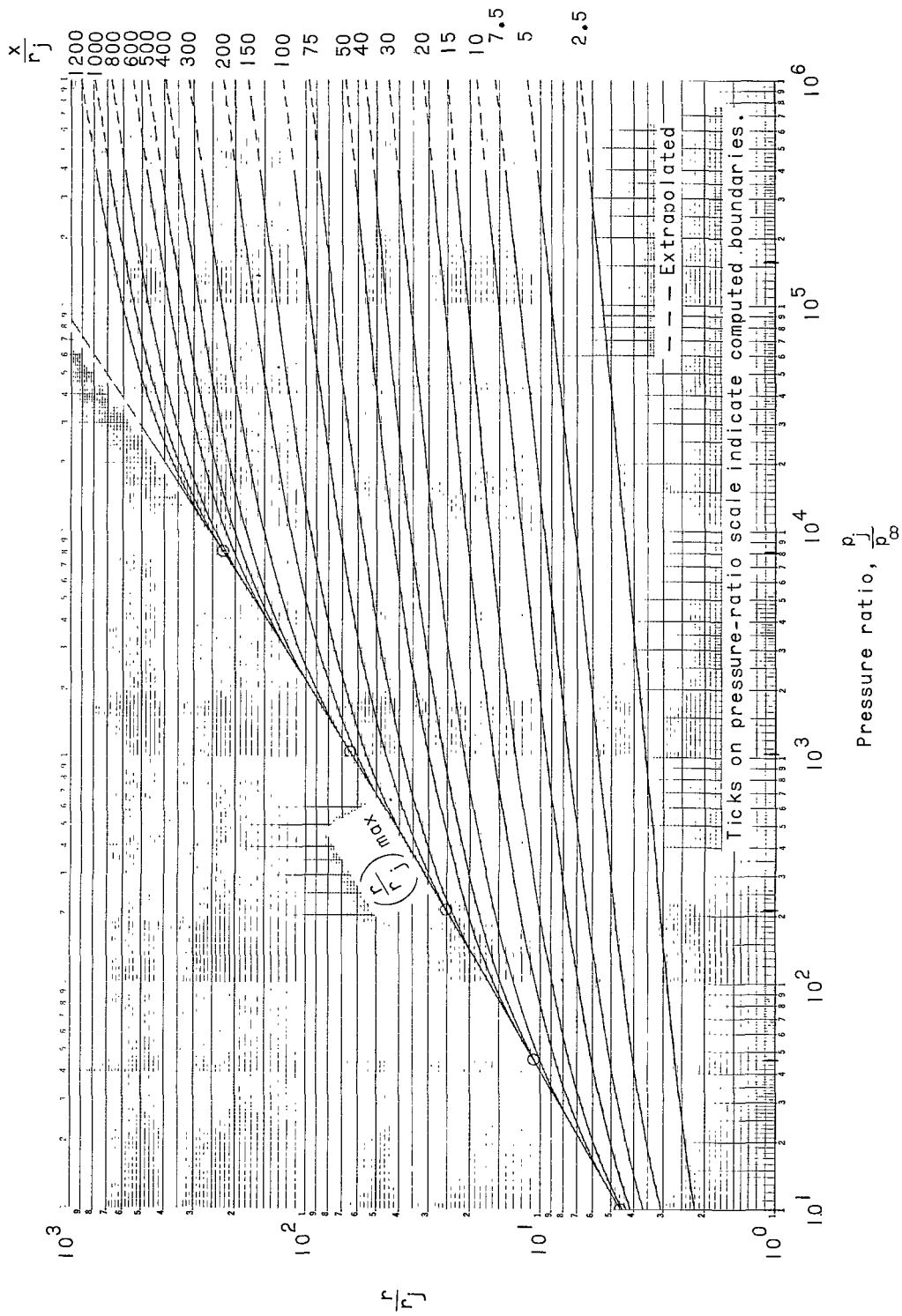
(a) $M_j = 1.0$; $\theta_N = 0^\circ$; $\gamma = 1.4$.

Figure 10.- Cross plot of jet boundaries from figure 8 at constant values of x/r_j to facilitate construction of boundaries at any intermediate pressure ratios.



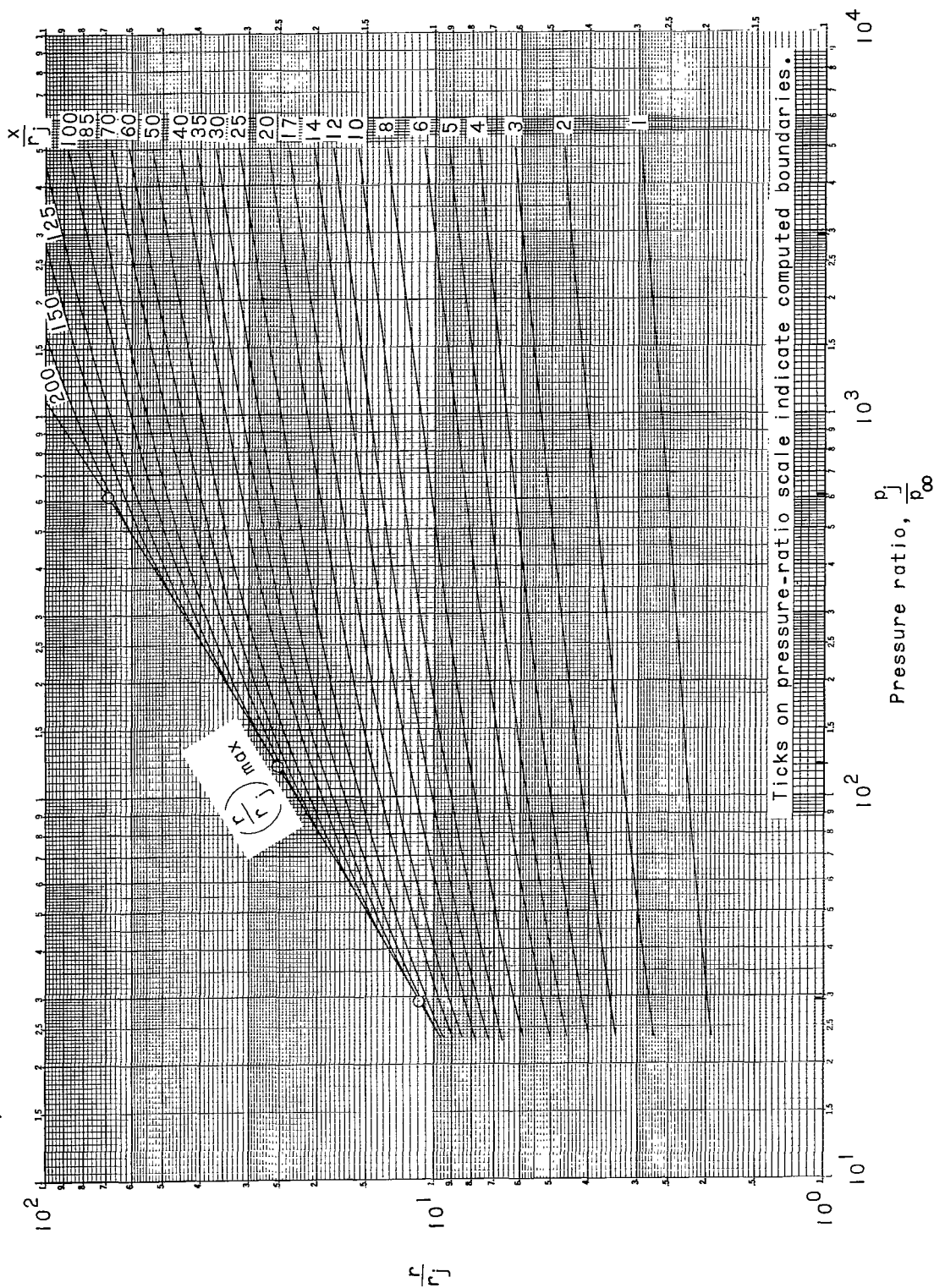
(a) $M_j = 1.0$; $\theta_N = 0^\circ$; $\gamma = 1.4$. Concluded.

Figure 10.- Continued.



(b) $M_j = 5.0$; $\theta_N = 15^\circ$; $\gamma = 1.4$.

Figure 10.- Continued.



(c) $M_j = 4.79$; $\theta_M = 26.5^\circ$; $\gamma = 1.4$.

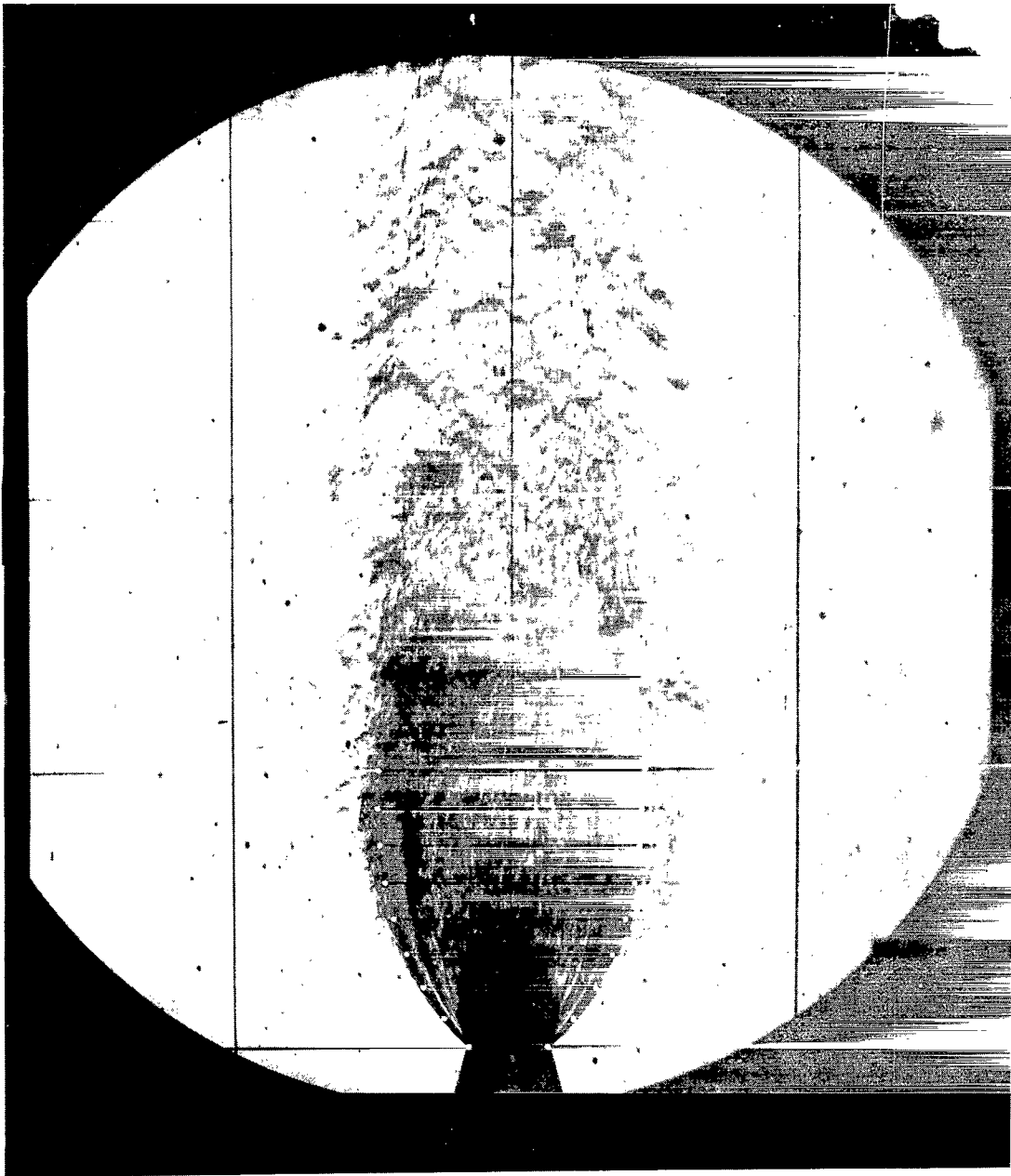
Figure 10.- Concluded.



(a) $M_j = 1.0$; $\theta_N = 0^\circ$; $p_j/p_\infty = 11.5$.

Figure 11.- Schlieren photographs of jet exhaust plumes with superimposed theoretical boundaries.

L-64-390



(b) $M_j = 1.0$; $\theta_N = 0^\circ$; $P_j/P_\infty = 20.9$.

Figure 11.- Continued.

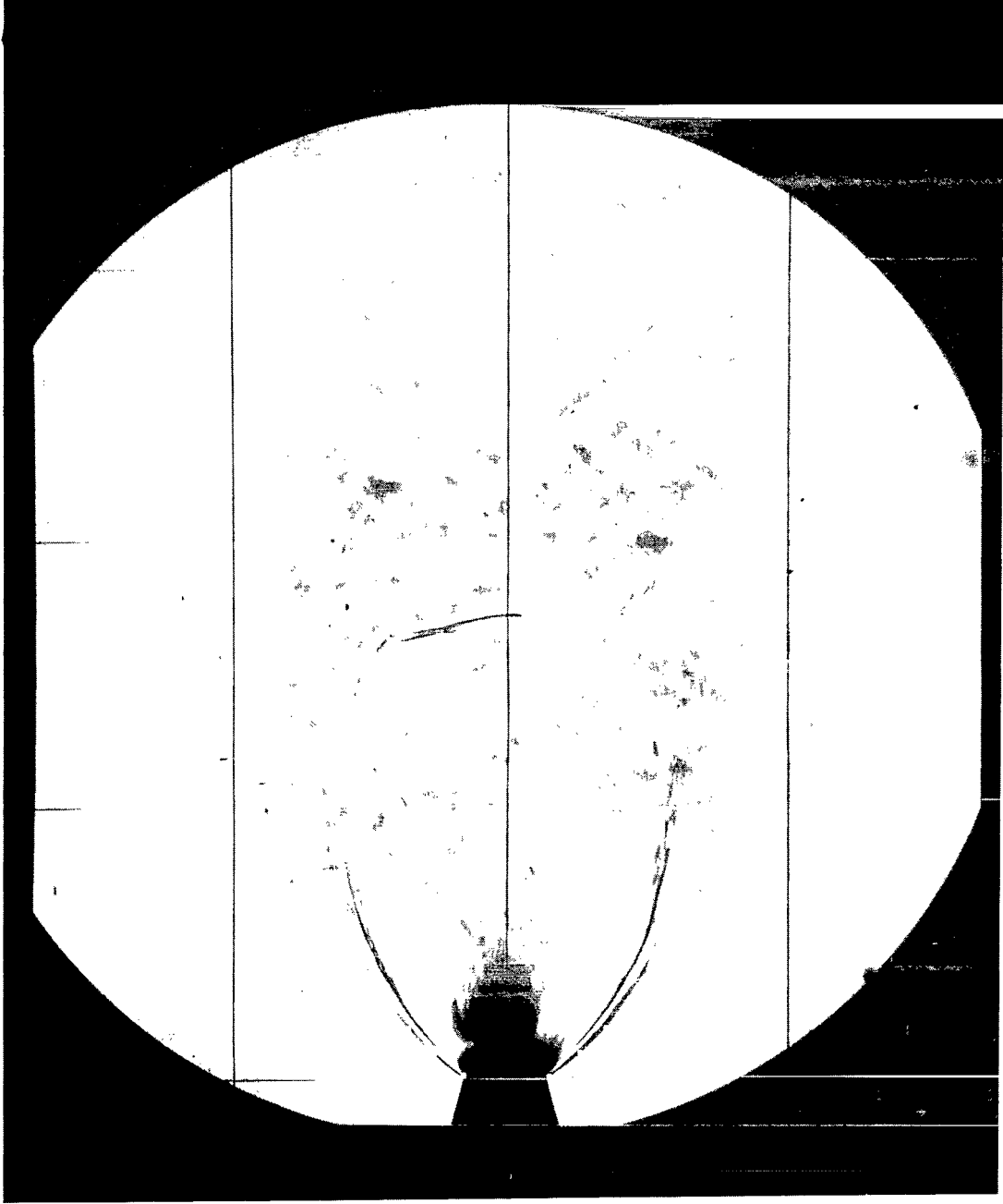
L-64-391



(c) $M_j = 1.0$; $\theta_N = 0^\circ$; $p_j/p_\infty = 39.1$.

Figure 11.- Continued.

I-64-392



(d) $M_j = 1.0$; $\theta_N = 0^\circ$; $P_j/P_\infty = 53.8$.

Figure 11.- Continued.

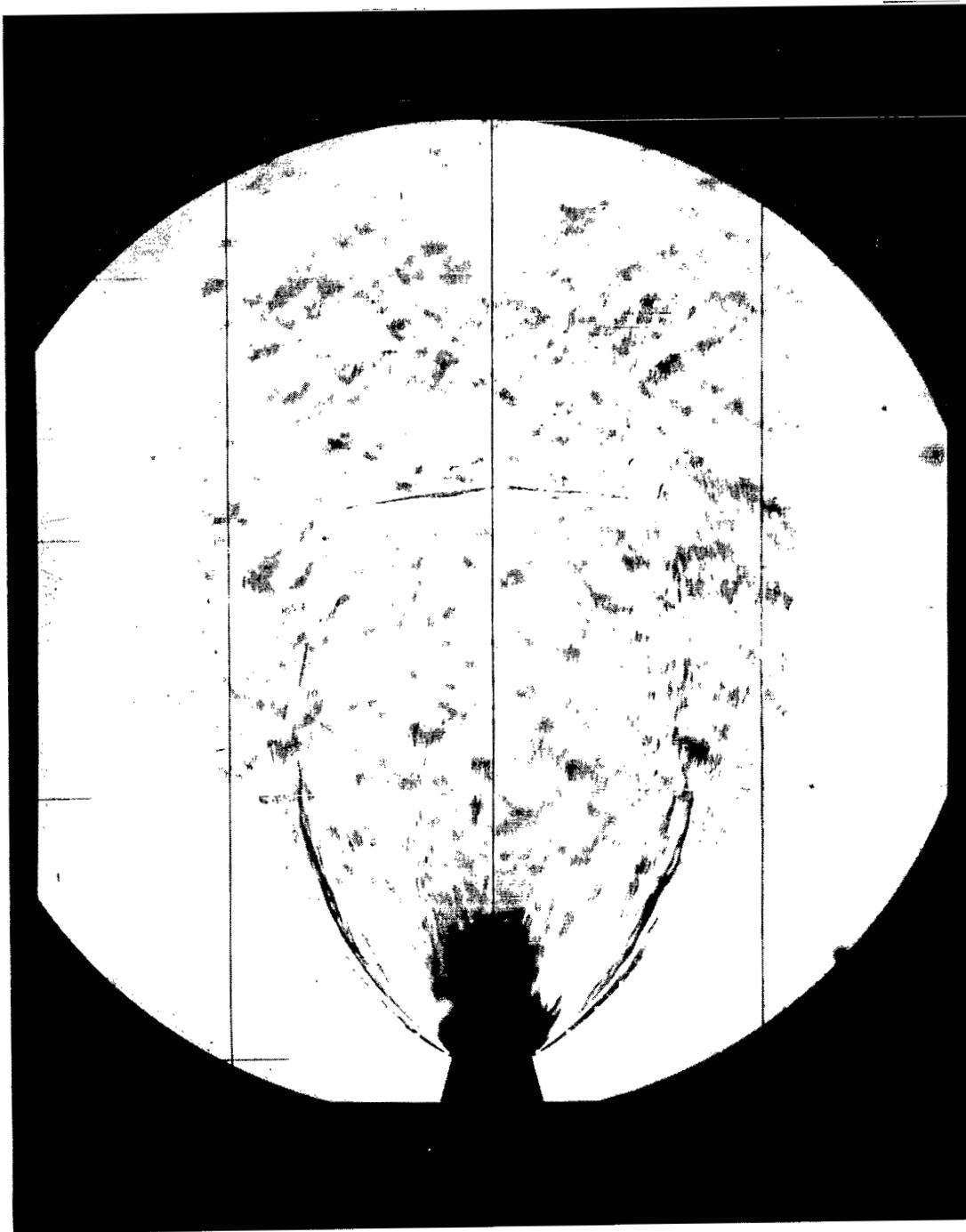
L-64-393



(e) $M_j = 1.0$; $\theta_N = 0^\circ$; $P_j/P_\infty = 66.3$.

Figure 11.- Continued.

L-64-394



(f) $M_j = 1.0$; $\theta_N = 0^\circ$; $P_j/P_\infty = 87.7$.

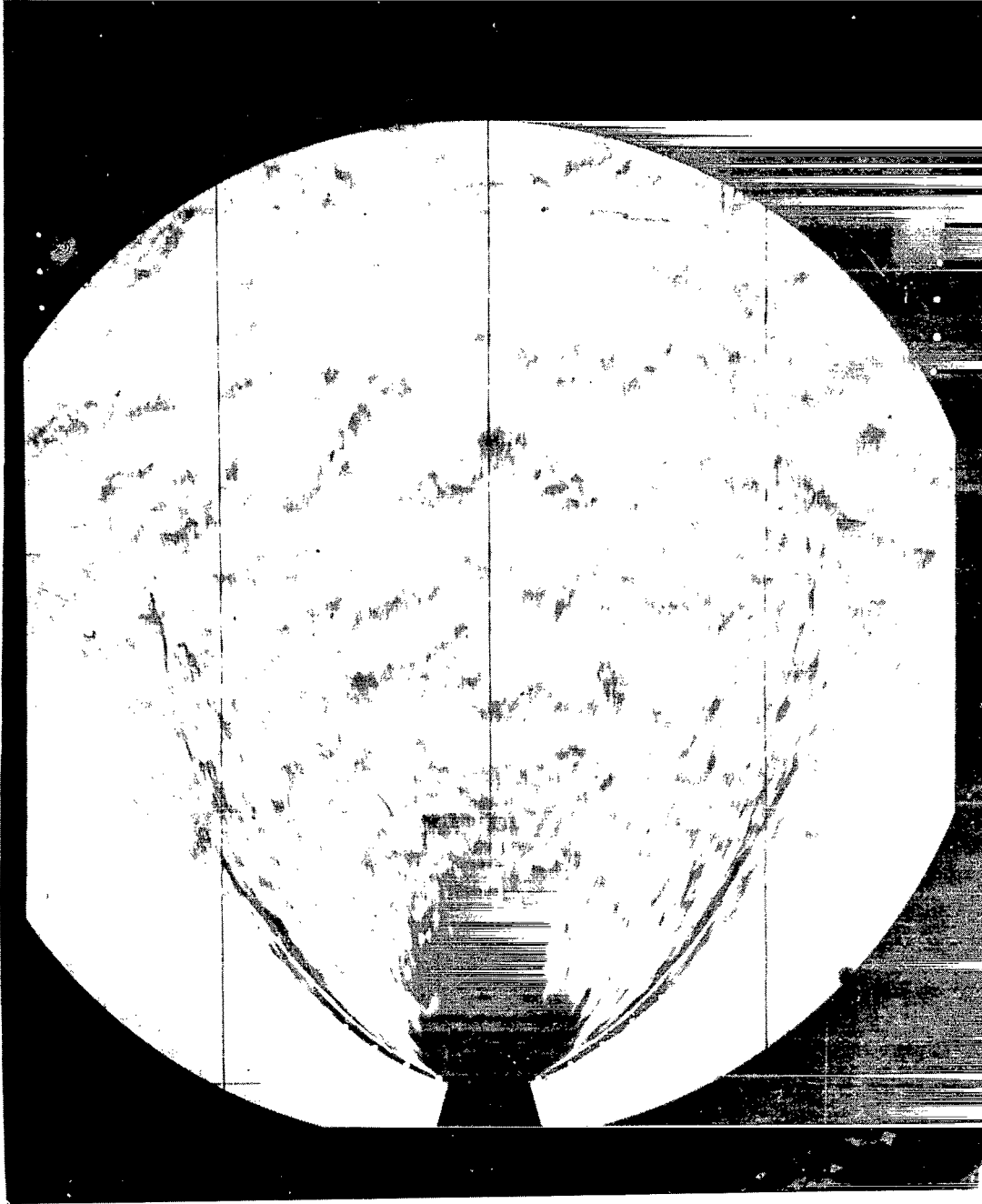
Figure 11.- Continued.



(ε) $M_j = 1.0$; $\theta_N = 0^\circ$; $P_j/P_\infty = 157.2$.

Figure 11.- Continued.

L-64-396



(h) $M_j = 1.0$; $\theta_N = 0^\circ$; $p_j/p_\infty = 194.2$.

Figure 11.- Continued.

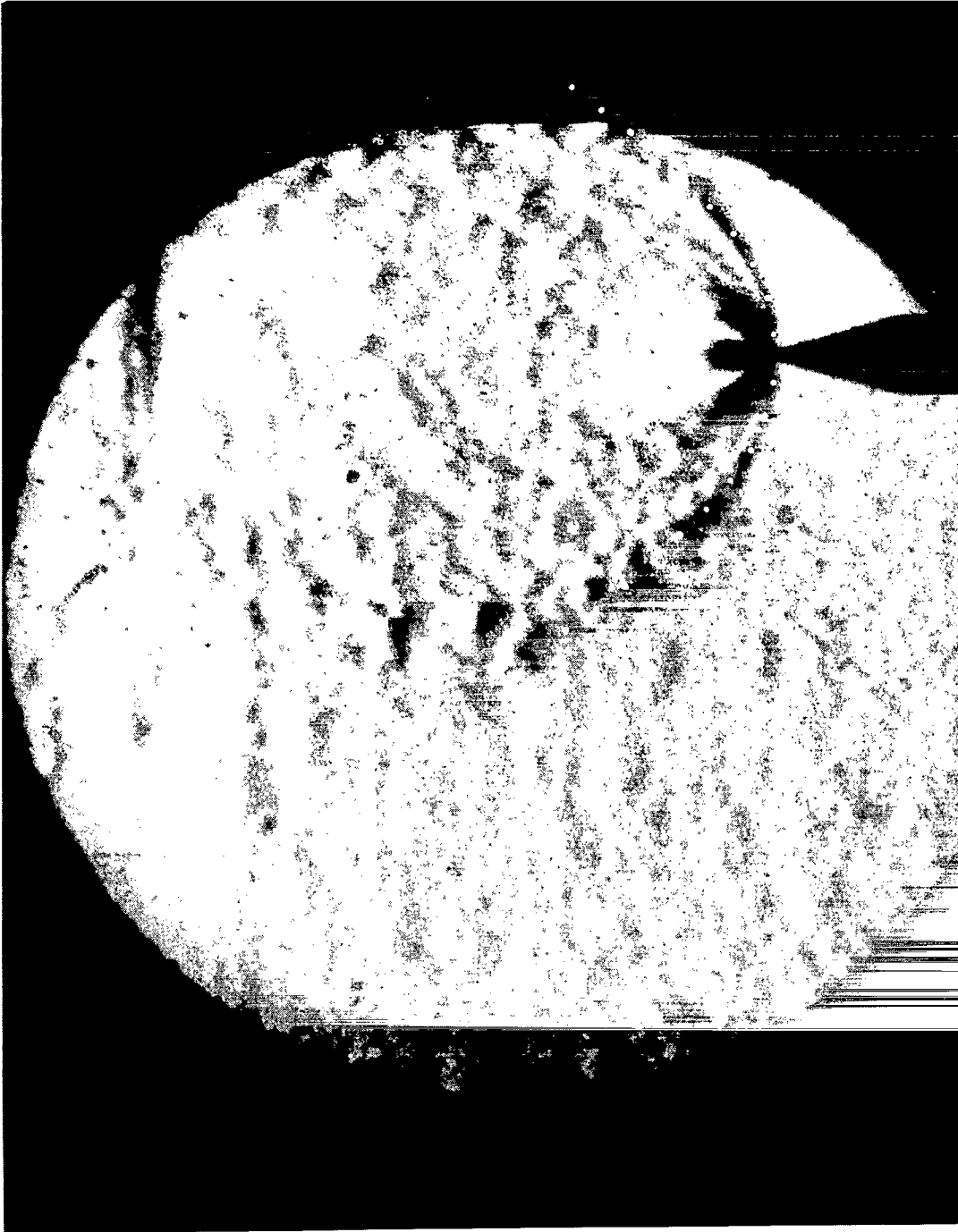
L-64-397



(1) $M_j = 1.0$; $\theta_N = 0^\circ$; $p_i/p_\infty = 9,190$.

Figure 11.- Continued.

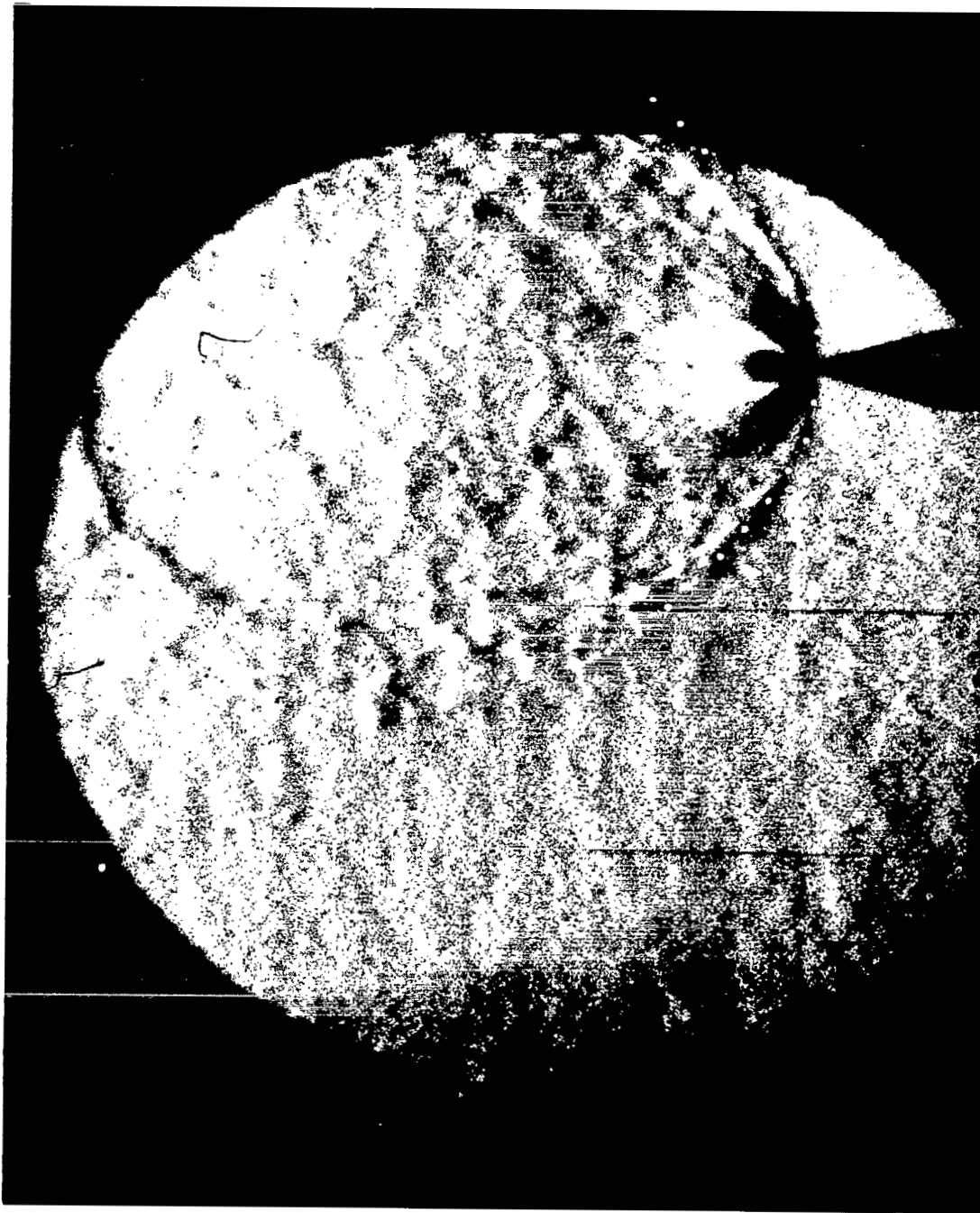
L-64-398



(j) $M_j = 1.0$; $\theta_N = 0^\circ$; $P_j/P_\infty = 12,030$.

Figure 11.- Continued.

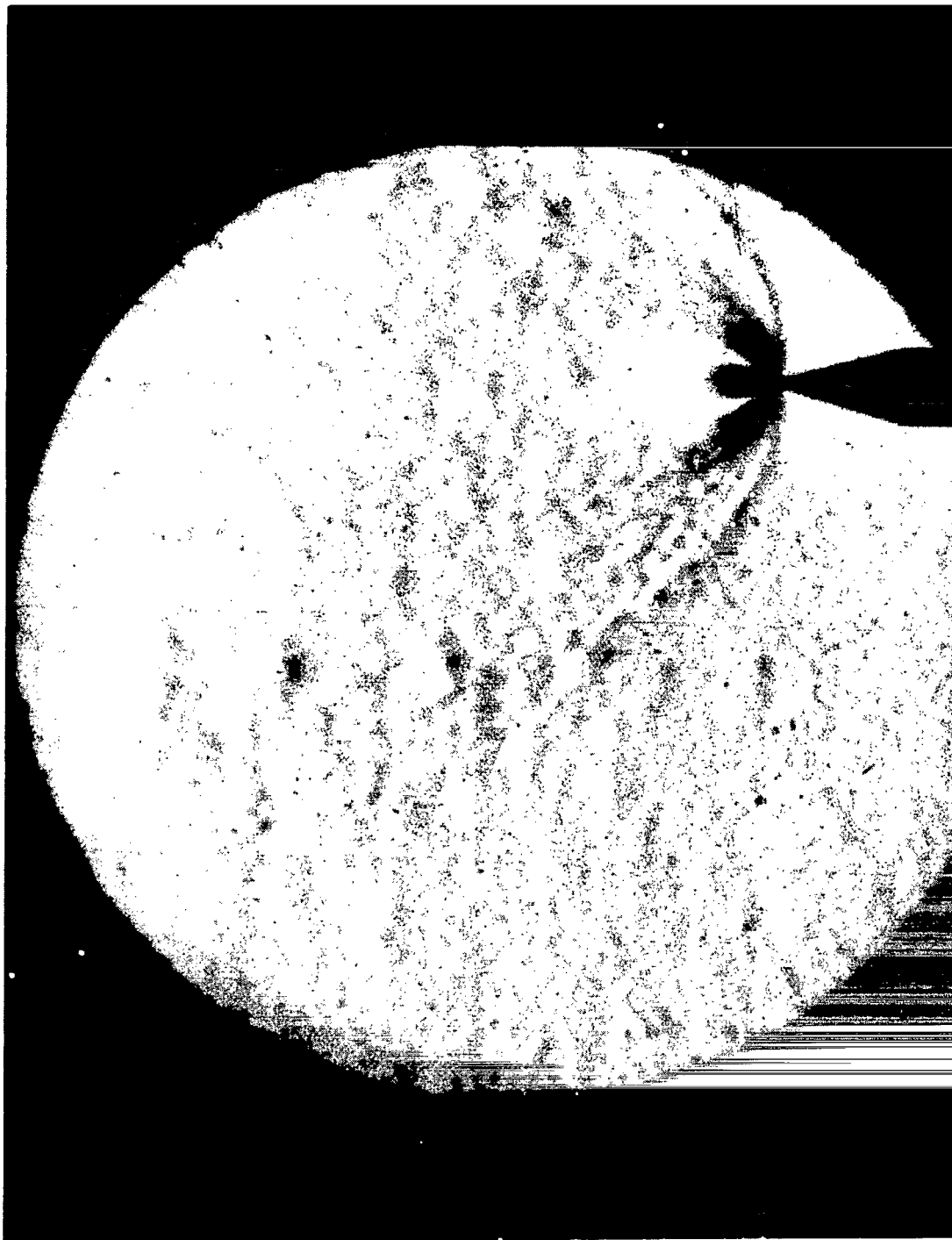
I-64-399



(k) $M_j = 1.0$; $\theta_N = 0^\circ$; $p_j/p_\infty = 15,500$.

Figure 11.- Continued.

L-64-400



(2) $M_j = 1.0$; $\theta_N = 0^\circ$; $p_j/p_\infty = 21,912$.

Figure 11.- Continued.

L-64-401



(m) $M_j = 1.0$; $\theta_N = 0^\circ$; $P_j/P_\infty = 30,590$.

Figure 11.- Continued.

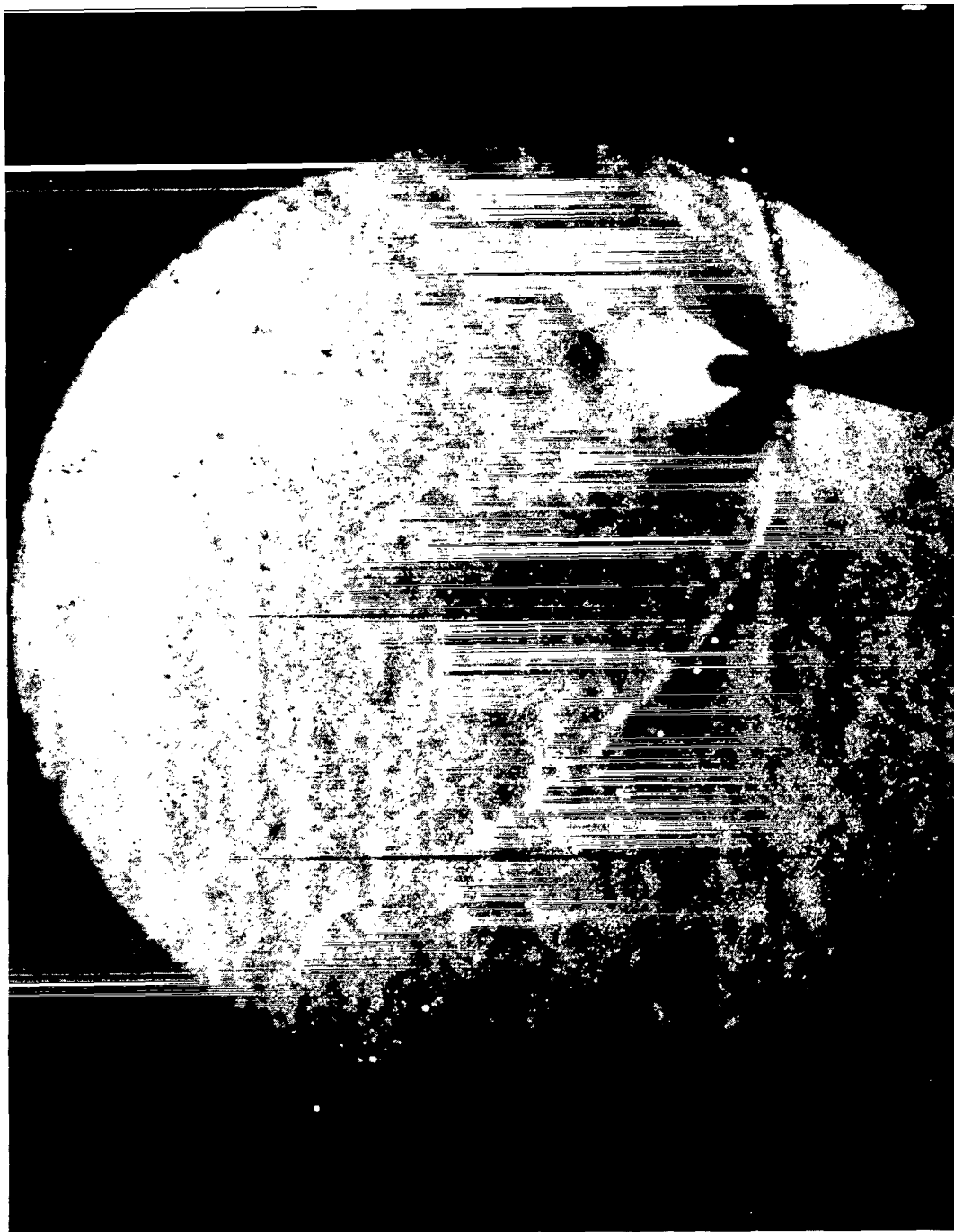
L-64-402



(n) $M_j = 1.0$; $\theta_N = 0^\circ$; $P_j/P_\infty = 52,980$.

Figure 11.- Continued.

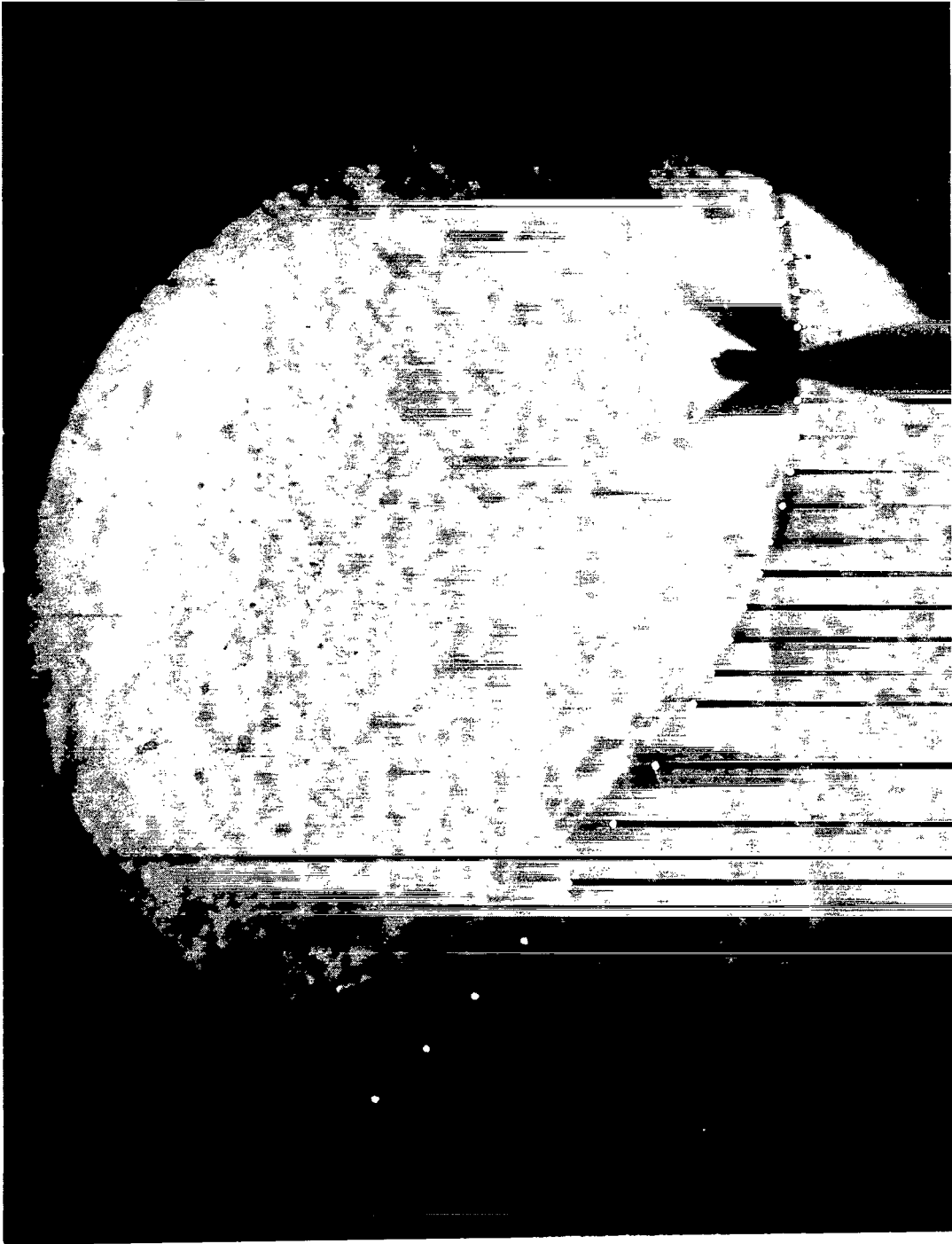
L-64-403



(o) $M_j = 1.0$; $\theta_N = 0^\circ$; $P_j/P_\infty = 82,030$.

Figure 11.- Continued.

L-64-404



(p) $M_j = 1.0; \theta_N = 0^\circ; P_j/P_\infty = 102,180.$

Figure 11.- Concluded.

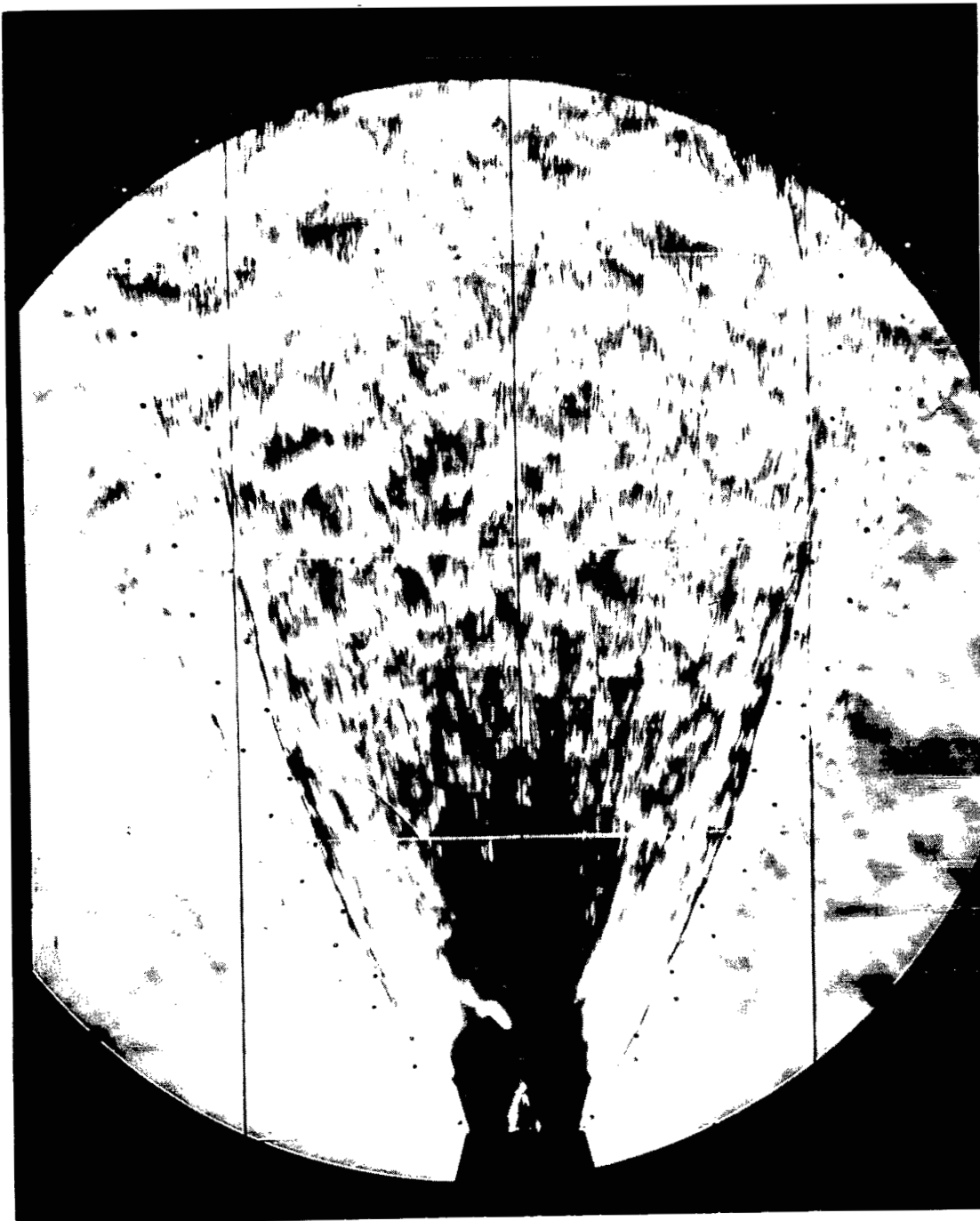
I-64-405



I-64-406

(a) $M_j = 2.22$; $\theta_N = 0^\circ$; $P_j/P_\infty = 14.4$.

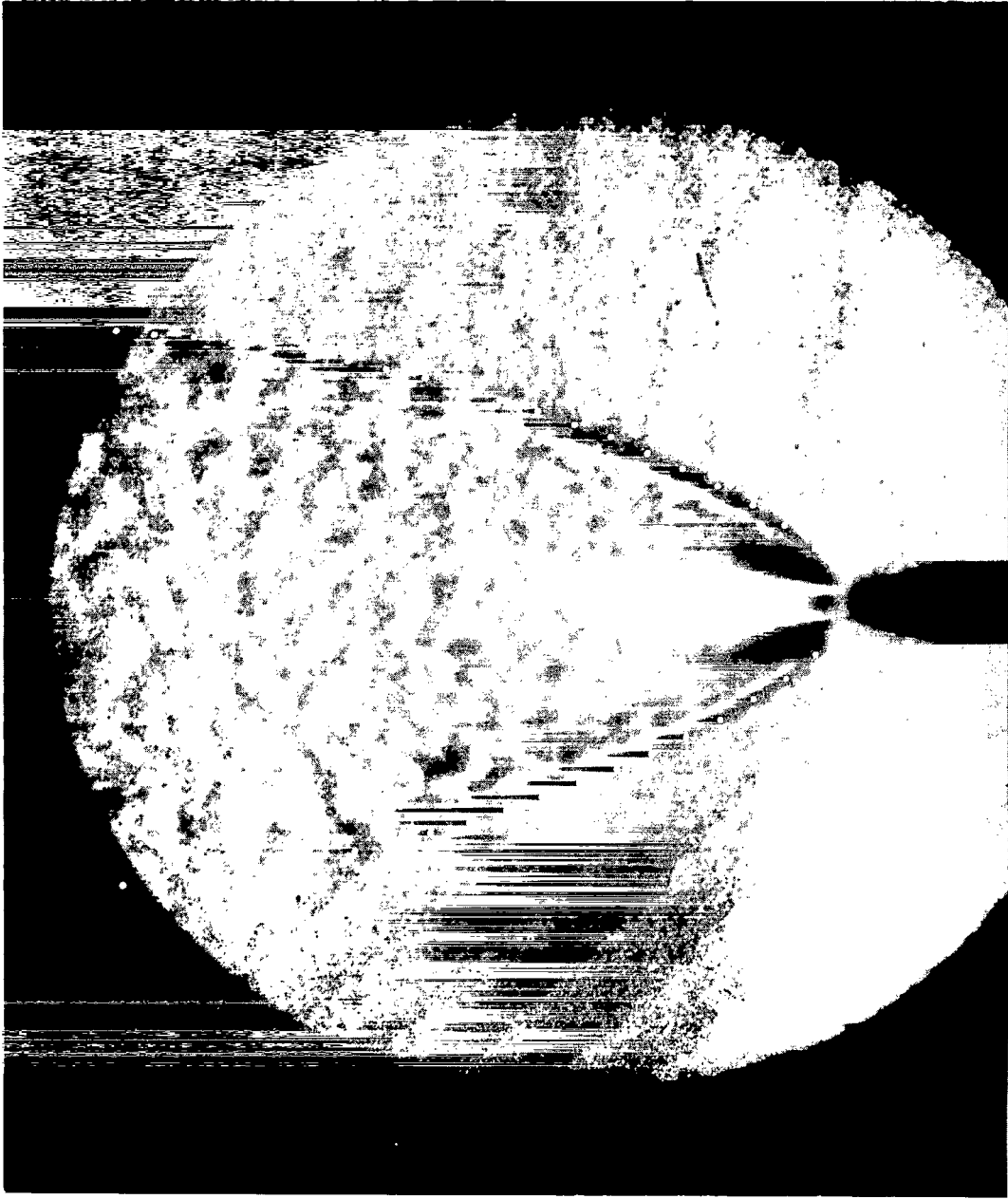
Figure 12.- Schlieren photographs of jet exhaust plumes with superimposed theoretical boundaries and internal shock.



(b) $M_j = 2.22$; $\theta_N = 0^\circ$; $P_j/P_\infty = 37.7$.

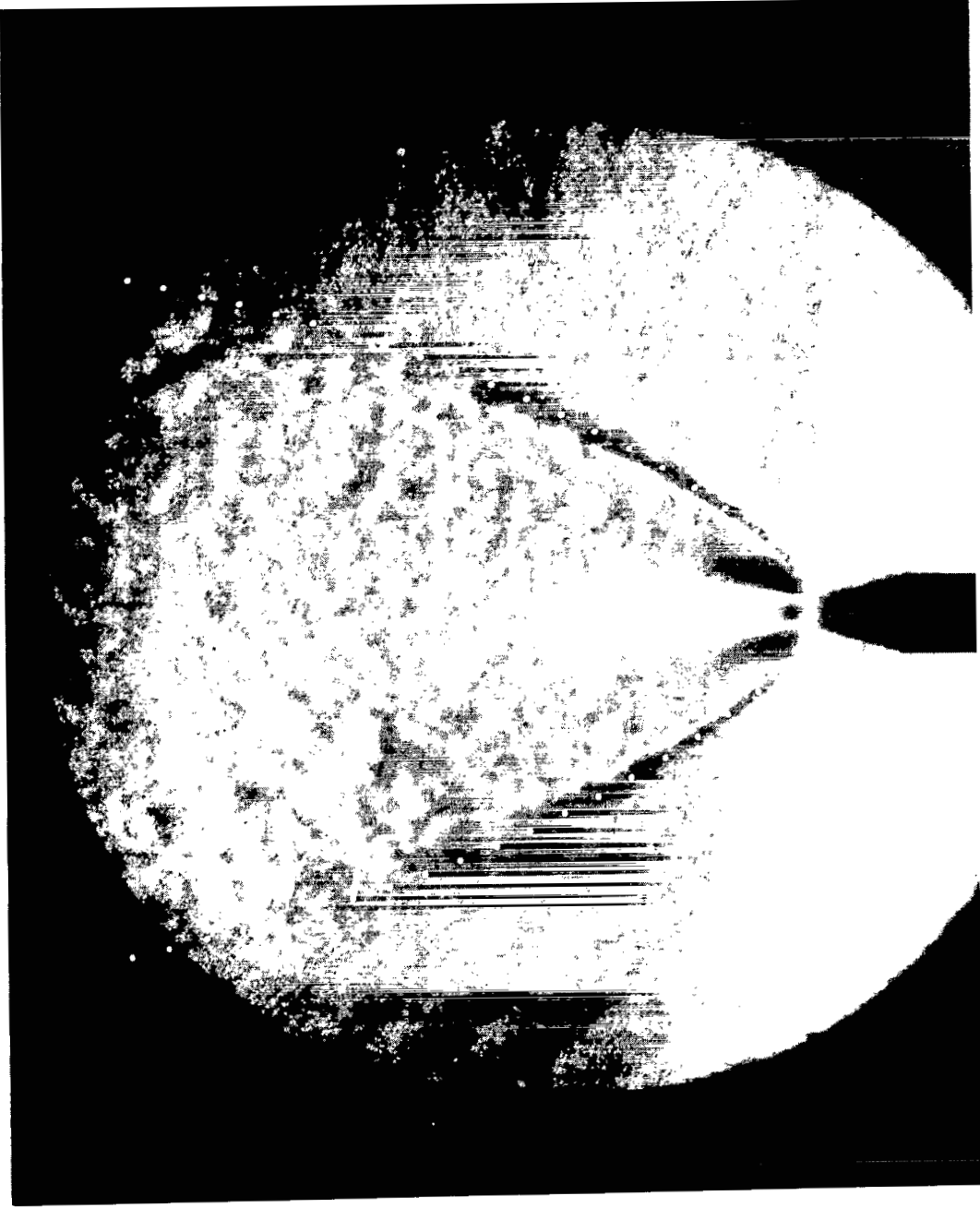
Figure 12.- Concluded.

I-64-407



(a) Nominal $M_j = 5.0$; $\theta_N = 26.5^\circ$; $P_j/P_\infty = 85$.

Figure 13.- Schlieren photographs of jet exhaust plumes with superimposed theoretical boundaries. I-64-408

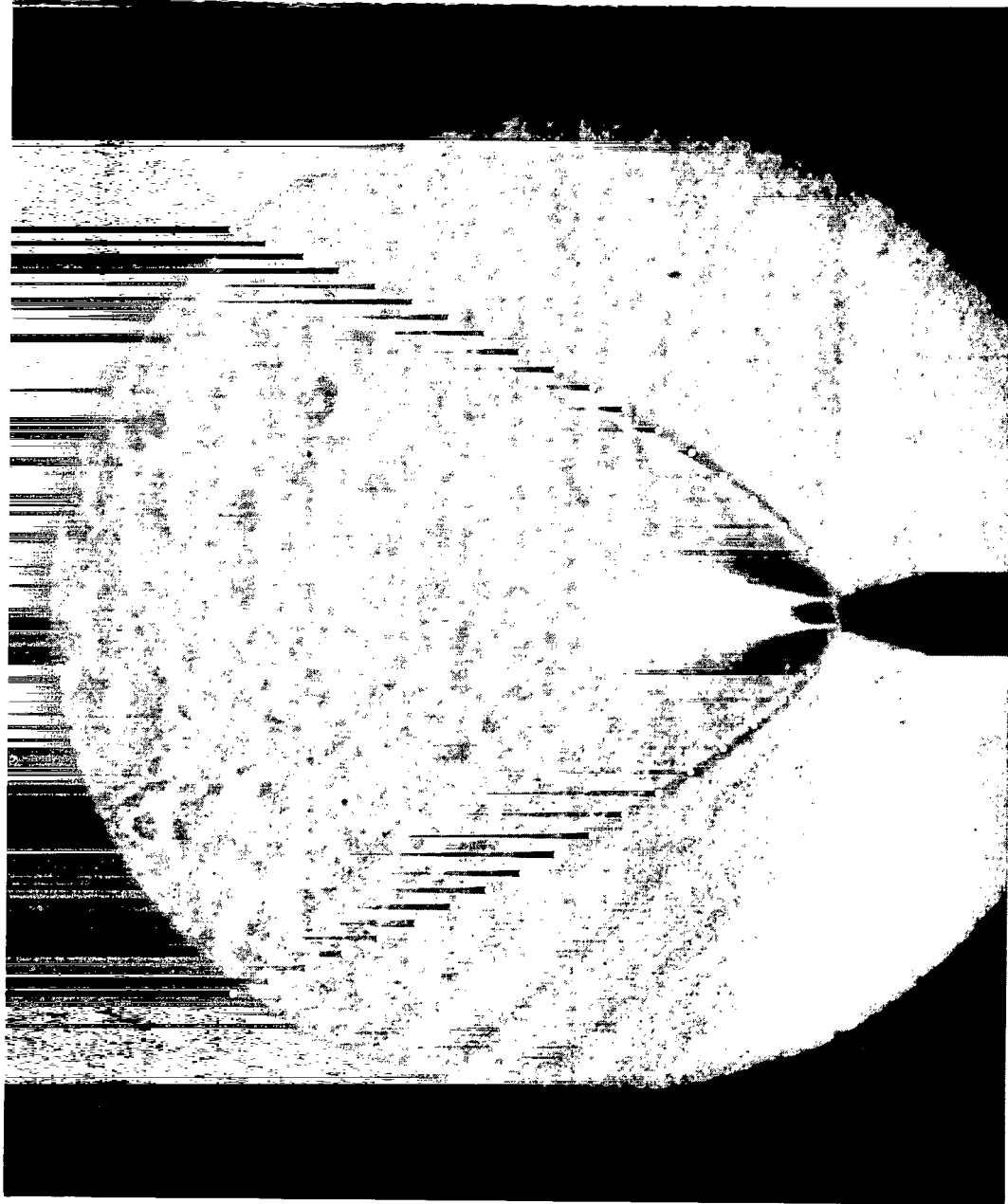


(b) Nominal $M_j = 5.0$; $\theta_N = 26.5^\circ$; $p_j/p_\infty = 147$.

Figure 13.- Continued.

I-64-409

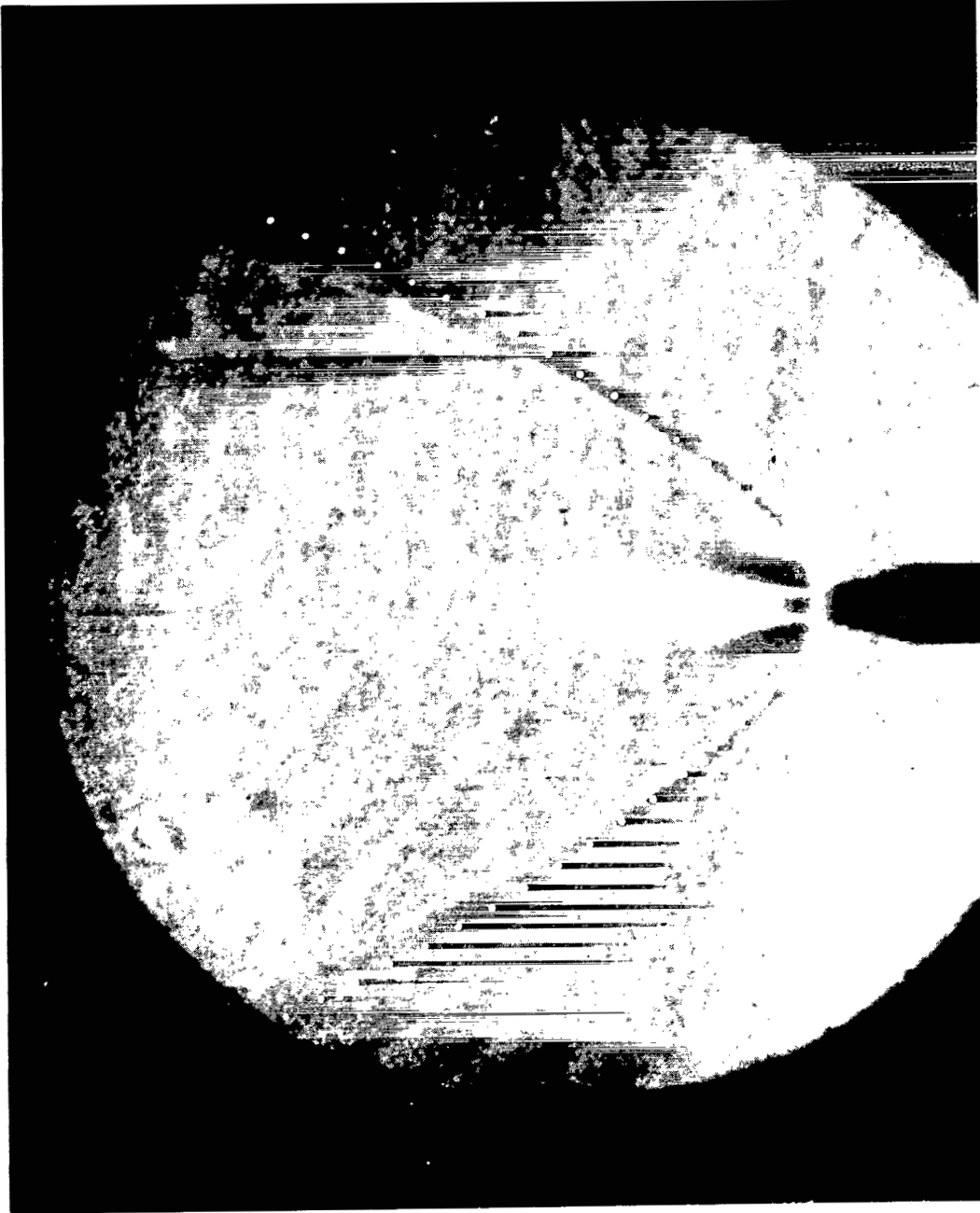




(c) Nominal $M_j = 5.0$; $\theta_N = 26.5^\circ$; $p_j/p_\infty = 286$.

Figure 13.- Continued.

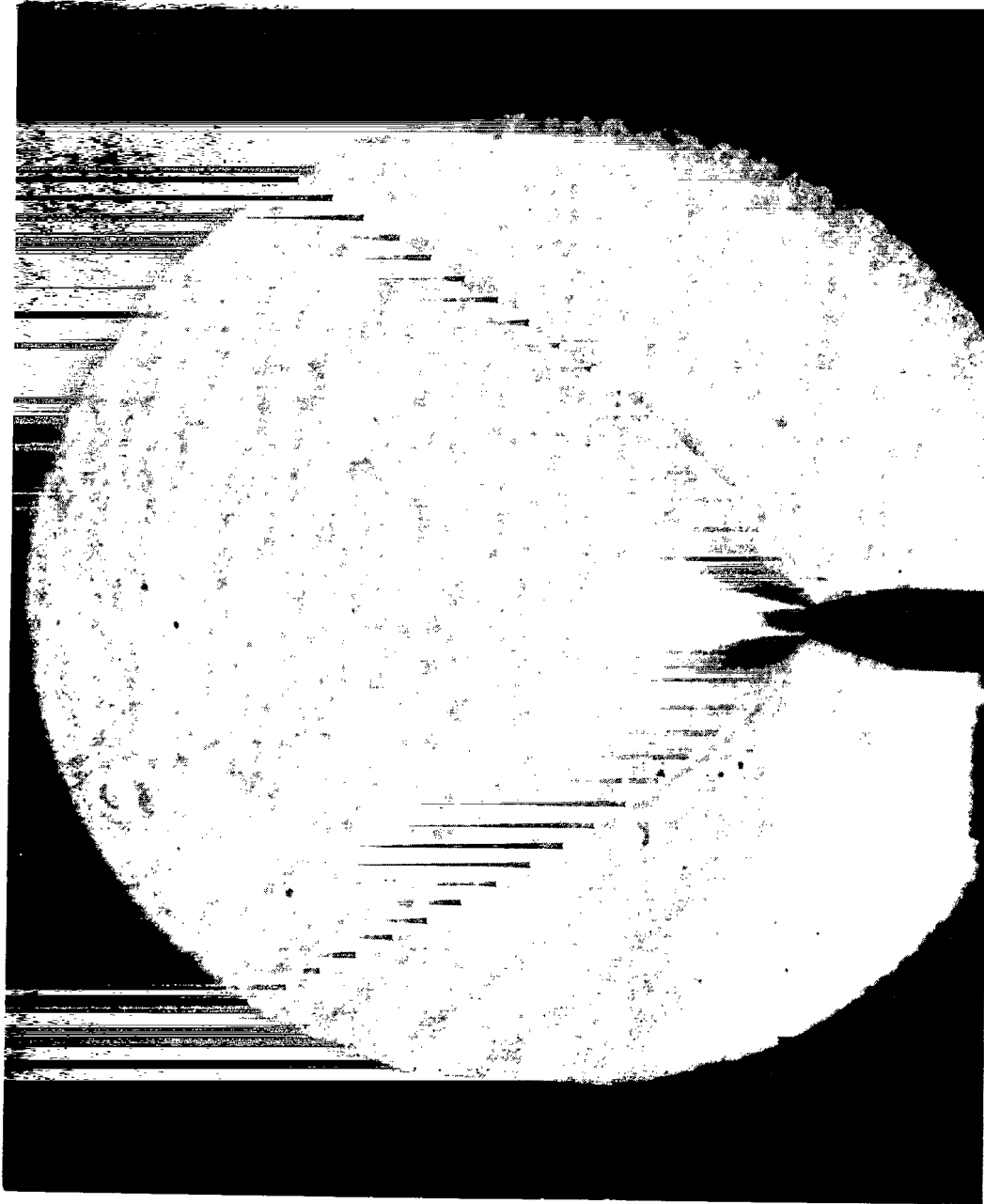
L-64-410



(d) Nominal $M_j = 5.0$; $\theta_N = 26.5^\circ$; $P_j/P_\infty = 418$.

Figure 13.- Continued.

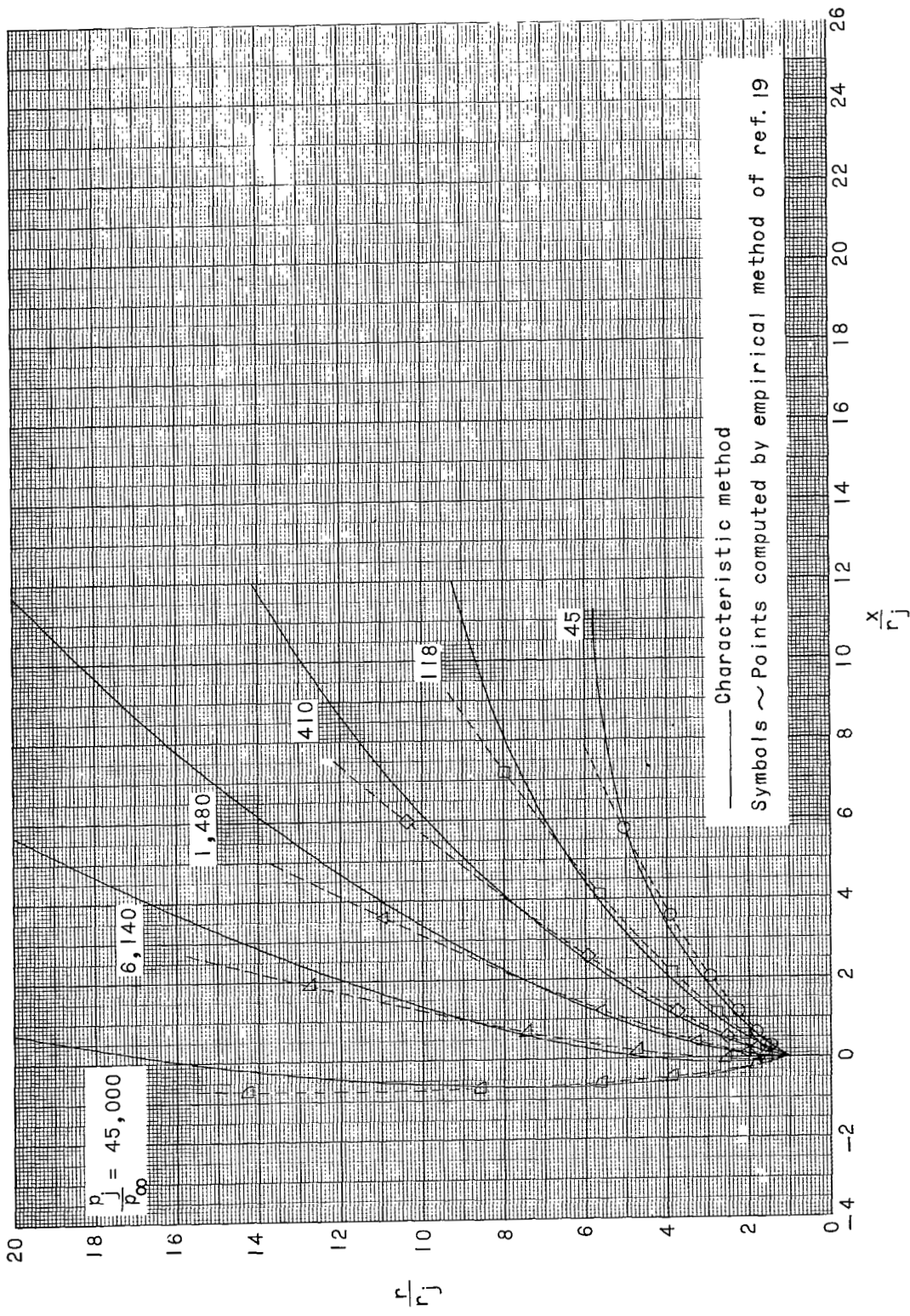
L-64-411



(e) Nominal $M_j = 5.0$; $\theta_N = 26.5^\circ$; $p_j/p_\infty = 580$.

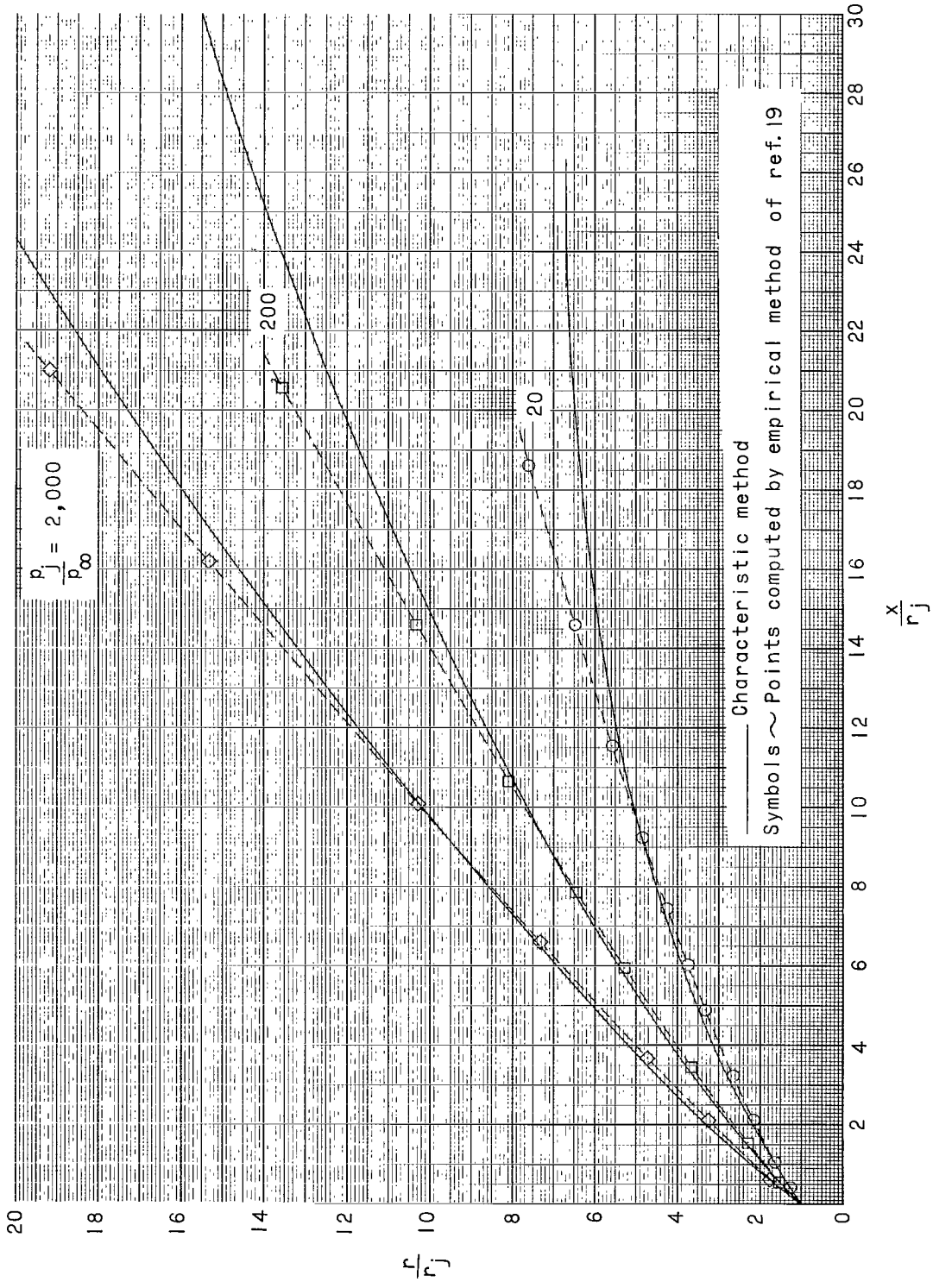
Figure 13.- Concluded.

L-64-412



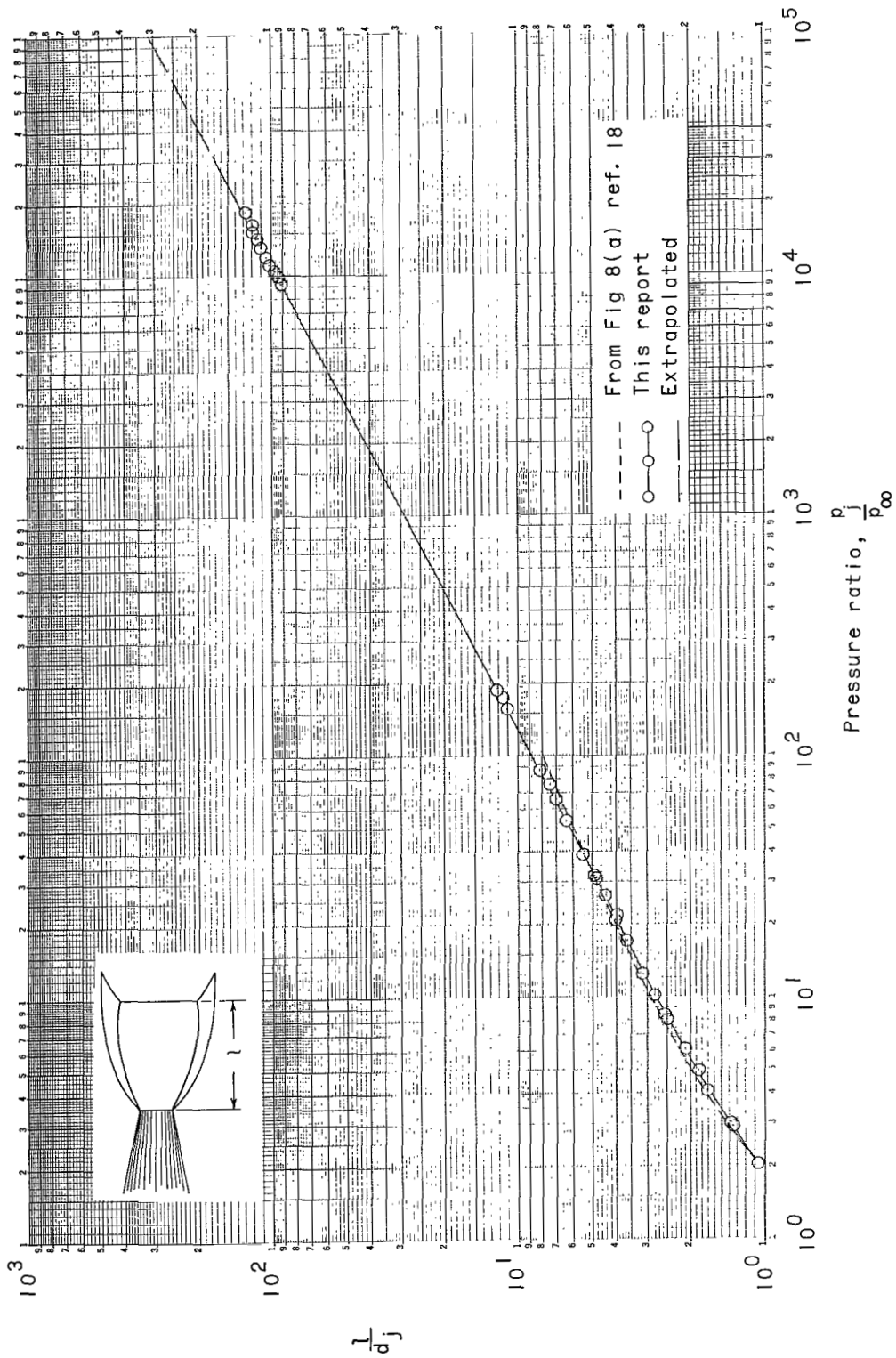
(a) $M_j = 1.0; \theta_N = 0^\circ; \gamma = 1.4.$

Figure 14.- Comparison of boundaries computed by characteristic method with those computed by empirical method.



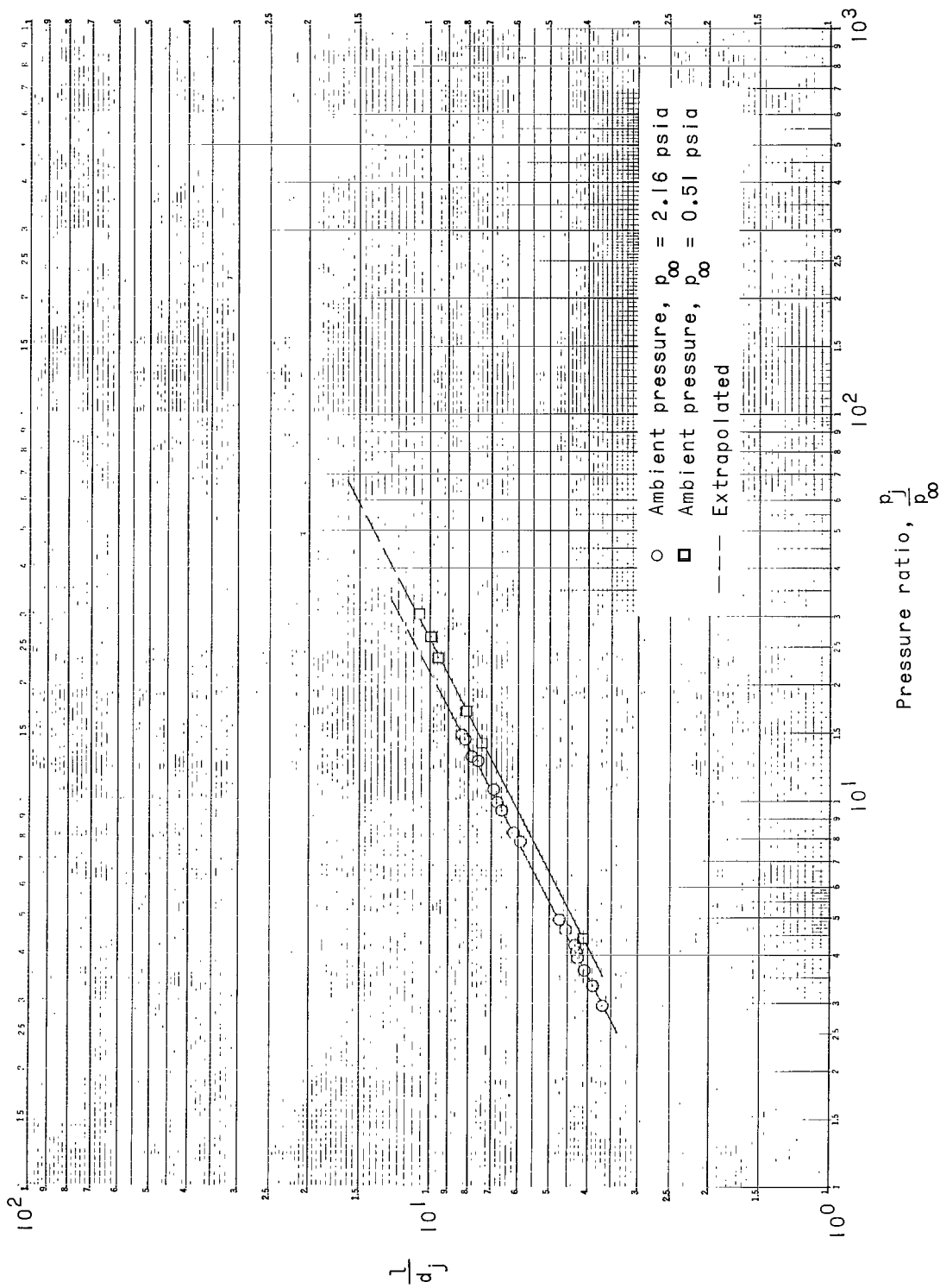
(b) $M_j = 5.0$; $\theta_N = 15^\circ$; $\gamma = 1.4$.

Figure 14.- Concluded.



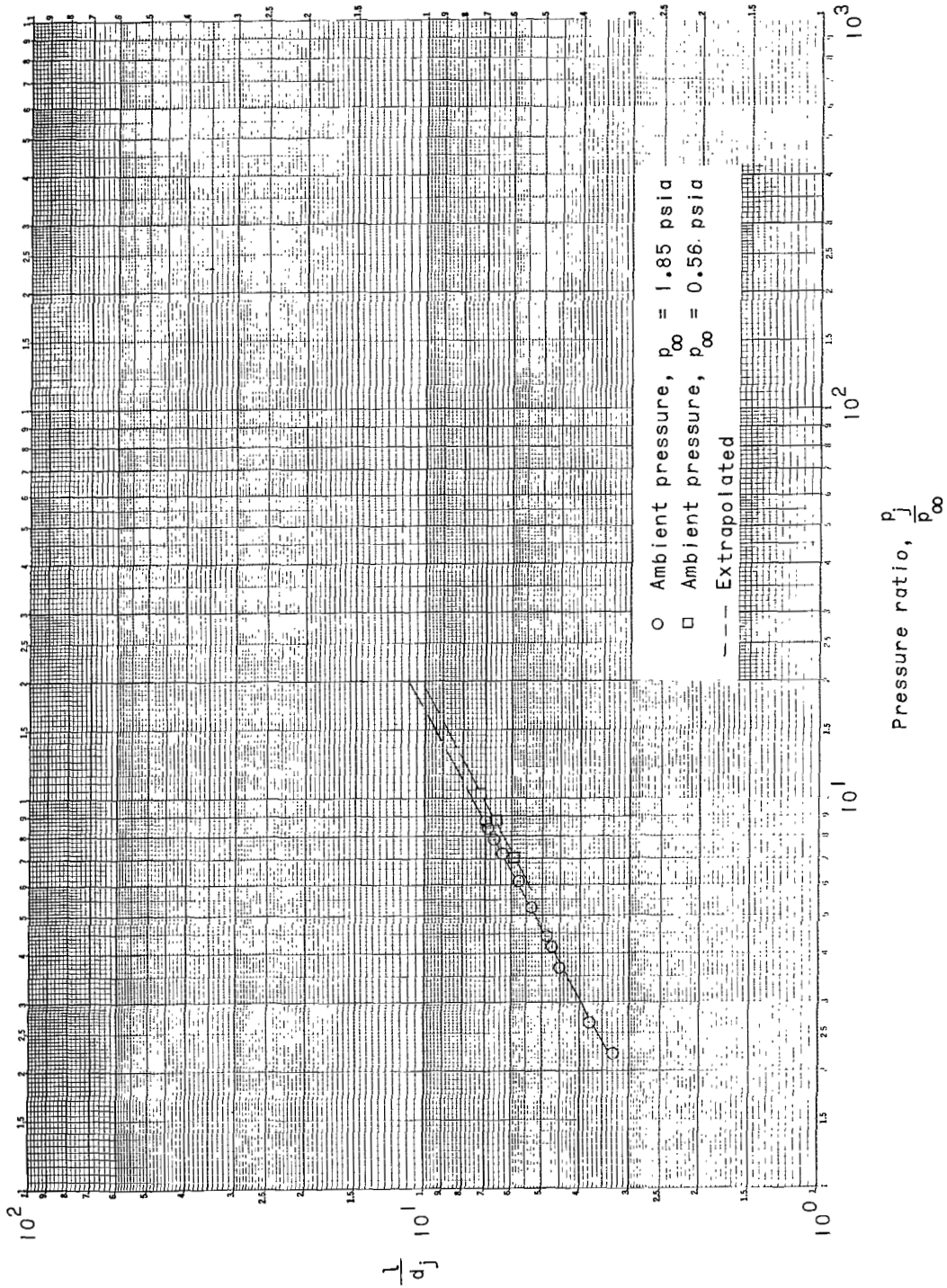
(a) $M_j = 1.0$; $\theta_N = 0^\circ$; $\gamma = 1.4$.

Figure 15.- Effect of jet pressure ratio upon nondimensional distance along jet axis from plane of nozzle exit to location of Riemann wave.



(b) $M_j = 2.22$; $\theta_N = 0^\circ$; $\gamma = 1.4$.

Figure 15.- Continued.



(c) $M_j = 2.63$; $\theta_N = 0^\circ$; $\gamma = 1.4$.

Figure 15.- Concluded.